SFEI | AQUATIC SCIENCE CENTER

NUMBER 913
DECEMBER 2018

Hydrodynamic and Water Quality Model Calibration and Application in San Francisco Bay

Prepared by:

Emma Nuss[1], Zhenlin Zhang[1], Rusty Holleman[2], Ariella Chelsky[1], Taylor Winchell[1], Jing Wu[1], and David Senn[1],

1 San Francisco Estuary Institute, 4911 Central Ave, Richmond, CA 94804

2 University California, Davis, 1 Shields Ave, Davis, CA 95616

SAN FRANCISCO ESTUARY INSTITUTE and the AQUATIC SCIENCE CENTER

4911 Central Avenue, Richmond, CA 94804 • p: 510-746-7334 (SFEI) • f: 510-746-7300 • www.sfei.org

CONTENTS

ACKNOWLEDGEMENTS

The report provides an overview and progress update of work related to the development and application of hydrodynamic and biogeochemical models for San Francisco Bay. This work received partial support from multiple funding sources and satisfies deliverable requirements for each of those funding sources: State Water Board Agreement #16-025-120 (Water Quality Modeling Progress Report); settlement of San Francisco Bay Water Board enforcement actions (Nutrient Calibration and Validation Report); and the San Francisco Bay Nutrient Management Strategy, including joint support from the Bay Regional Monitoring Program (Progress Report).
SFEI Contribution #913

1. Introduction

To answer management questions about nutrient related water quality in San Francisco Bay, hydrodynamic and biogeochemical models have been developed. This report outlines the development of both of these models. Section 2 is the description and validation of the hydrodynamic model, previously completed in December 2017 for the San Francisco Bay Interim Model Validation Report, but included here for completeness. Section 3 of this report covers the description and validation the biogeochemical model.

2. Hydrodynamic Model

2.1. Summary

As part of the Nutrient Management Strategy, a coupled hydrodynamic-biogeochemical model of San Francisco Bay is being developed. The process-based, numerical model will be used to inform nutrient management decisions, by:

- improving quantitative understanding of processes that shape current conditions,
- forecasting ecosystem response under future scenarios, and
- evaluating potential effectiveness of management actions.

This report describes the model in its present configuration and the status of its validation. Model development is necessarily an iterative process, with early stages focused on refining the model's representation of hydrodynamics and transport, and later stages of the effort including increasingly complex representations of biogeochemistry. Present validation efforts focus on assessing model skill with respect to hydrodynamics, salinity and transport. The final report will additionally consider model validation of water quality and biogeochemical processes.
The model inputs include tides, direct precipitation, evaporation, stormwater runoff, wastewater discharges, Delta outflow and wind. From these inputs, the model calculates water levels, salinity, currents and the force of the currents on the bed throughout the Bay. Simulations cover the period October 2012 through September 2013 (water year 2013).
A wide range of observations collected throughout the Bay are used to assess the model's predictive skill. Comparisons between observed and modeled data include tidal water levels, depth-averaged velocities and salinity from both shipboard and moored sensors.
Water levels are reproduced well from South Bay up to San Pablo Bay. Tidal comparisons upstream of Carquinez Strait show that the model generally overpredicts water levels, likely due to the truncated upstream Delta. Velocities are modeled similarly well in open areas of the Bay downstream of Carquinez Strait. Velocities upstream of Carquinez Strait likewise belie the lack of a resolved Delta.
Salinity is compared to monthly USGS transects along the channels of the Bay. Overall skill in predicting salinity is good, with a small bias fresh in the summer likely due to the absence of evaporation. Comparisons to transect data are augmented by moored, time-series data at three sites. These comparisons show that in the dry season the model exhibits a bias towards being too fresh, but wet season events are captured very well.
The hydrodynamic model in its current state has sufficient skill in representing transport in South Bay to support water quality studies with a South Bay focus. Velocities and water levels upstream of San Pablo Bay suffer from proximity to the Delta boundary condition. This may lead to unrealistic

transport in Suisun Bay, and has been part of the motivation for Suisun and Delta-specific modeling efforts which include the Delta. Further work is needed to achieve similar fidelity for exchange with the coastal ocean and transport in North Bay.
The remainder of this report provides details on the configuration of the model, analysis of its skill, and discussion of potential causes for model–data disagreements.

2.2. Model Setup

The San Francisco Bay hydrodynamic model is built on *D-Flow Flexible Mesh* (DFM). DFM is part of the Deltares suite of models which also includes *D-Water Quality*, the platform chosen for the biogeochemical phase of the NMS modeling project. DFM is a finite-volume, three-dimensional, unstructured hydrodynamic model Martyr-Koller *et al* 2017[1]. The unstructured nature of the grid allows for efficient and flexible resolution of flow features ranging from small perimeter sloughs and ponds up to a regional representation of the coastal ocean. This range of features is resolved without explicit seams or nesting boundaries as would be required for a structured grid model applied to the same area.
The original model setup was developed by Silvia Pubben and Mick van der Wegen, (Pubben, 2017), as a continuation of prior modeling efforts stemming from the USGS CASCaDE and San Francisco Bay-Delta Community Model projects.
We set up the model to simulate Water Year 2013 (WY2013), which spans October 30, 2012 to September 30th, 2013. The simulation begins two months earlier on August 1, 2012 to allow the model to spin up. WY2013 was chosen based on overlap with important recent data collection efforts (i.e. ADCP deployments), and the desire to avoid the more anomalous drought conditions of later years.
The model has been run on a Linux workstation utilizing 16 Intel Xeon E5-2680 2.40 GHz cores, communicating over MPI. The full 426 day run takes 7.0 days of wall-clock time, for a simulation speed of 61 times faster than realtime. DFM was compiled from SVN revision 52184 of the source code and GCC 5.4.0.

2.3. Model Domain and Grid

The model domain covers San Francisco Bay, including portions of Coyote Creek and Guadalupe River at the southernmost extent of the Bay, and extending north to the Sacramento and San Joaquin Rivers at Rio Vista and Jersey Point, respectively. A separate but related model includes a complete Delta, however the computational expense of that model currently limits its utility to studies with a North Bay focus, while the present model is optimized for South Bay applications. The domain extends into the Pacific Ocean, about 20km west of Point Reyes in the north and 40km west of Half Moon Bay in the south, roughly encompassing the San Francisco Bight. The horizontal grid resolution varies from 20 m in select sloughs of Lower South Bay, to over 2 km at Point Reyes. Nominal grid resolution in South Bay is 250 m, and 350–500 m in North Bay, for a total of 49,996 cells in the horizontal. The three-dimensional model utilizes a sigma coordinate in the vertical, such that all areas have 10 layers in the vertical, with the layer thicknesses varying in accordance with the overall depth.
Bathymetry for the model has been compiled from a combination of digital elevation models (DEMs):

[1] https://doi.org/10.1016/j.ecss.2017.04.024

- 10 m topo-bathymetry[2] from California Department of Water Resources (Wang and Ateljevich, 2012[3]).
- High resolution USGS bathymetry[4] in Lower South Bay (Foxgrover et al, 2014[5]).

Bathymetry is prescribed at the nodes of the grid by linear interpolation on the source DEMs, then internally extrapolated to edges and cells. All elevation data are relative to the NAVD88 vertical datum.

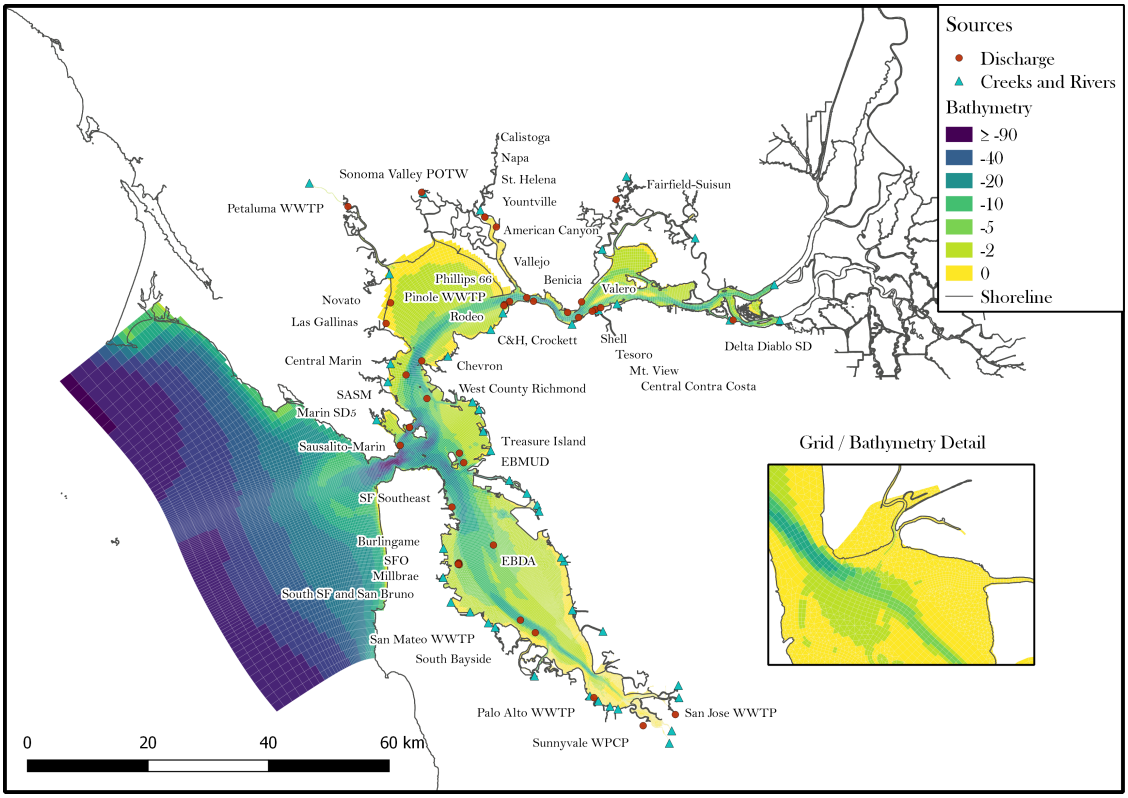

Figure 2.1: San Francisco Bay DFM grid

2.4. Boundary Conditions and Forcings

2.4.1. Tidal Ocean Boundary

The open ocean boundary is forced along the western edge by observed sea level data from Point Reyes, via NOAA gage 9415020. Observed 6-minute water levels are low-pass filtered with a 4th order Butterworth filter with a 3-hour cutoff period. Salinity at the ocean boundary is set to a constant 33 ppt. The shorter northern and southern edges of the ocean boundary are closed.

[2] http://baydeltaoffice.water.ca.gov/modeling/deltamodeling/modelingdata/DEM.cfm
[3] http://deltacouncil.ca.gov/sites/default/files/2015/05/A%20Continuous%20Surface%20Elevation%20Map%20for%20Modeling%20Chapter%206.pdf
[4] https://pubs.usgs.gov/of/2011/1315/
[5] http://www.southbayrestoration.org/documents/technical/Bathmetry%20SSF%20v3.pdf

2.4.2. Bay Area Rivers and Stormwater

Freshwater flows were derived from the *Bay Area Hydrologic Model* (BAHM)[6], an HSPF-based hydrologic model (see Appendix A for more details). This model has been calibrated against gage data over the 2000–2016 period, and includes 44 separate river and stormwater inputs to the Bay. All river and stormwater inputs are assumed to enter the Bay with negligible salinity.

2.4.3. Delta Inflow

To avoid undue computational complexity the hydrodynamic model does not extend into the Sacramento–San Joaquin Delta. The edge of the model domain is at Rio Vista on the Sacramento River and Jersey Point on the San Joaquin River, well within the tidal portion of the system. Boundary conditions here are taken from USGS streamflow gages, specifically USGS stations 11455420 (Sacramento River at Rio Vista) and 11337190 (San Joaquin River at Jersey Point) for the Sacramento and San Joaquin flows, respectively. Flows at Rio Vista and Jersey Point are assumed to have negligible salinity.

2.4.4. Wastewater Treatment Plants and Refineries

Given the goal to support nutrient-related studies in the Bay, special attention has been given to Wastewater Treatment Plant (WWTP) inputs. In parts of the Bay, especially South Bay, WWTP inputs are significant freshwater sources and it is therefore essential that they are accounted for in the hydrodynamics where they can properly influence the density field (as opposed to added as mass sources in the water quality model). Flow and load data for 37 WWTPs and 5 refineries have been compiled and made available online via ERDDAP[7] and github[8] (see Appendix B for more details). This compilation draws on observed flow rates where data exist. For dates when flow data is unavailable, a flow rate is estimated based on inter-annual trends and a seasonal flow climatology. Each of the 42 inflows have been added to the hydrodynamic model as a freshwater source located at the bed.

2.4.5. Winds

The model includes a wind field derived from observations at 5–10 stations near the Bay (depending on data availability). These observations have been extrapolated in space based on the method of Ludwig *et al* (1991)[9], which uses topographic data, atmospheric stability and observed winds to extrapolate a smooth, terrain-aware wind field. The hydrodynamic model includes the effects of wind in terms of surface stress and vertical mixing, but does not yet include wind-waves.

2.4.6. Precipitation and Evaporation

In addition to stormwater runoff which enters the model at prescribed locations along the boundary, we also include direct precipitation and evaporation acting directly on the water surface. The model incorporates measured precipitation and evapotranspiration ($ET_\circ$) from the CIMIS Union City station. $ET_\circ$ is scaled to pan evaporation[10] by dividing by a factor between 0.6 and 0.7

[6] https://www.sfei.org/projects/regional-watershed-spreadsheet-model#sthash.Rds0hLQn.dpbs
[7] http://sfbaynutrients.sfei.org/erddap/tabledap/sfei_sfbay_potw_201705.html
[8] https://github.com/rustychris/sfbay_potw
[9] https://doi.org/10.1175/1520-0450(1991)030<1490:UOMCAC>2.0.CO;2
[10] https://cals.arizona.edu/azmet/et1.htm

depending on temperature. The present model configuration further scales this evaporation down by a factor of 2 due to transient stability issues, though this factor will be removed in the near future as those stability problems are resolved. These inputs have the greatest effect in South Bay due to long residence times and minimal local freshwater inflows. Given these conditions, using a South Bay data source across the entire domain has not been problematic.

2.5. VALIDATION

Accurately predicting tidal water levels and velocities is fundamental and essential in a system like San Francisco Bay in which tides are the dominant driver of transport and mixing. Given the water quality applications of this model, skill in predicting salinity is perhaps even more important because the salinity field integrates the combined effects of sources, transport and mixing, both in the model and in nature. In this sense, a good validation for salinity is a much stronger indicator than water level or velocity that nutrients and plankton will also be transported correctly. Salinity is also important due to its role as an active driver of flows, where salinity gradients equate to density gradients which in turn drive circulation in marine environments.

The hydrodynamic model is validated against observations of tidal water level, velocity and salinity. Data from NOAA tide gages around the Bay are compared to model outputs for validation of tidal phase and amplitude. Validation of the velocity field draws on a series of short-term Acoustic Doppler Current Profiler (ADCP) moorings deployed by NOAA in 2012–2013. The modeled salinity field is compared to data from USGS cruises along the thalweg of the Bay. The cruises collect vertical profiles of salinity and other constituents at 36 stations, allowing for validation of both the longitudinal salinity field and salt stratification. Several USGS moored salinity sensors are also included which provide a more complete comparison of salinity variation at time scales from hours to weeks.

While in some systems temperature has an effect on transport similar to salinity, density variation in San Francisco Bay is dominated by salinity, leaving temperature with a negligible role. For this reason, temperature is not part of the present model or its validation. For the purpose of water quality modeling, in which process rates can be strongly temperature-dependent, we synthesize a spatially and temporally varying temperature field from observational data. A related modeling effort carried out by Deltares collaborators has included a mechanistic temperature model (Vroom et al., 2017[11]), which may be incorporated into this model in the future.

2.5.1. DEFINITION OF METRICS

In addition to graphical figures comparing modeled and observed quantities, we present several numeric measures of predictive skill, defined below. In these definitions a horizontal line ($\bar{x}$) indicates the arithmetic mean, and a subscript x_i indicates individual samples of the respective dataset.

Skill Model skill is calculated according to the formula proposed by Willmott, 1981[12],

$$SS = 1 - \frac{\sum_i (m_i - o_i)^2}{\sum_i \left(|m_i - \bar{o}| + |o_i - \bar{o}|\right)^2},$$

where o_i denotes samples in the observed data, m_i denotes samples in the model results. A perfect model achieves a skill score of 1. Unlike the correlation coefficient, the skill score takes into account both the correlation and the relative scales of the modeled and observed data.

[11] https://doi.org/10.1002/2016WR020062

[12] https://doi.org/10.1080/02723646.1981.10642213

Bias The average error, $\overline{m_i - o_i}$.

r^2 The squared correlation coefficient, defined as

$$r^2 \equiv \frac{C_{mo}^2}{C_{mm}C_{oo}},$$

where C_{ij} is the covariance matrix computed between the model and observed data. A value of 1.0 indicates perfect correlation or anti-correlation, and a value of 0.0 indicates no correlation between the model and observed data.

RMSE Root mean squared error, $\left(\overline{(m_i - o_i)^2}\right)^{\frac{1}{2}}$.

Lag The time shift, in minutes, between the model time series and the observed time series. A positive values means that the model *lags* the observations, and a negative value means that the model *leads* the observations.

Amplification factor The ratio of standard deviations between the model and the observations. A factor of 1.0 is perfect, while a factor greater than 1 indicates that the signal is amplified in the model, and a factor less than 1 indicates that the signal is attenuated or under-represented.

Threshold values separating success from failure are often difficult to generalize for these metrics. Here we describe some baseline expectations for a successful validation, with the caveat that the details of whether the validation is sufficient is often site and application specific. Water level is the most fundamental, and typically the easiest, quantity to validate, and we expect to have skill and correlation coefficients well above 0.9. Time lags should be much shorter than the period of the tides. Velocity, and specifically velocity magnitude, exhibits much greater small-scale variability than water levels. For this reason, individual ADCP comparisons tend to have larger RMSE and somewhat greater lags than water level comparisons. Where an amplitude error of 10% would be problematic for water levels, this is more often acceptable for velocity comparisons. Skill metrics for salinity at the scale of this model require nuanced interpretation due to the wide range of processes which contribute to salinity distributions. Where possible we include descriptions of specific patterns of errors which can be related to a specific aspect of the model. For the limited number of salinity time series stations, we also present skill metrics.

2.5.2. Water Level

NOAA tide gages record six minute water level data at numerous sites around the perimeter of the Bay. Validation of water levels at tidal time scales is an essential baseline metric for a coastal hydrodynamic model. The most relevant metrics for tidal validation in open areas of the Bay are the amplitude and lag. Tides are amplified and attenuated due to geometry and frictional characteristics of the Bay, a process which is capture by the comparison of amplitudes. The timing or phase of water level is driven by the same characteristics, with friction generally slowing the propagation of the tidal wave, and convergent or enclosed basin geometries causing an apparent acceleration of the tidal wave (a “standing wave”).
The model has been calibrated for tidal phase and amplitude at San Francisco by adjusting tidal conditions at Point Reyes before applying that water level as the ocean boundary condition. Performance within the Bay is quite good, with almost no additional amplification or attenuation aside from Port Chicago. Phase is also well represented at the open Bay sites, with phase leads less than 10 minutes. Phasing at Redwood City is complicated by local, dissipative features and the fact

that the tide gage is sited in a perimeter slough. Phase and amplitude at Port Chicago indicate the limitations of the northern portion of the domain and the lack of a resolved Delta.

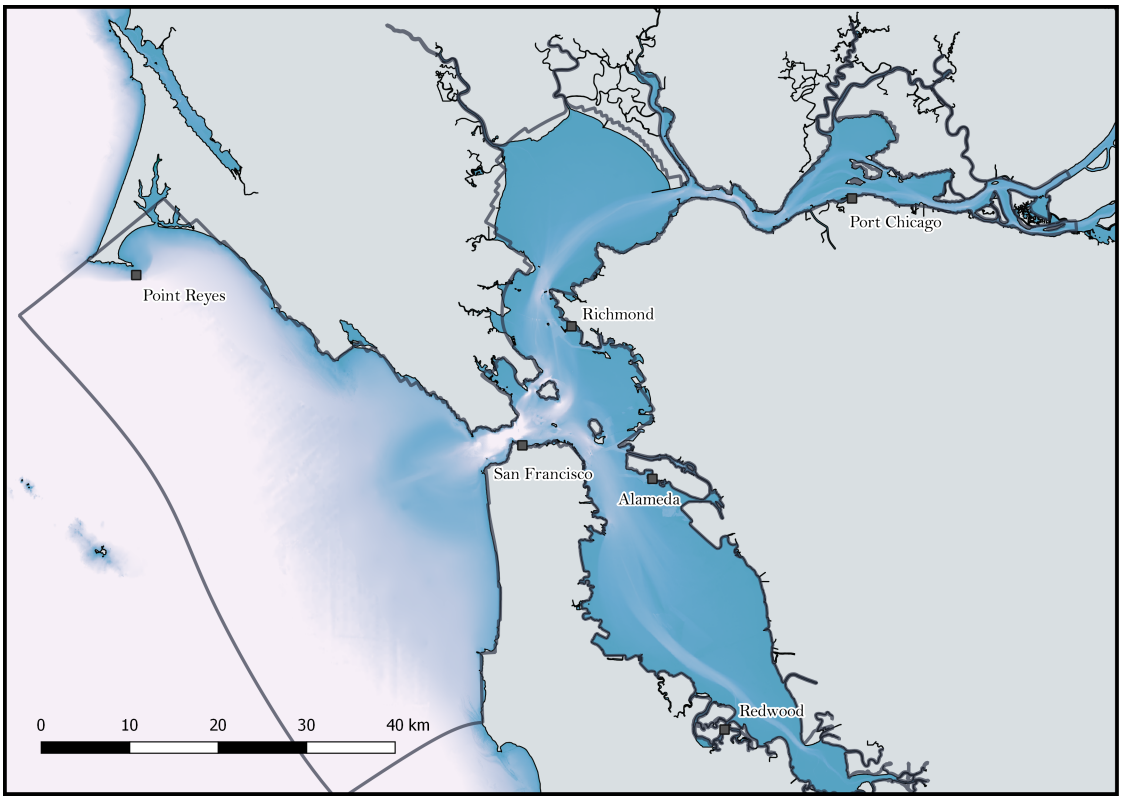

Figure 2.2: Locations of NOAA water level gaging stations

Name	Skill	Bias (m)	r^2	RMSE (m)	Lag (min)	Amp. factor
San Francisco	0.999	-0.010	0.996	0.035	0.1	1.00
Point Reyes	0.993	0.039	0.991	0.085	3.1	0.89
Richmond	0.998	–	0.992	0.055	-5.5	1.04
Alameda	0.997	0.024	0.991	0.068	-8.4	1.04
Redwood City	0.992	–	0.968	0.136	-19.7	1.02
Port Chicago	0.894	0.014	0.864	0.394	-37.7	1.72

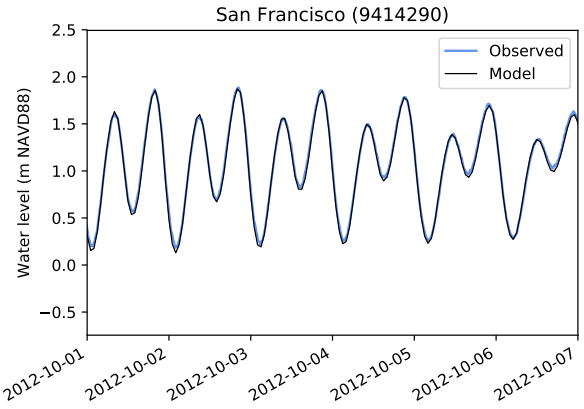

Figure 2.3: Water level comparison at San Francisco

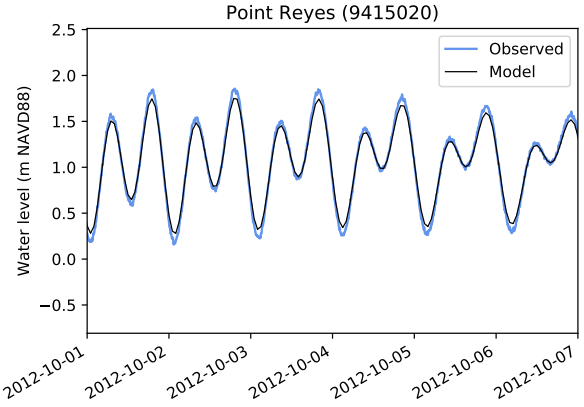

Figure 2.4: Water level comparison at Point Reyes

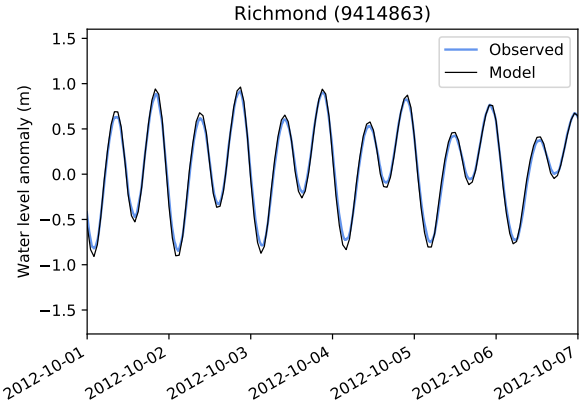

Figure 2.5: Water level comparison at Richmond

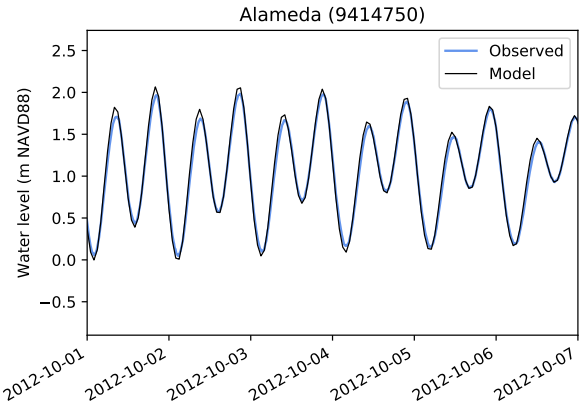

Figure 2.6: Water level comparison at Alameda

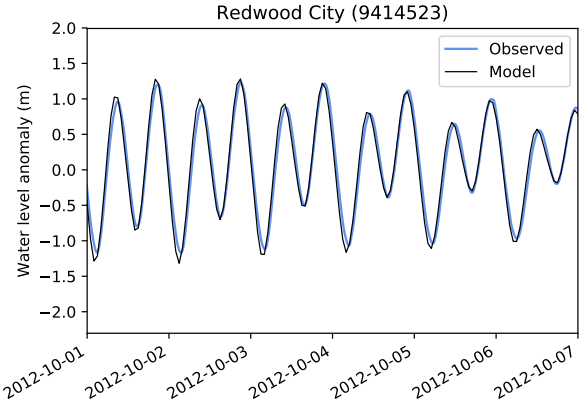

Figure 2.7: Water level comparison at Redwood City

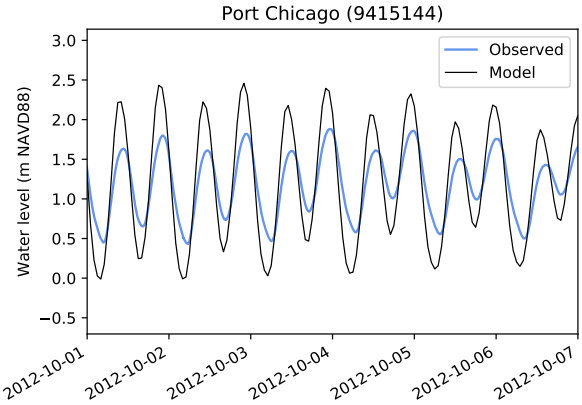

Figure 2.8: Water level comparison at Port Chicago

2.5.3. VELOCITY

Velocity data is taken from a series of NOAA ADCP deployments in 2012 and 2013, compiled from NOAA Tides and Currents[13]. Deployments were primarily in the summers of 2012 and 2013, with each station occupied for 1–3 months. Locations of the ADCP moorings are shown in Fig. 2.9. The unofficial compilation of the observational data used in these comparisons is also available for download[14].

Comparisons of observed and modeled velocities are presented below for the subset of the deployments that overlapped with the time period simulated. All comparisons are based on the depth-averaged observed velocity and the depth-averaged modeled velocity. Since most areas of the Bay experience linear tidal flows along a principal direction of the flow, plots and validation metrics are presented in terms of *principal* and *secondary* velocities, as opposed to east-west velocities and north-south velocities. In this context principal velocity means the velocity along the dominant orientation of the flow at the site, with the convention that positive velocity corresponds to flood-directed flow and negative velocity is ebb-directed flow. Principal velocity directions are calculated independently for each ADCP and each matching model output by maximizing variance along the principal direction. The secondary velocity direction is 90° counter-clockwise to the principal direction. Plots of velocity time series for both the principal and secondary components are truncated to a period of 8 days in order to keep the tidal variation and shape discernible in the plots. In addition to time series plots, model-data comparisons of principal velocity are shown in scatter plots, with the respective principal directions depicted by a pair of arrows inset in the scatter plot. The alignment of the pair of vectors indicates the agreement between observed and modeled current direction. In these scatter plots, a distribution more horizontal than the black 1:1 line indicates over-prediction of velocity, and a more vertical distribution indicates under-prediction. Time lag or lead is indicated by the point distribution tracing out an oval.

In general, we expect an estuarine hydrodynamic model to capture the timing and direction of currents very well, and generally resolve current speeds. Current speed can vary greatly over small distances, and interpreting errors in current speed requires more critical consideration of the specific deployment location as compared to water level comparisons. The emphasis of the validation is on the principal velocity. Secondary velocities are typically very small within the Bay, such that noise and errors which are small relative to the overall current speeds appear as large errors in the secondary velocity. While secondary velocity metrics are still presented, they are generally noisy and of much less concern than the principal velocities.

Timing is largely dictated by the tidal water levels, with bed friction and depth playing secondary roles. Assuming that bathymetry and tidal water levels are accurately modeled, the remaining errors in timing are largely related to friction and tidal prism. Directions of the tidal currents with the Bay are strongly forced by bathymetry, and we expect the model to capture current directions very well as long as the observations are not tucked away in an unresolved portion of the Bay. Currents outside the Bay are subject to a wider range of processes including variable winds and large scale coastal currents. We include comparisons for some of these locations, but with the simplicity of the present model's ocean boundary these comparisons are not expected to be favorable.

[13] https://tidesandcurrents.noaa.gov/cdata/StationList?type=Current+Data&filter=historic&pid=34
[14] https://drive.google.com/open?id=0B9IYEz9K_uS0MTY5TFZOWEtQSEE

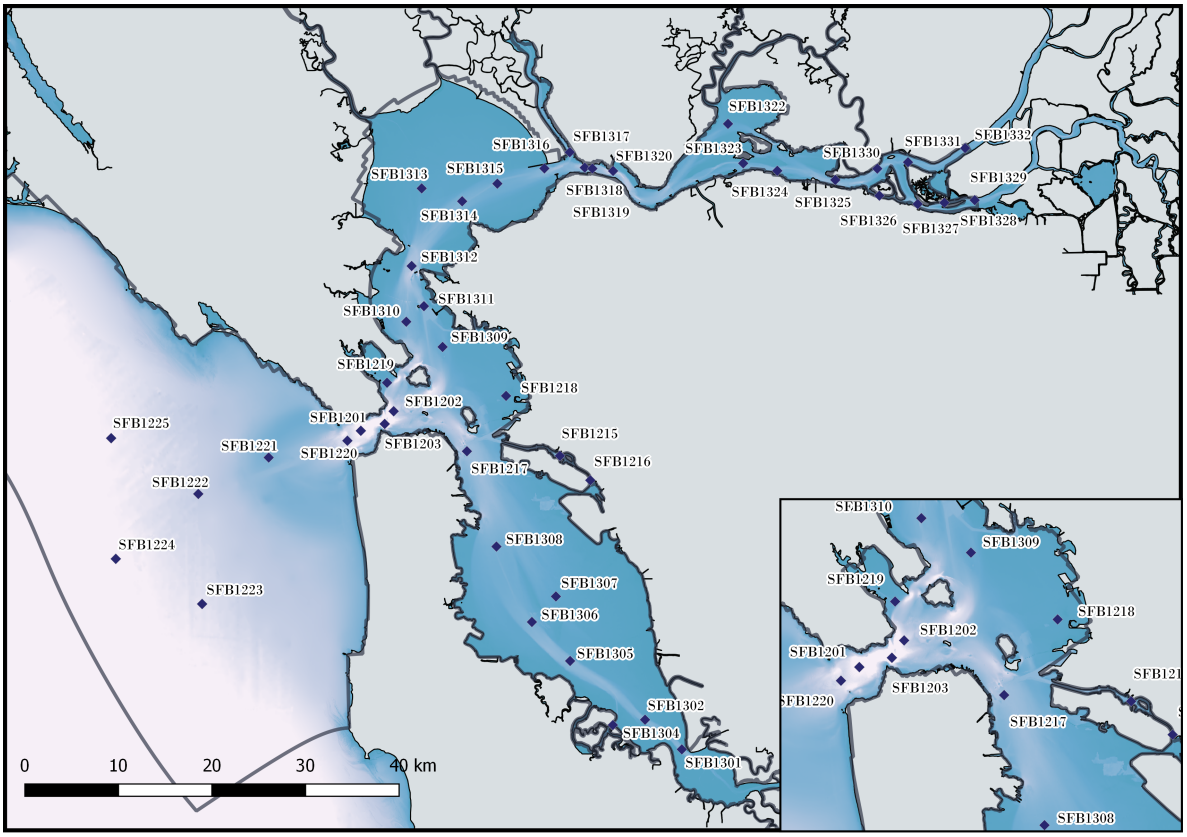

Figure 2.9: NOAA ADCP locations deployed during WY2013

South Bay

Velocity comparisons in South Bay are generally very good. In margin areas such as Redwood Creek the model is underpredicting velocity, likely due to a lack of small scale tidal prism and resolution limits in margin and slough areas. While Hunters Point appears to have a larger error in the principal velocity direction, this error has appeared across multiple models and is most likely linked to compass errors on the instrument rather than model error. The greatest errors are the velocity under-predictions at SFB1302, likely due to the relatively narrow channel mixing with adjacent shoals, and SFB1304 located in an area of under-resolved margins.

	Skill		Bias ($m\ s^{-1}$)		r^2		RMSE ($m\ s^{-1}$)		Lag (min)		Amp. factor	
Name	Pri.	Sec.	Pri.	Sec.	Pri.	Sec.	Pri.	Sec.	Pri.	Sec.	Pri.	Sec.
SFB1301	0.985	0.707	-0.013	-0.005	0.968	0.278	0.118	0.016	-15.60	8.4	0.85	0.99
SFB1302	0.973	0.562	0.050	-0.007	0.967	0.172	0.169	0.019	-14.70	8.5	0.77	0.49
SFB1304	0.920	0.520	-0.008	0.006	0.942	0.201	0.138	0.012	-20.85	9.0	0.59	0.34
SFB1305	0.984	0.447	0.055	0.065	0.959	0.085	0.126	0.077	-16.27	8.8	0.90	0.22
SFB1306	0.982	0.381	0.089	0.005	0.967	0.026	0.123	0.019	-16.50	8.1	0.95	0.32
SFB1307	0.984	0.488	-0.017	-0.021	0.942	0.066	0.083	0.037	-25.72	7.7	0.95	0.62
SFB1308	0.994	0.625	0.017	-0.005	0.989	0.226	0.075	0.022	1.27	8.7	1.11	0.56

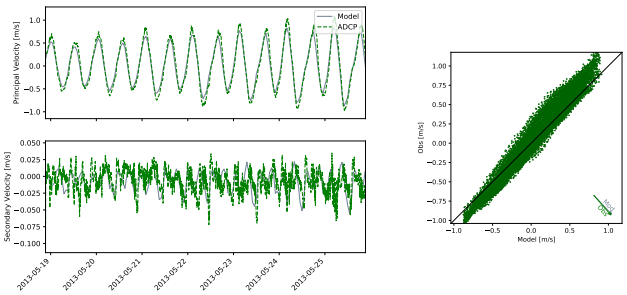

Figure 2.10: SFB1301 Dumbarton Bridge

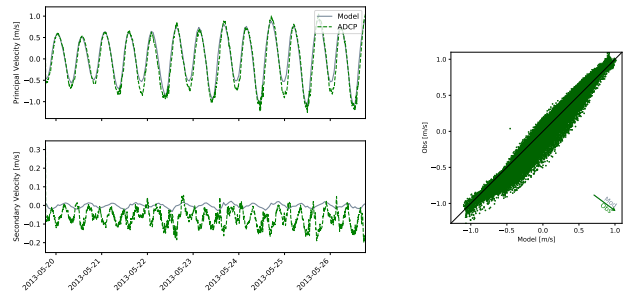

Figure 2.11: SFB1305 San Mateo Bridge

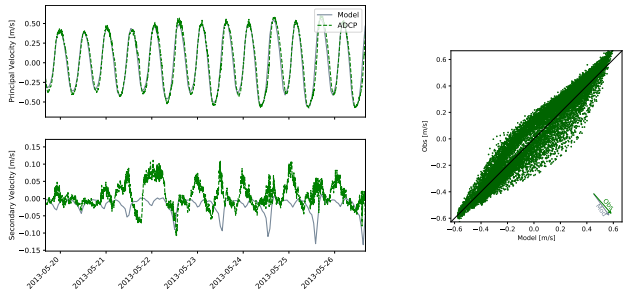

Figure 2.12: SFB1307 Mulford Gardens Channel Approach

Additional figures in Appendix A.

Central Bay

Central Bay is a particularly complex region for modeling hydrodynamics due to the high velocities, complex bathymetry, and its position at the junction of the two arms of San Francisco Bay. While velocities at Golden Gate are slightly over-represented, given the complexities of Central Bay the result here and at most open-water sites in the region is reasonably good. Previous models have shown a strong bias between tidal phases in this area, with the flood-tide jet under-represented due to horizontal numerical diffusion. The structured, flow-aligned grid in this region is effective at reducing that effect. Margin areas like Brooklyn Basin, which are non-energetic and driven primarily by secondary flows, are a weak point of the validation in Central Bay. Similarly, Richardson Bay is an area of interest for future water quality modeling, but is poorly resolved in the present model. The complicated character of the observed velocities, including periods of near-constant velocity, suggests that spatially variable frictional control is important here. This

terminal sub-basin may also be subject to wind-driven flows which are unlikely to be resolved by the model due to the low resolution of the atmospheric forcing.

	Skill		Bias ($m\ s^{-1}$)		r^2		RMSE ($m\ s^{-1}$)		Lag (min)		Amp. factor	
Name	Pri.	Sec.	Pri.	Sec.	Pri.	Sec.	Pri.	Sec.	Pri.	Sec.	Pri.	Sec.
SFB1202	0.989	0.408	-0.021	-0.021	0.968	0.005	0.160	0.086	-12.88	-15.5	1.12	0.84
SFB1215	0.948	0.226	0.003	0.005	0.881	0.001	0.041	0.018	-33.00	6.0	0.75	0.10
SFB1216	0.951	0.252	-0.028	0.001	0.933	0.005	0.144	0.009	-22.27	9.6	0.70	0.22
SFB1217	0.992	0.337	-0.020	0.002	0.968	0.002	0.121	0.037	-14.47	6.0	1.00	0.58
SFB1218	0.875	0.576	-0.022	0.015	0.902	0.175	0.050	0.032	-15.07	7.6	0.56	0.55
SFB1219	0.884	0.808	-0.009	0.004	0.679	0.532	0.135	0.062	7.27	8.4	1.36	0.65
SFB1309	0.980	0.873	0.013	-0.033	0.936	0.682	0.150	0.084	-20.40	-20.7	1.12	1.31
SFB1310	0.959	0.689	0.039	0.006	0.904	0.250	0.260	0.039	-31.42	7.6	1.29	0.83
SFB1311	0.982	0.412	-0.007	0.044	0.930	0.004	0.169	0.070	-22.20	6.1	1.03	0.48
SFB1312	0.963	0.388	-0.077	-0.014	0.911	0.007	0.343	0.041	-28.57	7.0	1.24	0.41

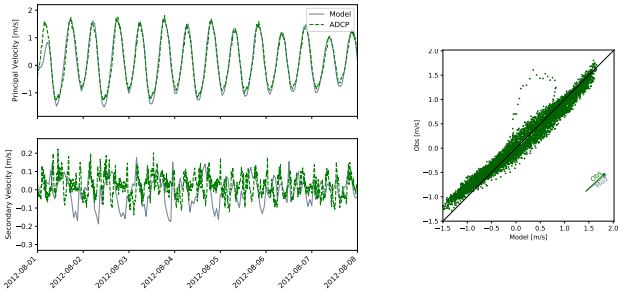

Figure 2.13: SFB1202 Golden Gate Bridge

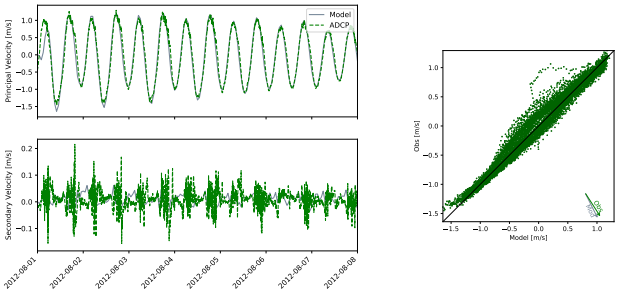

Figure 2.14: SFB1217 Rincon Point

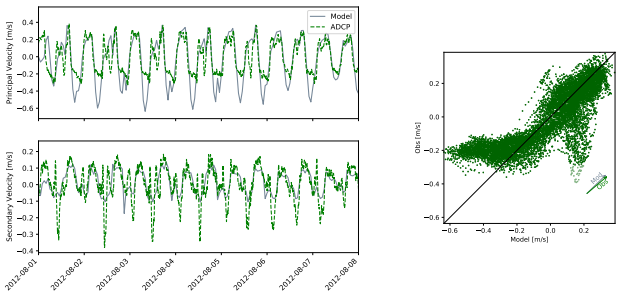

Figure 2.15: SFB1219 Richardson Bay

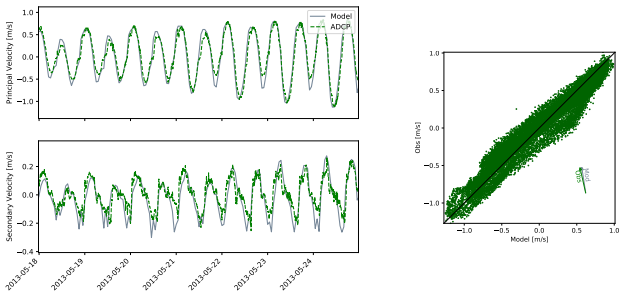

Figure 2.16: SFB1309 Point Chauncey, 1.3 nm E of.

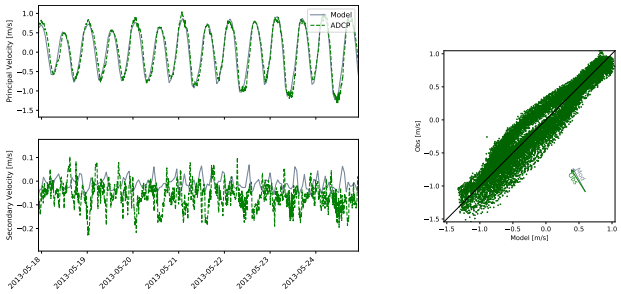

Figure 2.17: SFB1311 Red Rock, 0.2 nm E of.

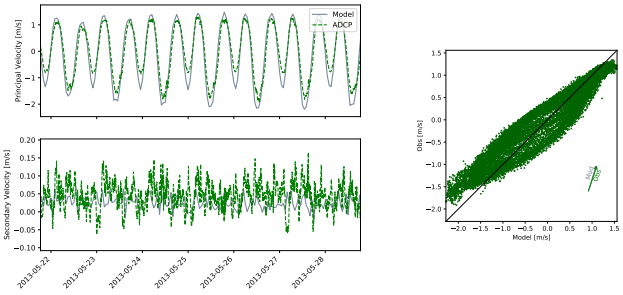

Figure 2.18: SFB1312 Point San Pablo, Midchannel

Additional figures in Appendix A.

COASTAL

Where station SFB1202, just inside the Golden Gate, has a small bias in overpredicting ebb, its mirror station SFB1201, just outside the Gate, has a similar bias in overpredicting floods. As opposed to the expected bias low on ebbs (i.e. an under-resolved ebb-tide jet), the error is an over-predicted flood tide. This may be related to details of the grid in this region, or may be the combined effects of an under-resolved ebb-tide jet and an overall bias high. The drivers of this bias are not entirely clear, as the comparison at the next station out, SFB1220, are quite good and presumably still sampling the ebb-tide jet. Points beyond the SF Bar are included for completeness, but are not expected to validate given the simplicity of the ocean boundary condition.

	Skill		Bias ($m\ s^{-1}$)		r^2		RMSE ($m\ s^{-1}$)		Lag (min)		Amp. factor	
Name	Pri.	Sec.	Pri.	Sec.	Pri.	Sec.	Pri.	Sec.	Pri.	Sec.	Pri.	Sec.
SFB1201	0.977	0.492	0.062	-0.044	0.947	0.046	0.253	0.121	-14.63	13.1	1.19	1.37
SFB1220	0.994	0.801	-0.007	-0.024	0.977	0.461	0.118	0.076	-8.77	8.9	0.96	1.20
SFB1221	0.981	0.647	0.007	-0.038	0.963	0.179	0.104	0.109	-8.62	-20.5	1.22	1.07
SFB1222	0.845	0.398	-0.041	-0.065	0.594	0.010	0.084	0.105	-19.95	56.6	1.03	1.37
SFB1223	0.654	0.367	-0.021	0.004	0.203	0.001	0.097	0.059	-68.77	44.6	0.73	1.55

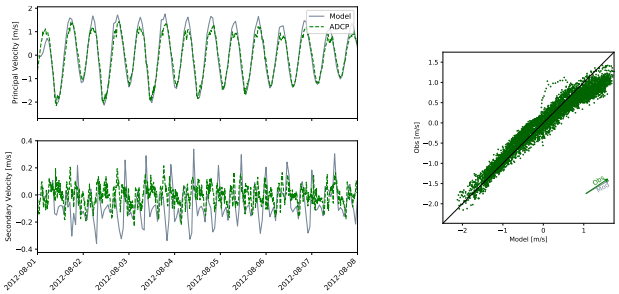

Figure 2.19: SFB1201 San Francisco Bay Entrance

Additional figures in Appendix A.

NORTH BAY

The North Bay velocity comparisons are dominated by significant phase errors (the model leads the observations) and over-predicted amplitudes. The truncated Delta of this model is likely at the center of this discrepancy, as it does not adequately dampen the landward propagating tide. The tide is then free to reflect seaward, leading to overpredicted water levels near the boundary, and overpredicted velocities farther from the boundary. The phase lead of the velocity further supports this interpretation.

	Skill		Bias ($m\ s^{-1}$)		r^2		RMSE ($m\ s^{-1}$)		Lag (min)		Amp. factor	
Name	Pri.	Sec.	Pri.	Sec.	Pri.	Sec.	Pri.	Sec.	Pri.	Sec.	Pri.	Sec.
SFB1313	0.958	0.559	-0.013	-0.016	0.881	0.109	0.161	0.040	-33.97	7.2	1.23	0.76
SFB1314	0.943	0.712	0.003	-0.009	0.877	0.376	0.342	0.027	-38.25	8.0	1.37	0.61
SFB1315	0.916	0.526	0.025	0.000	0.816	0.094	0.367	0.030	6.04	8.7	1.46	0.60
SFB1316	0.905	0.376	0.024	-0.026	0.708	0.026	0.400	0.044	-67.57	6.0	1.23	0.47
SFB1317	0.244	0.407	0.023	-0.019	0.700	0.004	0.642	0.040	34.57	-98.8	0.08	0.49
SFB1318	0.871	0.371	0.048	-0.004	0.586	0.064	0.514	0.043	-81.30	9.1	1.05	0.32
SFB1319	0.849	0.428	-0.014	-0.074	0.528	0.004	0.639	0.115	-87.52	-74.5	1.05	0.30
SFB1320	0.813	0.321	0.049	-0.010	0.535	0.000	0.423	0.061	-81.45	-75.1	1.48	0.37
SFB1322	0.774	0.540	0.020	-0.035	0.361	0.199	0.291	0.106	-105.00	-116.8	1.09	0.42
SFB1323	0.883	0.335	0.008	0.006	0.616	0.004	0.330	0.027	-75.60	87.1	0.92	0.54
SFB1324	0.873	0.534	-0.024	0.003	0.633	0.206	0.323	0.034	-74.25	6.5	0.77	0.40
SFB1325	0.846	0.148	-0.005	-0.001	0.801	0.089	0.373	0.026	-46.05	6.0	0.52	0.40
SFB1326	0.872	0.255	0.051	0.001	0.901	0.014	0.294	0.016	-14.85	7.9	0.52	0.22
SFB1327	0.922	0.372	0.011	-0.008	0.947	0.000	0.243	0.019	20.10	6.0	0.59	0.57
SFB1328	0.895	0.351	0.048	-0.008	0.959	0.001	0.247	0.019	21.07	6.0	0.54	0.09
SFB1329	0.939	0.409	-0.060	-0.006	0.878	0.008	0.193	0.020	33.45	9.7	0.74	0.70
SFB1330	0.804	0.319	0.001	-0.009	0.847	0.049	0.333	0.030	-32.17	9.0	0.43	0.17
SFB1331	0.821	0.494	0.007	0.003	0.839	0.026	0.298	0.021	-33.30	9.5	0.46	1.27
SFB1332	0.943	0.296	-0.016	-0.003	0.969	0.013	0.156	0.011	16.35	8.9	0.64	0.27

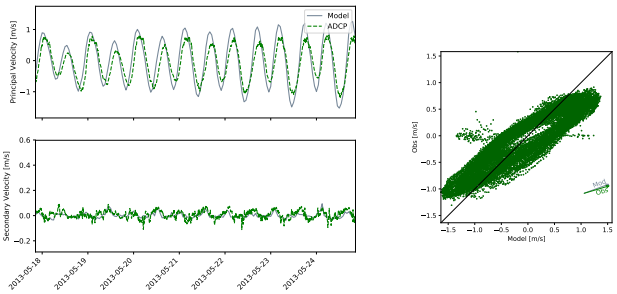

Figure 2.20: SFB1315 Pinole Shoal

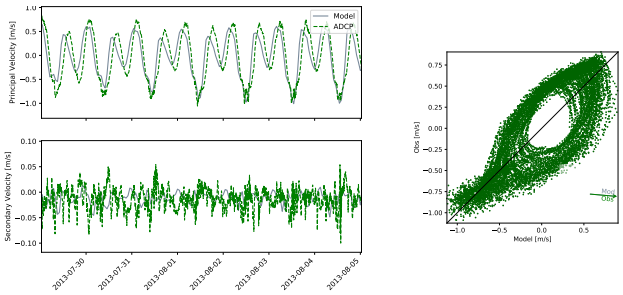

Figure 2.21: SFB1323 Roe Island Channel

Additional figures in Appendix A.

2.5.4. Salinity

Accurately predicting salinity is important both as a diagnostic for transport and as a driver for hydrodynamic circulation. We compare the model's output to two USGS data sources: periodic

transects along the thalweg of the Bay and four moored sensors providing continuous, 15-minute data.

Transects

The USGS completes a cruise along the transect of the Bay on a monthly to bimonthly basis taking water property measurements at 36 stations (Fig. 2.22). We validate our modeled salinity field against these monthly cruises, comparing both depth-averaged salinity and estimated stratification. Although some USGS cruises cover only the South Bay, we include plots of model output for the full Bay in all cases for consistency and context. Depth-averaged salinity in both the model output and observations is calculated as a simple mean of the samples within each vertical profile. Stratification is calculated within each profile as

$$\frac{\partial s}{\partial z} \approx \frac{s_{max} - s_{min}}{/} z_{max} - z_{min},$$

essentially enforcing stable or neutral stratification. Transects are plotted south to north, with Lower South Bay on the left and the Sacramento River on the right. Thin black lines denote 5 ppt contours, with more subtle color shifts at 1 ppt intervals. The vertical dimension from the model output has been adjusted to depth below the surface. There is some variation of the profile of the bed elevation between the observations and the model due to differences in the exact location of the observations, and bathymetric details which are not resolved in the model.

In general the model performs well, with a good representation of the stratification and shape of the longitudinal salinity profile. There is a persistent bias low during low-flow periods. The causes of this bias are being investigated, and likely related to a combination of evaporation, Delta boundary condition, and insufficient flushing in the coastal ocean.

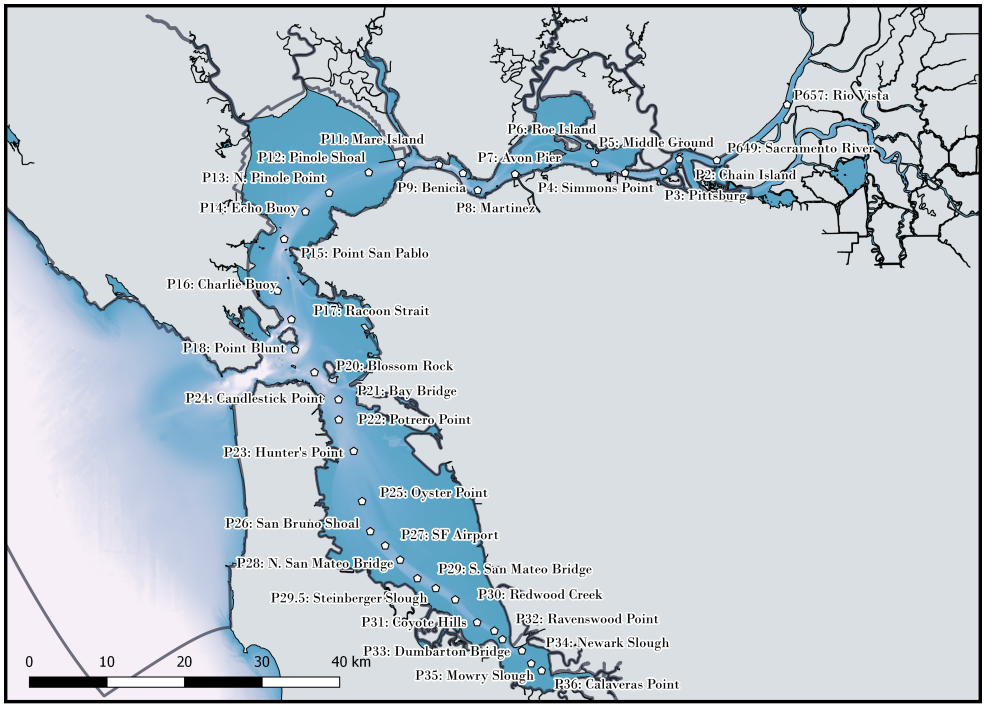

Figure 2.22: Locations of USGS stations during transect cruises

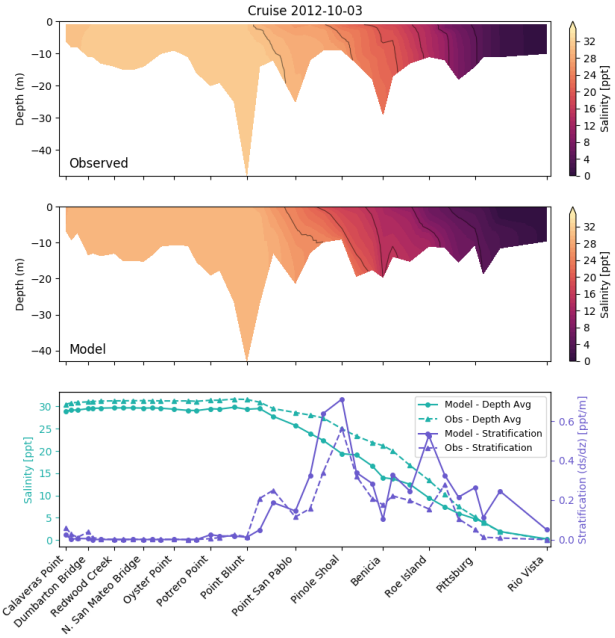

Figure 2.23: USGS Transect, 2012-10-03

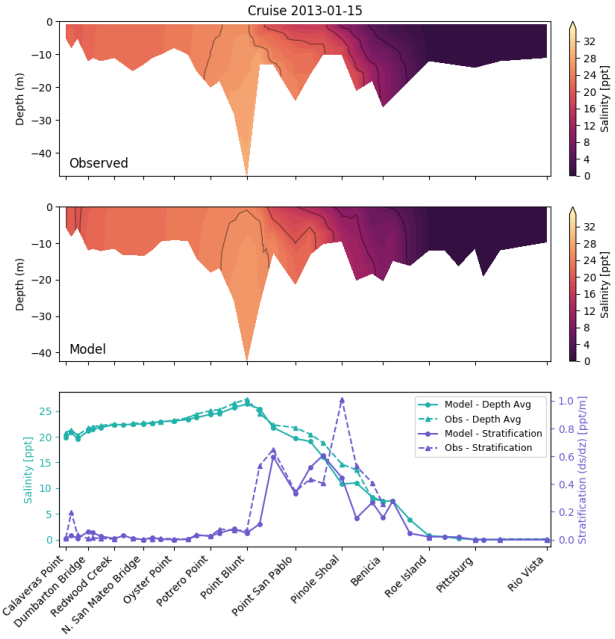

Figure 2.24: USGS Transect, 2013-01-15

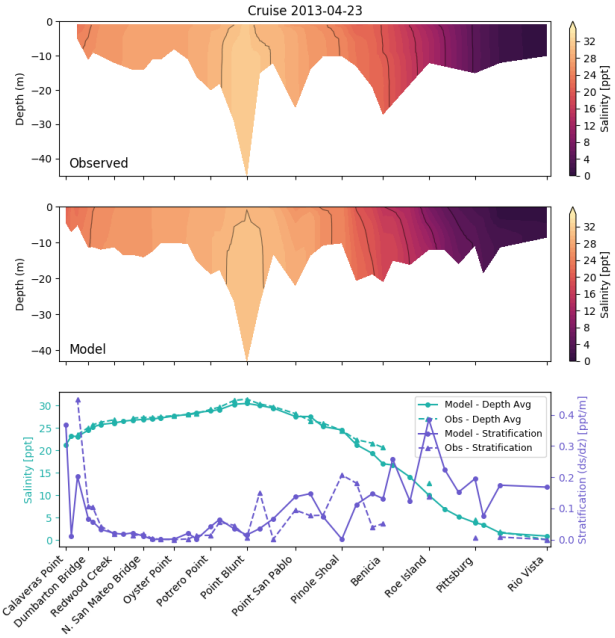

Figure 2.25: USGS Transect, 2013-04-23

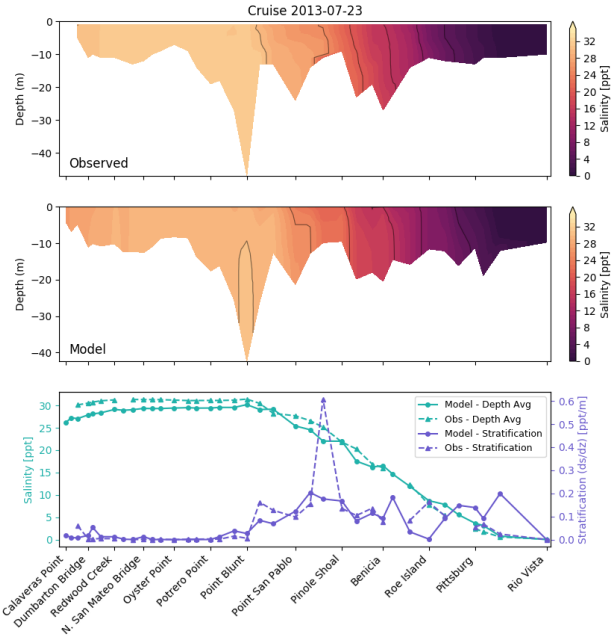

Figure 2.26: USGS Transect, 2013-07-23

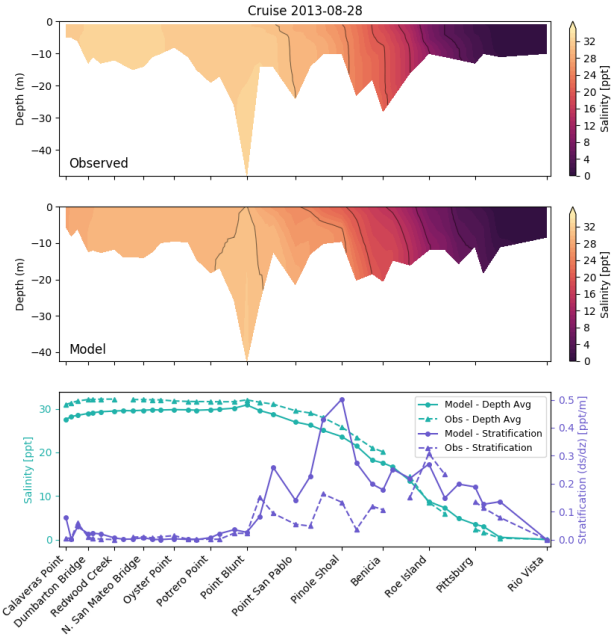

Figure 2.27: USGS Transect, 2013-08-28

Additional figures in Appendix A.

In addition to the transect data shown in the previous section, USGS maintains a limited number of mooring sites within the Bay. Four of these sites have salinity data overlapping the simulation period, and model-data comparisons for these are included below. While many of the large-scale patterns of salinity in the Bay can be extracted from the monthly transect data, high-frequency measurements allow for more rigorous skill metrics, and analysis of daily and spring-neap time scales. Sites at the Richmond-San Rafael Bridge and the San Mateo Bridge consist of sensors at two fixed elevations. Alcatraz and Alviso each have a single sensor. Error metrics are calculated for the depth-averaged salinity. Skill and bias are reasonable for the open-Bay sites, with errors on the order of 2 ppt largely due to the previously mentioned bias low. Alviso Slough has been included for completeness, though its location in the margins is unlikely to validate well given the coarse representation of this region in the present model. A related modeling effort in the Nutrient Management Strategy is developing a hydrodynamic model focused on small scale features in Lower South Bay.

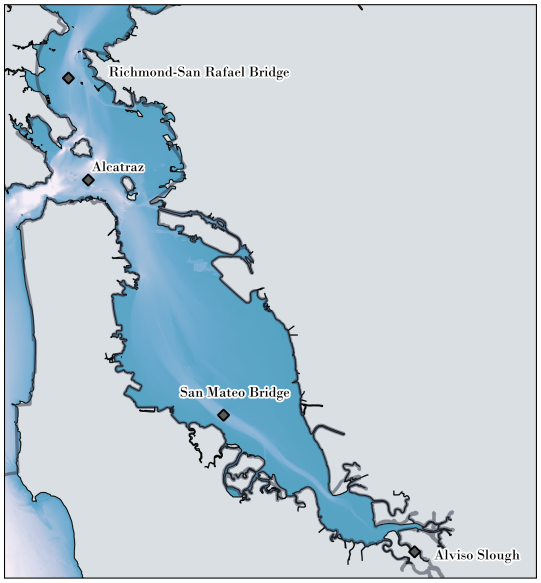

Figure 2.28: Location of USGS moorings used for salinity time series comparison.

Name	Skill	Bias (ppt)	r^2	RMSE (ppt)
San Mateo Bridge	0.956	-0.50	0.972	1.06
Alcatraz	0.879	-0.88	0.925	1.43
Richmond Bridge	0.889	-1.53	0.924	1.89
Alviso Slough	0.556	8.88	0.598	10.35

Individual time series are shown below. For each site, salinity is extracted from the model at elevations matching the sensor(s) for that site. The upper panel in each of the figures below shows the average salinity (average of top and bottom sensors where available) with a 40 h low-pass filter (Hanning FIR). The shaded regions around the lines show the salinity range, as an approximation for tidal variability.

The lower figure shows an estimate of stratification. For sites with two sensors, stratification is calculated as the gradient between the two sensor elevations. For sites with a single sensor, stratification cannot be inferred from the observations, and the modeled stratification is extracted across the full water column.

Though the model output is not expected to validate well in the spinup period before October 1, 2012, these figures include that period to help evaluate the duration of the spinup period and potential drivers of dry-weather salinity bias.

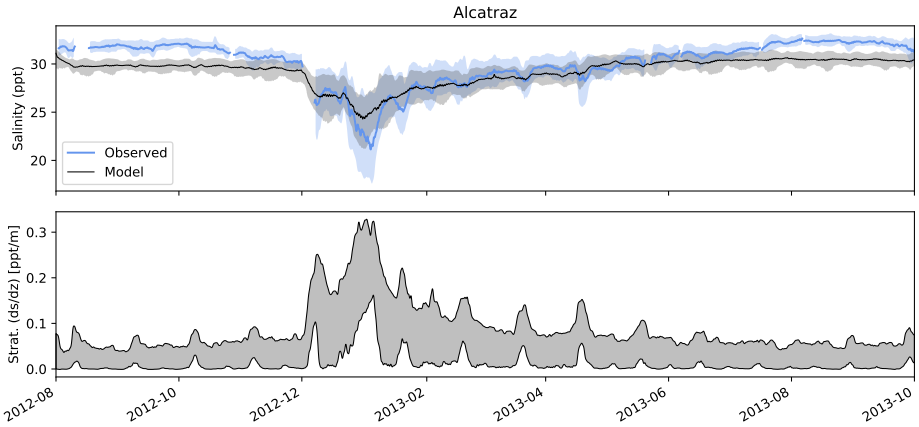

Figure 2.29: Salinity time series: Alcatraz, USGS 374938122251801

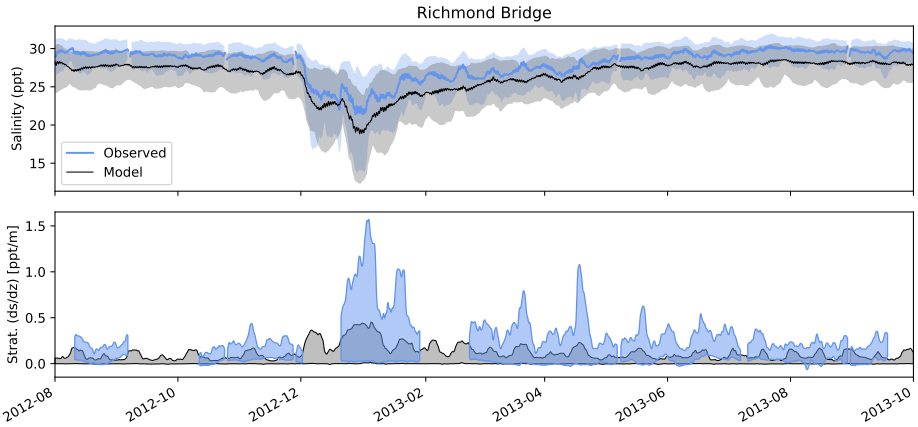

Figure 2.30: Salinity time series: Richmond / San Rafael Bridge, USGS 375607122264701

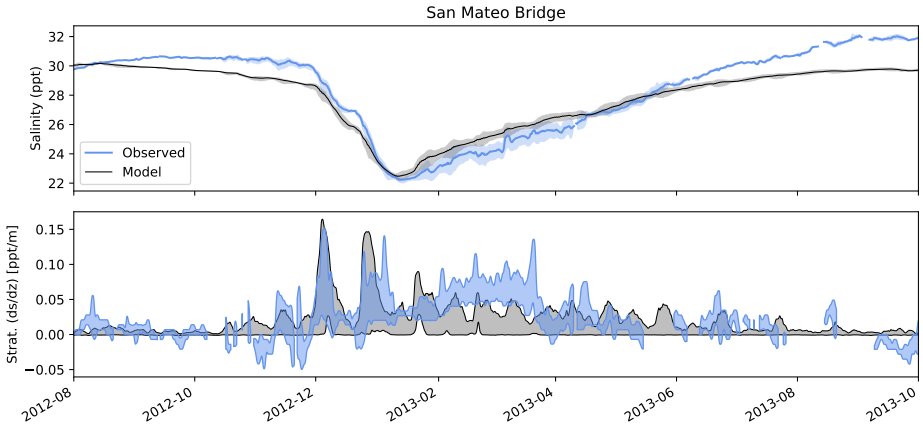

Figure 2.31: Salinity time series: San Mateo Bridge, USGS 11162765

Additional figures in Appendix A.

2.6. Next Steps

The above model-data comparisons show that the model does well resolving the important transport processes in South Bay, and adequately resolves mixing and transport in Central Bay and San Pablo Bay. At the same time, the comparisons point to several potential improvements which will be tested and incorporated in the future.

Refine the forcing of the open ocean boundary The closed boundaries on the north and south sides of the coastal portion of the domain appear to decrease flushing of the San Francisco Bight, leading to too much retention of fresh water in Central Bay. We anticipate that allowing fluxes through these boundaries would improve salinity validation. Some experimentation is needed to determine the exact type of boundary condition to impose, as instabilities may arise when an open boundary is close to a high-gradient location like Point Reyes.

Delta Inflows Boundary conditions at the Delta currently come from a pair of high frequency velocity gaging stations. In the existing configuration these flows enter with zero salinity, but in particularly dry conditions flows here may have significant salinity. This discrepancy would lead to a non-physical loss of salt. Forcing with time-varying salinity or imposing this boundary farther upstream would avoid this issue.
The Delta flows are also incomplete, and should be extended to include Dutch Slough and Threemile Slough. These channels carry much smaller fluxes than the Sacramento and San Joaquin Rivers, but given the importance of Delta flows overall, even these secondary inputs could be significant to downstream conditions.
The poor tidal phasing in the current model is also a point of potential improvement. This may be remedied to some extent by including the two additional flows mentioned above. To make more significant gains may require either a schematized Delta (e.g. a pair of dissipative channels mimicking the effects of the true Delta), or a Riemann boundary condition which would allow excess tidal energy to propagate out of the domain.

Evaporation Direct precipitation and evaporation are currently included in the model as time-varying but spatially constant quantities. Evaporation is under-represented due to stability issues in earlier iterations of the model. This factor will be relaxed in future runs, which we expect to cause an increase in modeled summer salinities in South Bay. Spatially-varying precipitation and evaporation would be more realistic, although this enhancement is not expected to make a large difference in the modeled salinities.

3. Biogeochemical Model

3.1. Introduction

Nutrient concentrations throughout San Francisco Bay (SFB) are elevated relative to natural conditions (Cloern and Jassby 2012[15]; SFEI 2014a[16]). Nutrient sources include wastewater treatment plants (WWTPs) that discharge directly to SFB or Bay Area watersheds ($50,000\ kg\ N\ d^{-1}$), seasonally varying inputs from the upstream Delta ($5,000 - 50,000\ kg\ N\ d^{-1}$) (SFEI 2014b[17]), and stormwater runoff. SFB has been considered resistant to the impacts of classic eutrophication observed in other nutrient-enriched estuaries (Cloern and Jassby 2012[1]; SFEI 2014[2]), with that resistance attributed to limited light availability to phytoplankton, caused by high suspended sediment concentrations that diminish light penetration into the water column and strong tidal mixing that allows for only short periods of vertical stratification in the water column; and strong benthic grazing pressure (Cloern and Jassby 2012[1]; SFEI 2014[2]). Recent increases in phytoplankton biomass (Cloern et al. 2007[18], Cloern et al. 2010[19]) have raised concerns that SFB's resistance to elevated nutrients may be changing.
In 2012, to begin addressing these concerns, regulators and stakeholders launched the SFB Nutrient Management Strategy, an applied science program aimed at building the scientific foundation to inform major nutrient management decisions. Through a combination of monitoring, field investigations, and numerical modeling, the NMS science program targets two overarching management questions:

1. What nutrient loads can SFB (subembayments) assimilate without adverse impacts?
2. What management actions would be effective at achieving protective nutrient loads or concentrations?

This report summarizes the progress on the development and application of coupled biogeochemical - hydrodynamic models for SFB, which aim to mechanistically model the fate of nutrients, the influence of those nutrients on phytoplankton dynamics, and dissolved oxygen concentrations. This report describes: the basic structure of the current model, including major processes, parameterizations, and model inputs; current model performance; and plans for future work.

3.2. Model Structure

To model SFB water quality, we use a hydrodynamic model to simulate physical transport (Fig. 2.28) and a biogeochemical model to simulate concentrations and transformations of constituents in the water. Hydrodynamics are simulated using the D-Flow Flexible Mesh (DFM) model, a three-dimensional, finite-volume, unstructured hydrodynamic model. A detailed description of the hydrodynamic model and its validation can be found in Section 2 of this report. Output from the DFM model serves as input to the biogeochemical model, D-Water Quality (D-WAQ), which simulates nutrient cycling and phytoplankton-zooplankton dynamics, while subject to realistic hydrodynamic conditions. D-WAQ is coupled to DFM offline, meaning, the hydrodynamic model is

[15] https://doi.org/10.1029/2012RG000397
[16] http://sfbaynutrients.sfei.org/sites/default/files/SFBNutrientConceptualModel_Draft_Final_Oct2014.pdf
[17] http://sfbaynutrients.sfei.org/sites/default/files/NutrientLoadsFINAL_FINAL_Jan232014.pdf
[18] https://doi.org/10.1073/pnas.0706151104
[19] https://doi.org/10.1007/s12237-009-9195-3

run for the entire period of interest and then the DFM output is used as an input into the D-WAQ model. In the following sections, the biogeochemical processes included in the model and the data needed for model input are discussed in further detail.

3.2.1. Nutrient Cycling

The D-WAQ model simulates multiple nutrient cycling processes and computes concentrations of relevant water quality parameters (or state variables) as a function of space and time (Fig. 3.1). In the water column, both nitrification and denitrification contribute to nitrogen transformations. Nitrification is the oxidation of ammonium (NH_4^+) to nitrate (NO_3^-) which is carried out by specialized bacteria and archaea. As an autotrophic process (produces energy), nitrification requires oxic conditions, whereas denitrification is a heterotrophic process and requires anoxic conditions. Typically, denitrification is carried out by facultative anaerobes, in which bioavailable nitrate (NO_3^-) is converted to nitrogen gas (N_2) through a multistep process and released to the atmosphere. Denitrification is dependent on both the presence of NO_3^- and an organic carbon source, e.g., organic matter from prior phytoplankton production within the system or organic matter produced elsewhere and transported into the system by tributaries. In SFB, where the water column is generally oxygen-rich, because of the anoxic requirement, the majority of denitrification is expected to occur in surficial layers of bed sediments; however, some denitrification may also occur within anoxic microzones associated with suspended particulate matter in the water column. The model simulates transformations in the water column and in the bed sediments, as well as constituent fluxes between the water and bed sediment. The sediment diagenesis model includes two layers: the first (S1) is the oxic or aerobic layer of the sediment, and the second (S2) is the anoxic or anaerobic layer of the sediment. The sediment layers are divided this way because oxygen regulates most processes simulated by the model in the sediment. Nitrogen cycling processes are divided between sediment layers as they are sensitive to the presence of oxygen, with nitrification only included in S1, and denitrification in S2. Bioturbation (vertical mixing of sediment layers by benthic organisms) is included in the sediment diagenesis model as it causes the dispersion and transport of dissolved substances across the sediment-water interface. Other important processes include the settling and resuspension of detrital material (from algal predation, algal and zooplankton metabolism, and external inputs), mineralization of organic matter, fluxes of nutrients from the sediment and sediment oxygen demand.

3.2.2. Primary Production and Biomass

Primary production in the model is represented through the growth and mortality of phytoplankton. In general, phytoplankton growth rates vary as a function of nutrient concentrations, light availability, and temperature. Phytoplankton take up nutrients based on their physiological requirements for photosynthesis; and in SFB, light availability typically determines the rate of photosynthesis; however, under some conditions, nutrient concentrations can decrease to low enough levels that they limit (or co-limit) phytoplankton growth rates.
Phytoplankton biomass represents the balance of production and loss processes. Simulated phytoplankton loss processes include: death via natural mortality, settling, transport/export from a grid cell, and grazing by primary consumers. After phytoplankton die, D-WAQ simulates their gradual remineralization, both in the water column and within the sediment layers (after settling), including recycling of nutrients and consumption of oxidants (e.g., oxygen, nitrate).

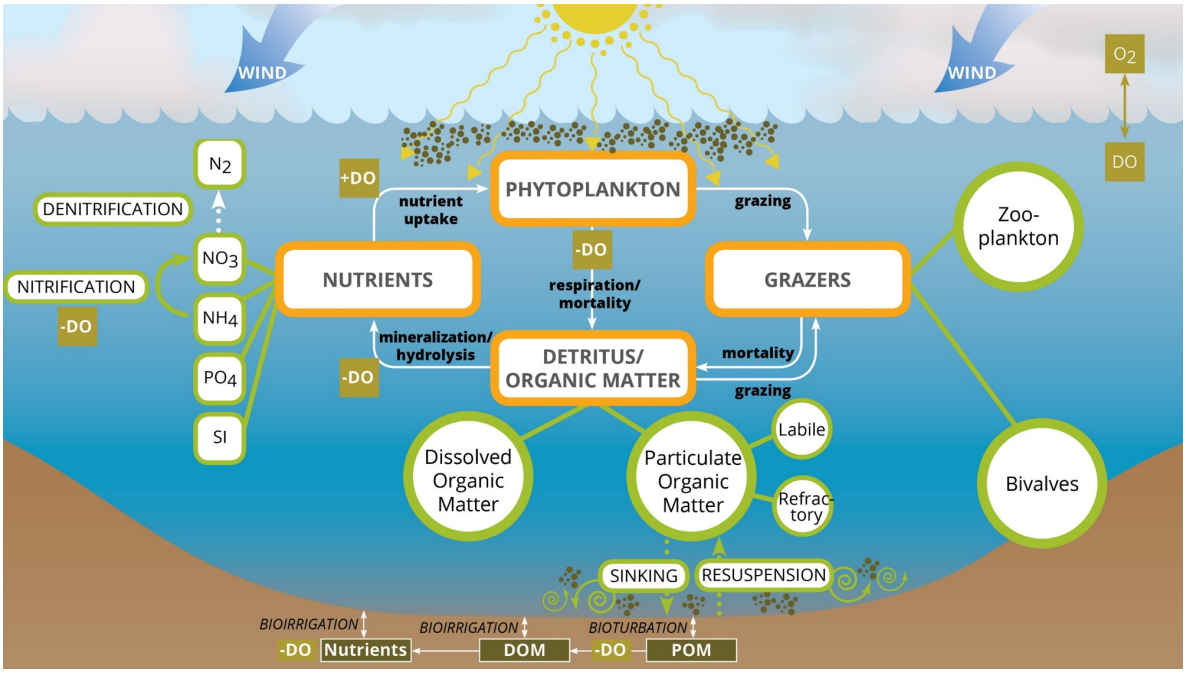

Figure 3.1: Diagram of the biogeochemical processes included in D-WAQ.

3.2.3. Grazers

D-WAQ offers multiple options for simulating grazing. Grazing can occur in the water column by zooplankton or at the sediment-water interface by benthic grazers. In both cases, grazing can be incorporated into the model by specifying grazing rates (constant or time-varying) and by simulating grazer abundance. In the current model, we are simulating grazer abundance and grazing rates through a dynamic energy budget (DEB) model. Using this approach, the energy needed by an individual organism changes throughout its life cycle. Food ingestion is proportional to the organism size and scales up or down as the biomass changes. As food is ingested, a proportion is ejected as feces, but the rest is assimilated into the organism and has three fates: energy storage or reserve, biovolume, and reproduction. For computational reasons, these divisions of energy are not tracked for each individual, but instead are tracked for the community. Both passive and active mortality are applied to the grazers as well. The current SFB simulations, in general, utilize D-WAQ's DEB approach, but incorporate a minor modification to grazer behavior under low phytoplankton biomass conditions.

3.2.4. Other Required Data or Forcings

The DFM and D-WAQ models require a range of forcing data to simulate realistic conditions. A detailed description of the physical forcing data and model setup for DFM can be found in Section 2.4 of this report. Biogeochemical forcing data input to the D-WAQ model are discussed below.

Nutrient Sources

The current biogeochemical model includes multiple time-varying freshwater flows and nutrient loads to SFB, entering at discrete locations, including (Fig. 2.28): WWTP (and refinery) effluent discharges; stream/creek flows exiting Bay Area watersheds; and contributions from the Delta. These flows are prescribed as external forcings, and provided during model setup. The relevant

datasets were developed prior to model runs using observational data or, in some cases, output from other models (hydrological model for river/creek flowrates). Developing the datasets typically involved several steps: acquiring observational original dataset; QA/QC; addressing data gaps through basic interpolation or statistically-based approaches to account for seasonality and long-term trends; converting to daily data (e.g., from monthly).
Of the major nutrient sources, the Bay Area's 37 WWTPs account for the majority of nutrient loads on an annual-average basis. As part of model development, we built a daily time step dataset for the 37 WWTPs and 5 refineries extending from 2000-2017 (available via ERD-DAP[20] and github[21]) (see Appendix B for details). Since July 2012, all WWTPs have been conducting biweekly or monthly effluent monitoring for a fairly complete set of nutrient analytes; therefore, beyond some limited QA/QC, calculating daily flow and load estimates for 2012-2017 was fairly straightforward, and the values are known with a high degree of confidence. For 2000-June 2012, available data varied greatly by WWTP in terms of completeness (e.g., analytes, frequency, duration). For this time period, missing analyte concentrations were estimated based on the assumptions described in SFEI (2014b)[22], and temporal gaps were addressed by accounting for seasonal variations and long-term trends. Refinery data were handled similarly to WWTPs data. Flow and nutrient loads from the WWTPs and refineries are released into the deepest grid cell at the approximate latitude and longitude of the discharge site. Flow and nutrient concentration data from the Delta were compiled for 2000-2017, converted to daily values, and applied at the domain's northeastern boundary. Temporal gaps in concentration/load data were filled through accounting for inter-annual trends and seasonality based on long-term data records, following an approach similar to Novick et al, (2015)[23]. Lastly, freshwater flows from 20 smaller streams are included in the model as stormwater input. Daily flows were simulated for 2000-2017 using a calibrated hydrologic model that includes all San Francisco Bay Area watersheds. Nutrient concentrations for both the stormwater input and ocean boundaries were set to constant values; $NH_4^+ = 2\ \mu M$, $NO_3^- = 10\ \mu M$, $PO_4 = 0.6\ \mu M$, and $Si = 100\ \mu M$.

Light Field
To determine the light levels phytoplankton are exposed to, we need to know the incident light reaching water surface (solar radiation) and light extinction coefficient within the water column. To quantify incident light, we used measured hourly solar radiation at Union City from the California Irrigation Management Information System (CIMIS). To realistically capture the impact of wind-wave driven sediment resuspension particularly in the shoal region, we modeled the light extinction coefficient as a function of hourly wind stress (from CIMIS) based on a regression between Secchi depth observed by Department of Fish and Wildlife in South Bay and Lower South Bay and wind stress (Fig. 3.2). Currently, the light extinction coefficient varies temporally, but is spatially constant. We are in the process of compiling and validating a spatially and temporally varying light field based on spatial interpolation of high frequency USGS suspended sediment concentrations, which can potentially improve our modeling results (see Appendix C for details).

Observational Data for Model Tuning and Evaluating Model Performance
To tune the model and evaluate model performance, we relied primarily on observational data from

[20] http://sfbaynutrients.sfei.org/erddap/tabledap/sfei_sfbay_potw_201705.html
[21] https://github.com/rustychris/sfbay_potw
[22] http://sfbaynutrients.sfei.org/sites/default/files/NutrientLoadsFINAL_FINAL_Jan232014.pdf
[23] https://www.sfei.org/documents/delta-nutrient-sources

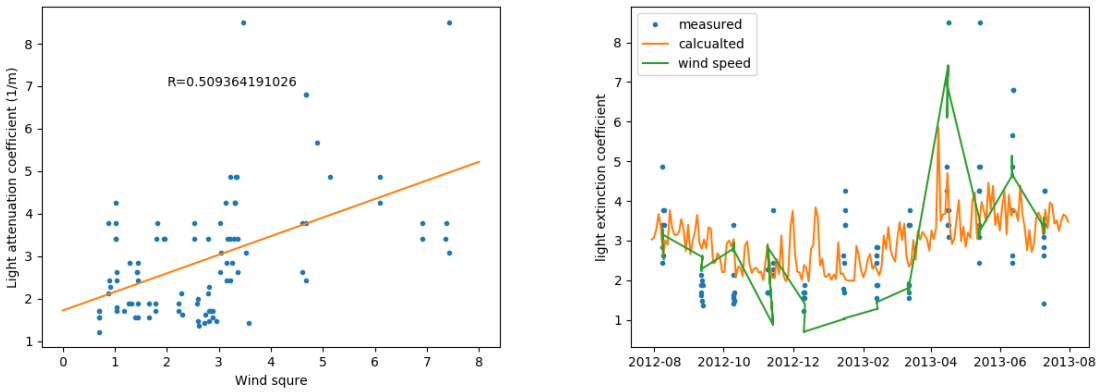

Figure 3.2: Light Field. (left) Regression between observed wind magnitude and light attenuation coefficient. (right) The calculated light extinction coefficient used in the model (orange) with measured light extinction coefficients (blue) and wind (green).

USGS ship-based sampling (Schraga and Cloern[24]), which include a suite of biogeochemical analytes including discrete and calculated chlorophyll-a, discrete and calculated oxygen, oxygen saturation, discrete and calculated suspended particulate matter (SPM), nitrite + nitrate, ammonium, phosphate, and silicate. Cruises occur 1-2 times per month, with discrete samples collected at 5-10 stations per cruise (Fig. 2.22). When discussing nitrate (NO_3^-) below, although the measurement technique detects both NO_3^- and nitrite (NO_2^-), here-
after it is referred to only as NO_3^-, because, in general, NO_3^- is much greater than NO_2^- in this dataset.

3.3. Results - WY2013

Output from the coupled biogeochemical - hydrodynamic model of WY2013 (October 2012 to September 2013) for concentrations of DIN ($NO_3^- + NH_4^+$), NO_3^-, NH_4^+, $chl-a$, and dissolved oxygen are presented in Figures 3.3 - 3.8. The panels within each figure present data from seven locations across SFB (top = northeast; bottom = south). The smooth curve represents daily-average modeled concentrations, and the shaded area around the curve depicts the daily range (modeled). In some cases the daily ranges are large relative to the daily average, with that variability being indicative of spatial gradients in water quality, and tidal transport moving water masses of different chemical compositions up- and down-estuary. Modeled and measured data are also presented in terms of concentration vs. distance from Station 36 and as a function of Date (Figs. 3.9-3.14).

Nitrogen Concentrations

Modeled DIN (NO_3^-+NH_4^+) concentrations (Fig. 3.3) broadly capture DIN spatial patterns in SFB, with highest DIN concentrations in Lower South Bay (Fig. 3.3H), lowest concentrations in Central Bay (Fig. 3.3D), and increasing concentrations in Suisun Bay (Fig. 3.3A). At locations where measured DIN concentrations exhibits substantial seasonal changes, (Fig. 3.3H, G, A, and B), comparable changes are evident in modeled DIN, including the large DIN decrease in Lower South Bay in February and March and subsequent rebound (Fig. 3.3G and H). Overall, the reasonably

[24] https://doi.org/10.1038/sdata.2017.98

good agreement between modeled and observed DIN (generally within ± 20%) suggests that the model captures the major loads, transport, and overall DIN losses (denitrification, assimilation by phytoplankton). However, there is an apparent bias toward the model moderately (but consistently) underpredicting DIN at some locations, and there is clearly room for improvement.

The model's performance with predicting N speciation (NH_4^+ vs. NO_3^-) is also informative. At most locations and times, modeled and measured NO_3^- concentrations also agree well (Figure 3.2). Station 27, near the San Mateo Bridge, is a notable exception with the model substantially underpredicting NO_3^- throughout October - December 2012. At first glance, the model appears to poorly predict measured NH_4^+ concentrations, on a percentage basis. However, that perspective does not take into account the fact that, throughout most of SFB (except LSB), most WWTPs discharge DIN primarily as NH_4^+, yet the majority of ambient DIN occurs as NO_3^-, requiring most of the NH_4^+ to have undergone nitrification to NO_3^-. Viewed through that lens, the model performs reasonably well with predicting NH_4^+ concentrations.

Chl-a and Dissolved Oxygen

Predicting phytoplankton blooms is difficult because numerous processes can play important roles that influence bloom timing, magnitude and duration: stratification vs. well-mixed water column, light attenuation, nutrient availability, growth rate, grazing, settling, horizontal transport or export. In Lower South Bay, the model captures the timing and approximate magnitude of a major bloom (Fig. 3.7). The February and March increase of both modeled and measured chl-a coincide with the substantial decreases in DIN, consistent with a large phytoplankton bloom drawing down nutrients by assimilation and growth. However, field data around the time of the bloom are quite limited: only one observation date during what the model suggests was a 6-week event, which limits what we can confidently infer about important factors.

Comparisons of modeled and measured chl-a data also highlight some of the model's limitations. For example, the model substantially overpredicts chl-a levels at two other South Bay stations which correspond to a large area of South Bay, indicating that additional model refinements are needed. Interestingly, the chl-a overpredictions at Station 27 and Station 21 help explain the DIN underpredictions there (Fig. 3.3E and F). Modeled chl-a also exceeded measured chl-a in San Pablo Bay and western Suisun Bay for an extended period (March - April, Fig. 3.7C and B), although the actual magnitude is fairly small. A sizable chl-a jump, observed in eastern Suisun field observations, was not captured by the model. However, this missed event is not surprising, because chl-a-enriched water masses are commonly transported from the Delta to Suisun Bay, and the Delta falls outside the current model's domain.

The good agreement between modeled and measured DO was somewhat unexpected, since only limited effort has gone thus far toward refining DO predictions. Small differences between modeled and measured values during October 2012 - January 2013 are not surprising, since observed and simulated concentrations remain close to DO-saturation levels because of limited biological activity (short days, cooler temperatures). During the Lower South Bay bloom, the similar magnitudes of increase in modeled and measured DO during the bloom (DO production), and similar decreases post-bloom (increased heterotrophic activity after large organic carbon input), suggest that the balance between, production rates, respiration rates, and air-sea exchange rates were well modeled.

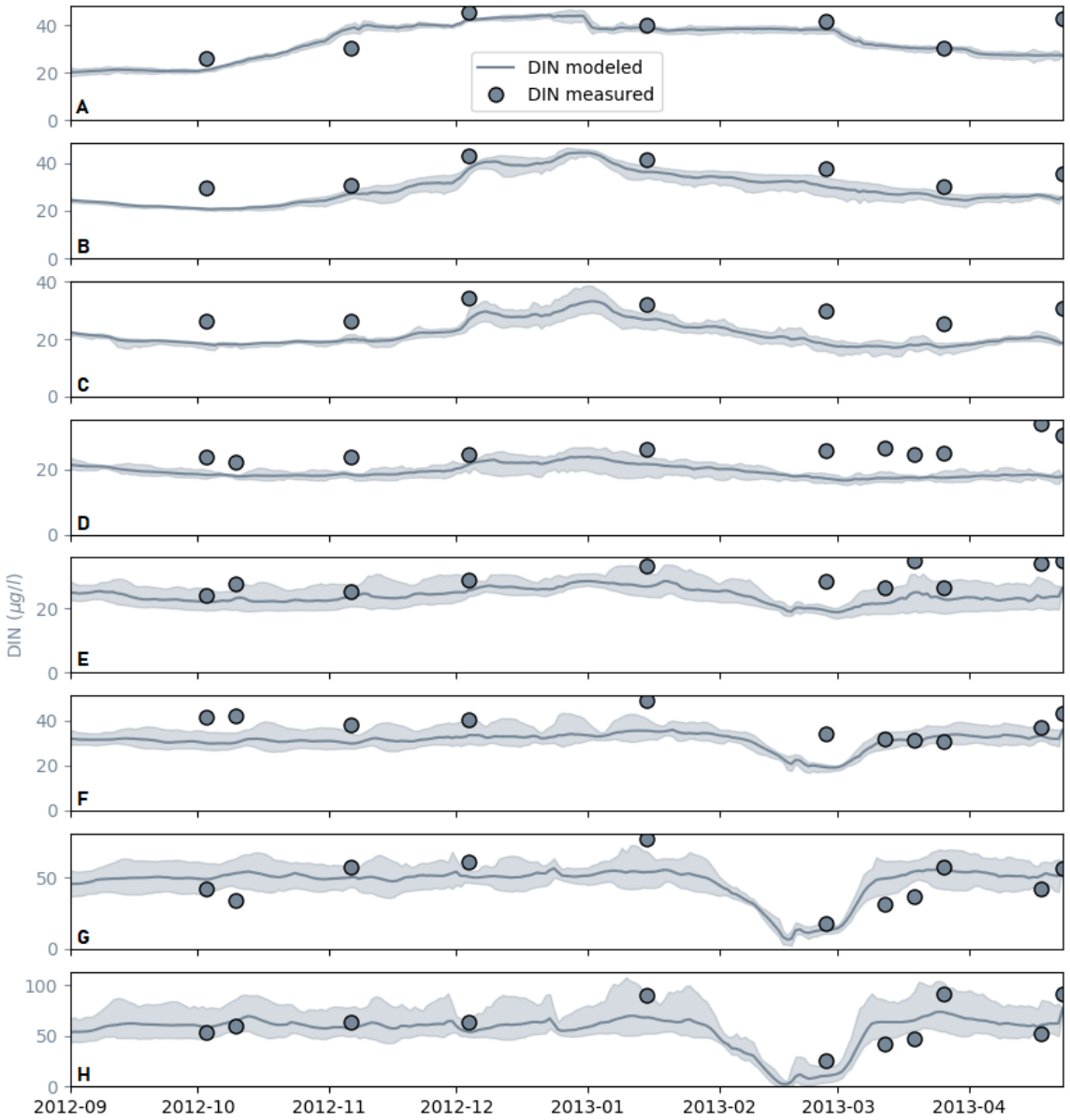

Figure 3.3: Modeled and observed surface DIN concentrations over the model run at USGS Station 3 (A), Station 9 (B), Station 15 (C), Station 18 (D), Station 21 (E), Station 27 (F), Station 32 (G), and Stations 34-36 (H).

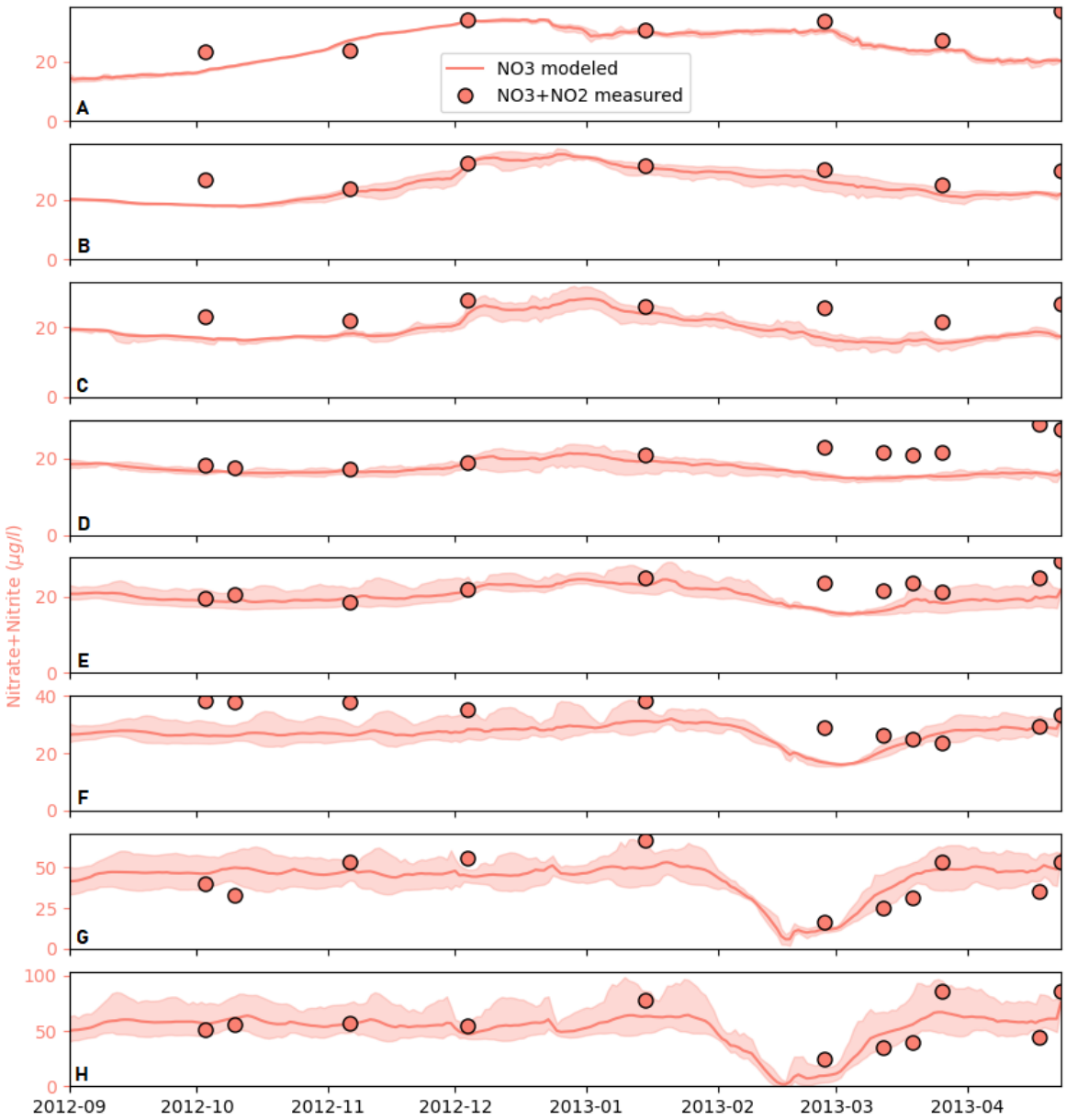

Figure 3.4: Modeled and observed surface nitrate concentrations over the model at USGS Station 3 (A), Station 9 (B), Station 15 (C), Station 18 (D), Station 21 (E), Station 27 (F), Station 32 (G), and Stations 34-36 (H).

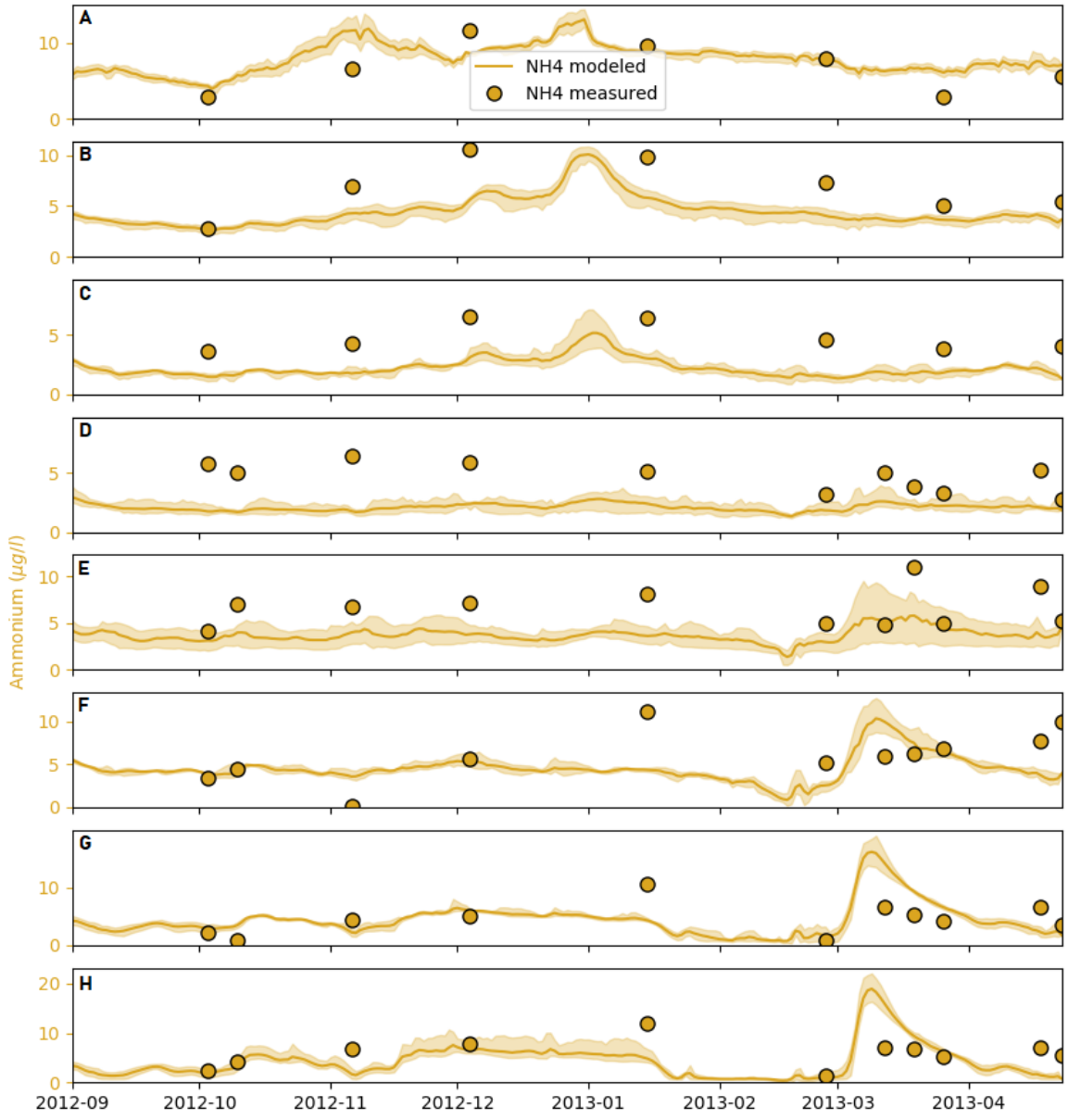

Figure 3.5: Modeled and observed surface ammonium concentrations over the model at USGS Station 3 (A), Station 9 (B), Station 15 (C), Station 18 (D), Station 21 (E), Station 27 (F), Station 32 (G), and Stations 34-36 (H).

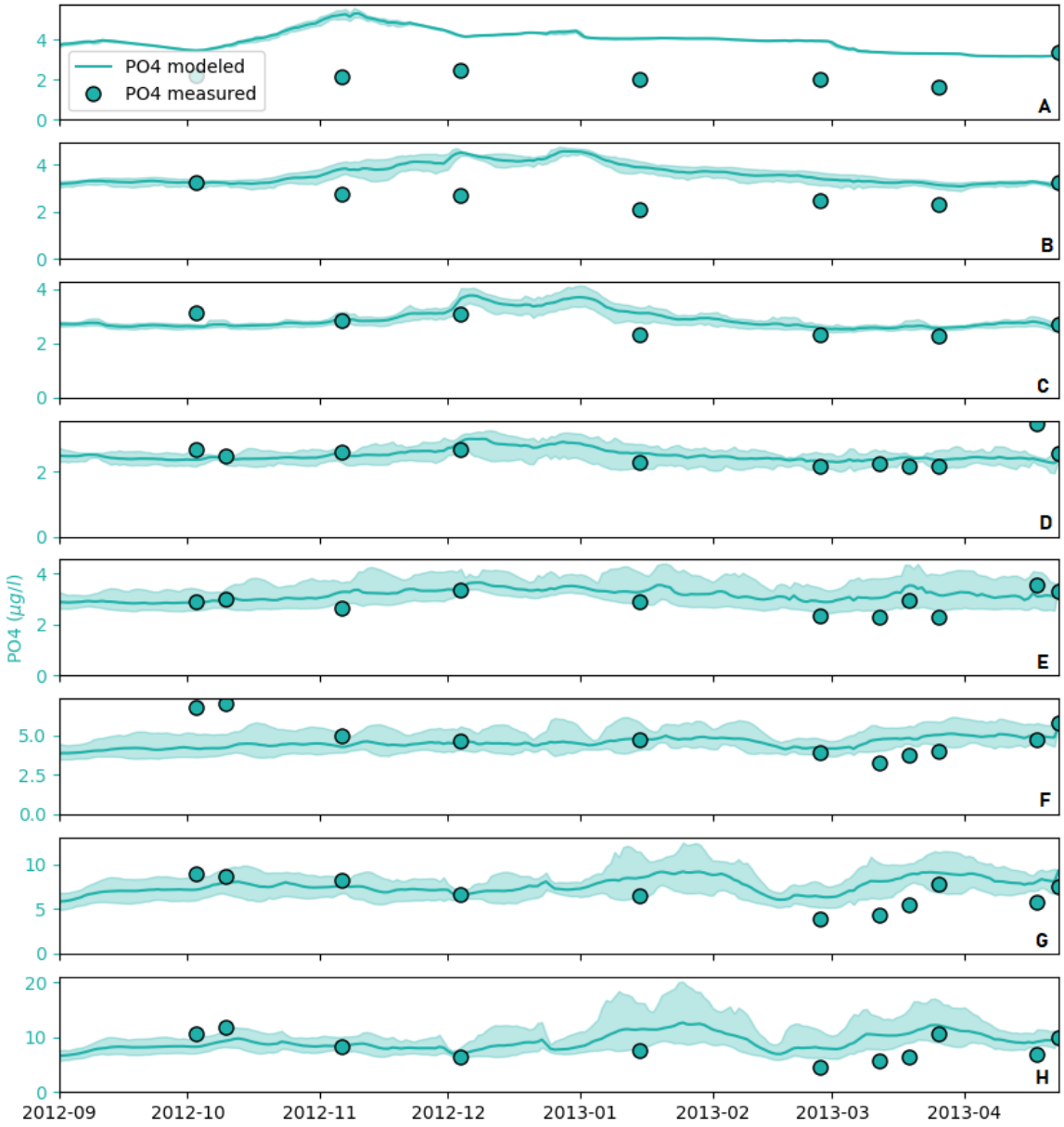

Figure 3.6: Modeled and observed surface phosphate concentrations over the model at USGS Station 3 (A), Station 9 (B), Station 15 (C), Station 18 (D), Station 21 (E), Station 27 (F), Station 32 (G), and Stations 34-36 (H).

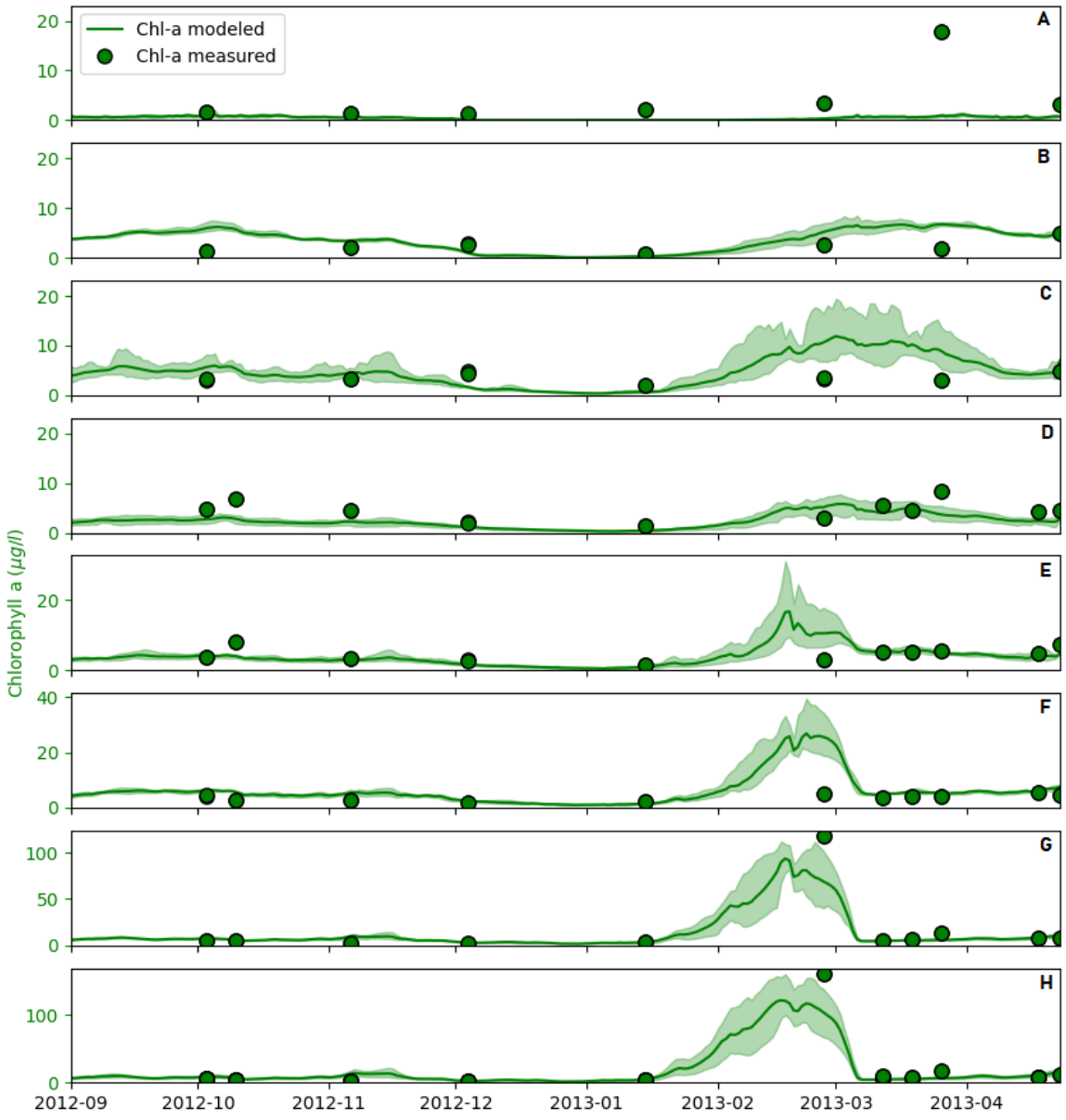

Figure 3.7: Modeled and observed surface chlorophyll-a concentrations over the model at USGS Station 3 (A), Station 9 (B), Station 15 (C), Station 18 (D), Station 21 (E), Station 27 (F), Station 32 (G), and Stations 34-36 (H).

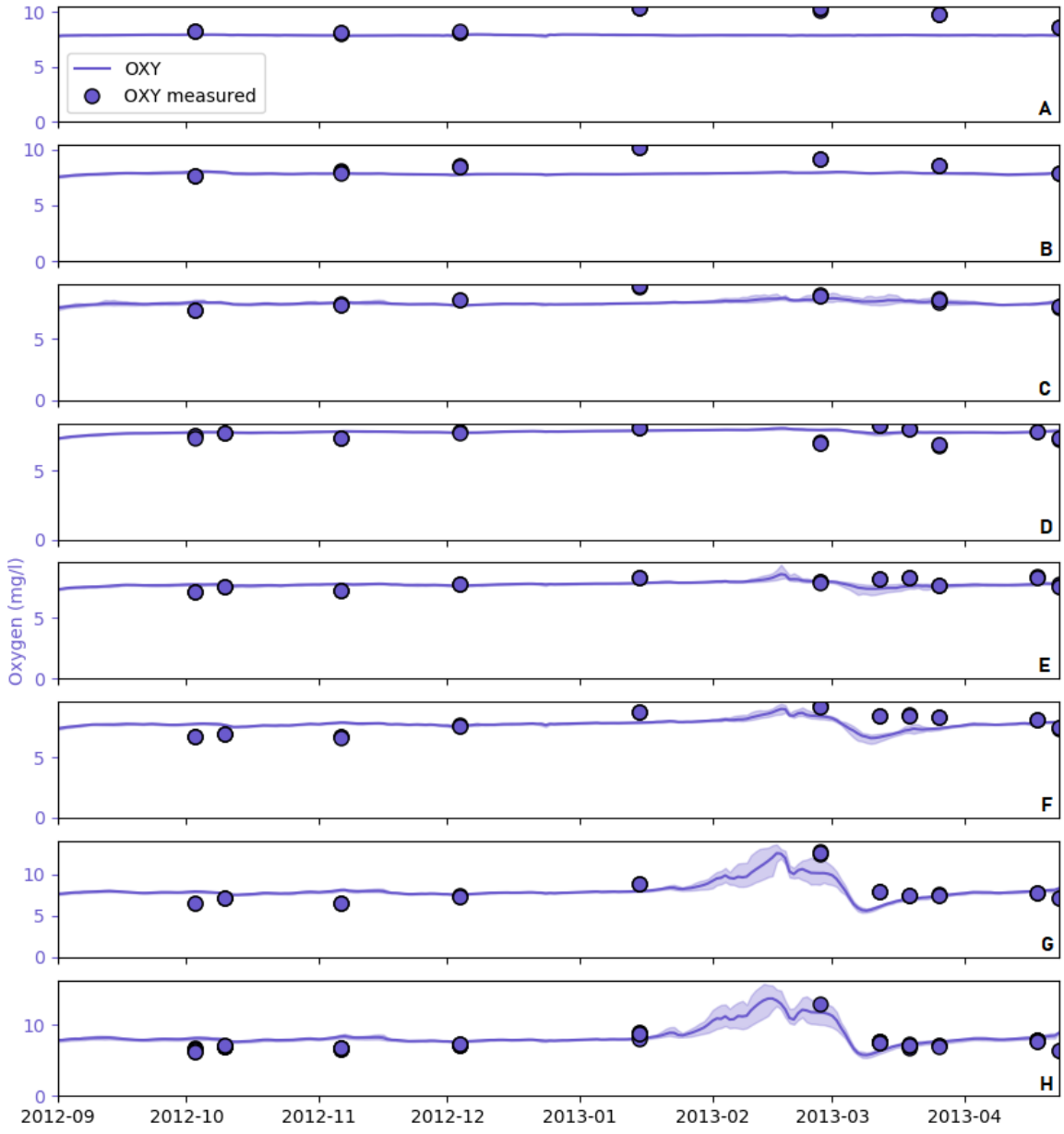

Figure 3.8: Modeled and observed surface oxygen concentrations over the model at USGS Station 3 (A), Station 9 (B), Station 15 (C), Station 18 (D), Station 21 (E), Station 27 (F), Station 32 (G), and Stations 34-36 (H).

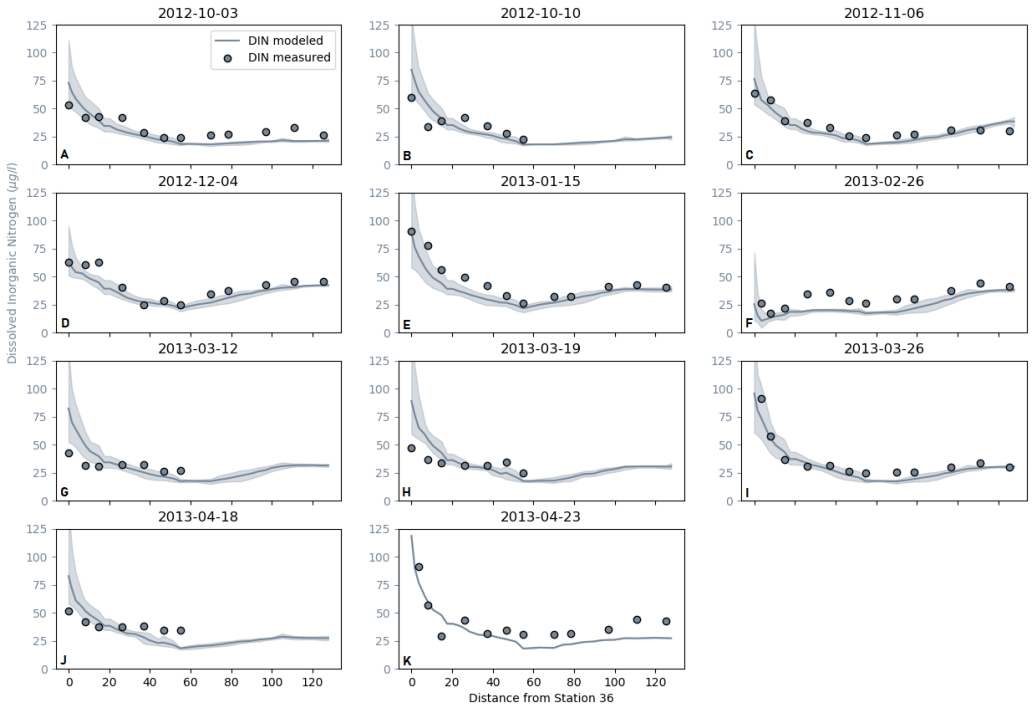

Figure 3.9: Modeled and observed surface DIN concentrations vs. distance from Station 36, by Date.

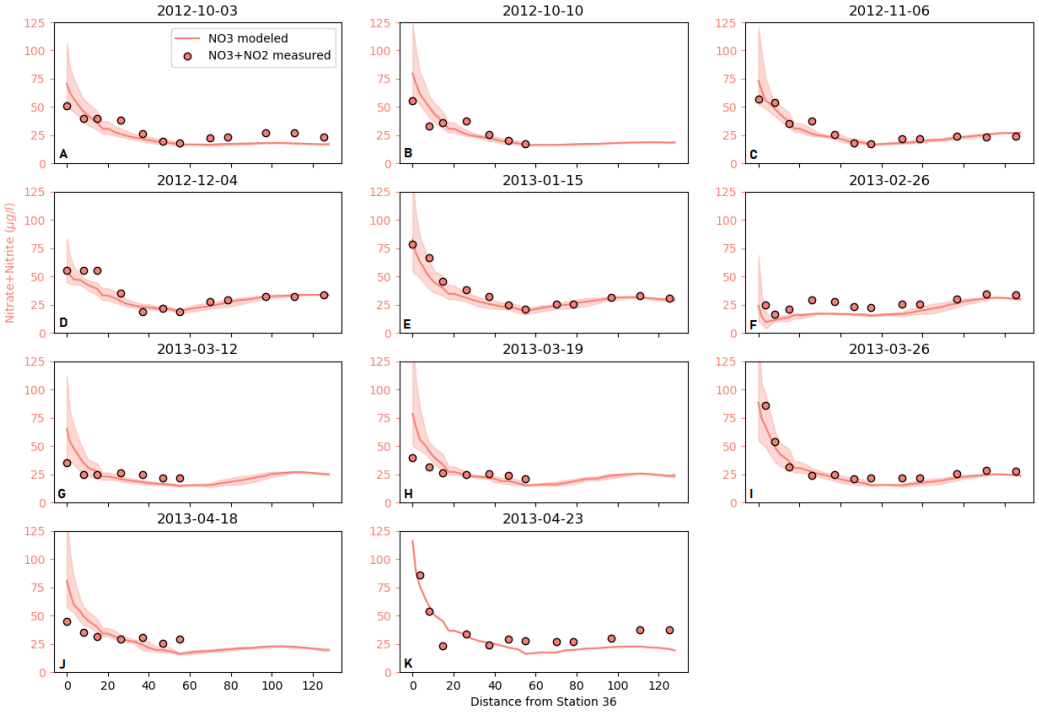

Figure 3.10: Modeled and observed surface nitrate concentrations vs. distance from Station 36, by cruise date

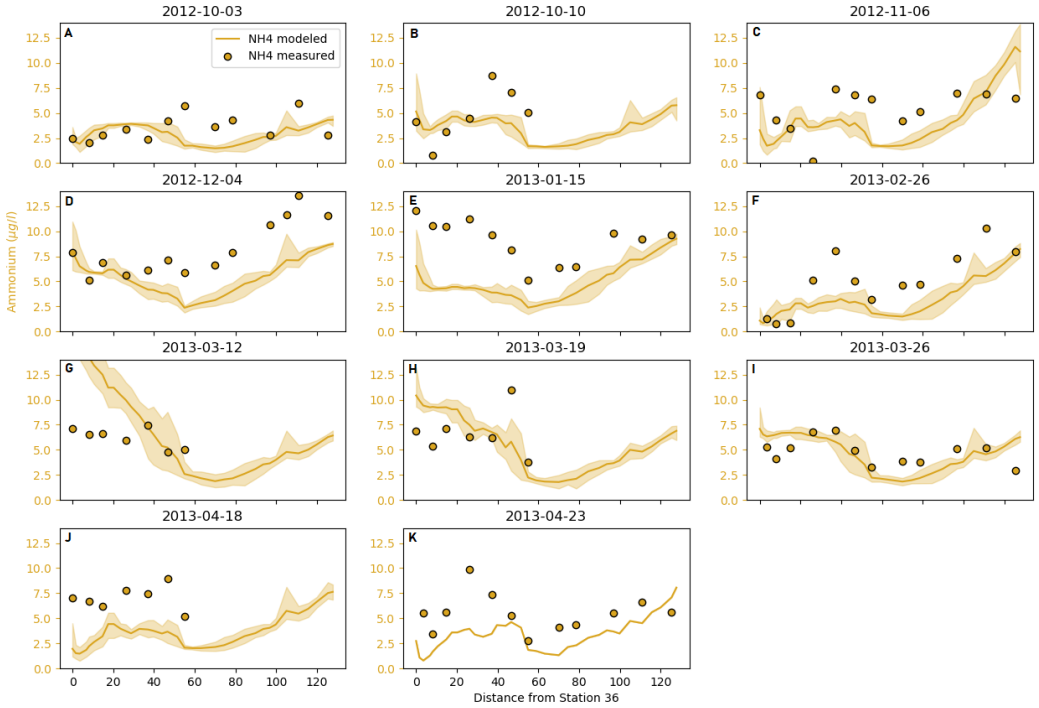

Figure 3.11: Modeled and observed surface ammonium concentrations vs. distance from Station 36, by cruise date.

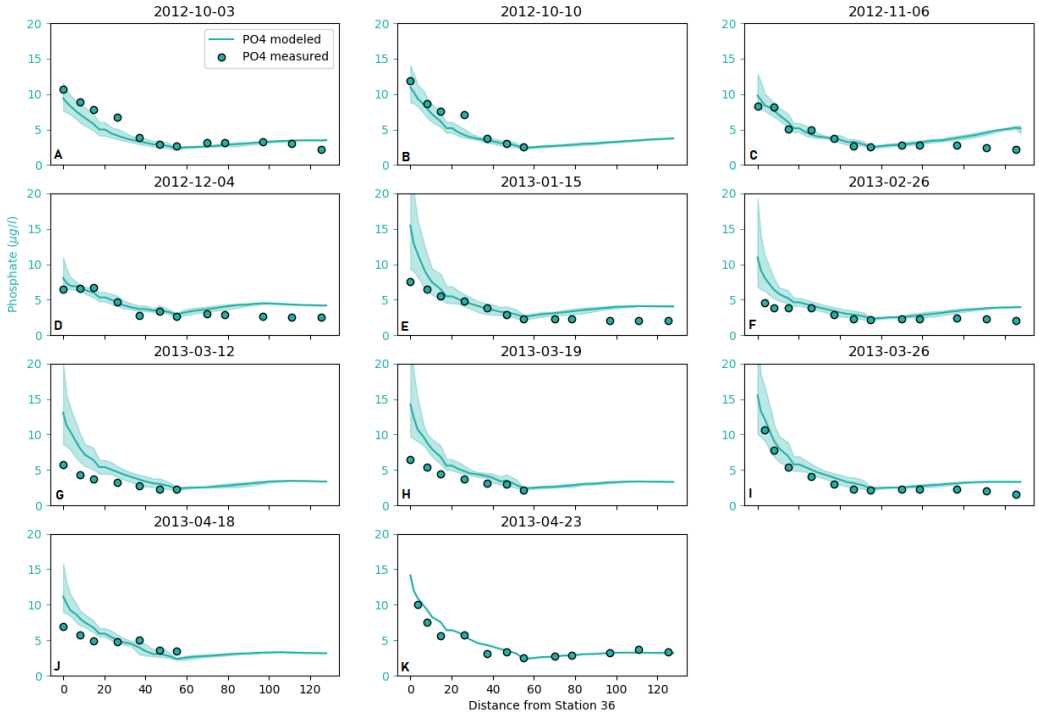

Figure 3.12: Modeled and observed surface phosphate concentrations vs. distance from Station 36, by cruise date.

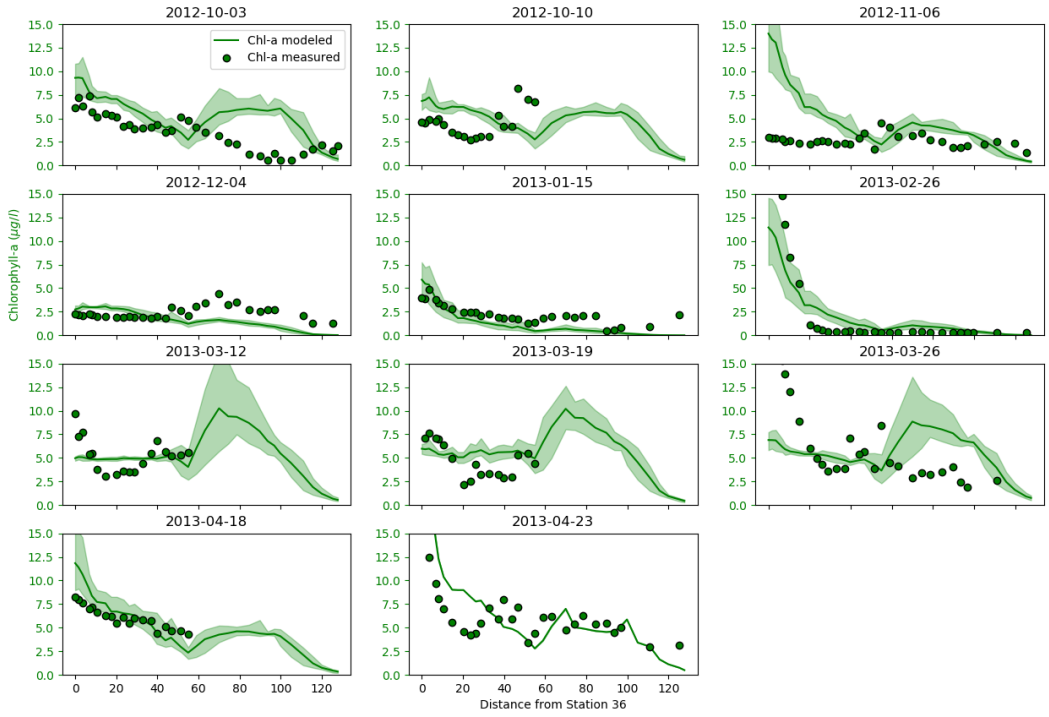

Figure 3.13: Modeled and observed surface chlorophyll-a concentrations vs. distance from Station 36, by cruise date.

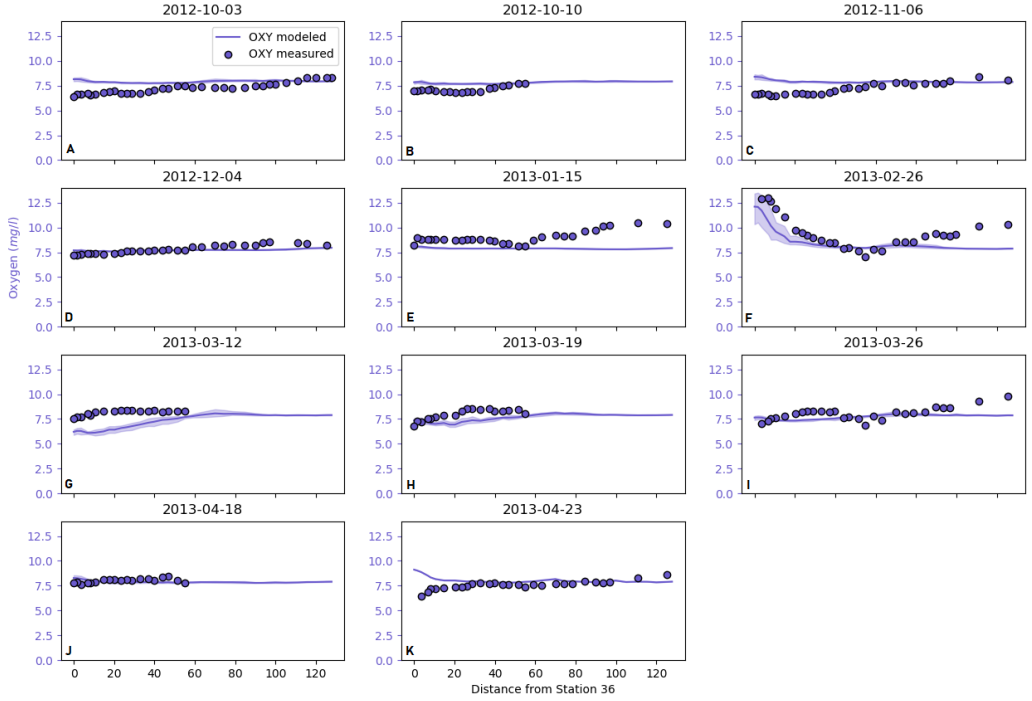

Figure 3.14: Modeled and observed surface oxygen concentrations vs. distance from Station 36, by cruise date.

Chlorophyll-a Spatial Variability

Since the model yields 3D predictions, it is also possible to view snapshots of modeled spatially-varying chl-a concentrations (Fig. 3.15 and 3.16). In late February 2013, the model predicts that chl-a was elevated throughout all of Lower South Bay, and dropped off fairly rapidly, decreasing to low levels north of the San Mateo Bridge (station 27, Fig. **??**). Although modeled chl-a and measured chl-a are comparable in the deep channel (i.e. USGS sampling sites), model output suggests that chl-a concentrations were highly elevated along the eastern shoal in South Bay and, to a lesser extent, along the shoal in San Pablo Bay. While no shoal field observations are available during that time, we know from limited observations during other time periods that chl-a concentrations can be substantially higher along the shoals than in the channel channel (e.g.,Huzzey et al. 1990[25]; Thompson et al. 2008[26]; SFEI (2017)[6]). Post-bloom (April 2013), modeled chl-a concentrations are low Bay-wide, including along the shoals (Fig. 3.16).

Figures comparing modeled and measured chl-a and DO versus depth are presented in the Appendix. Vertical structure is not easily observed in these plots due to the small magnitude of difference in chl-a over the water column compared to the much larger change in chl-a levels over the model run.

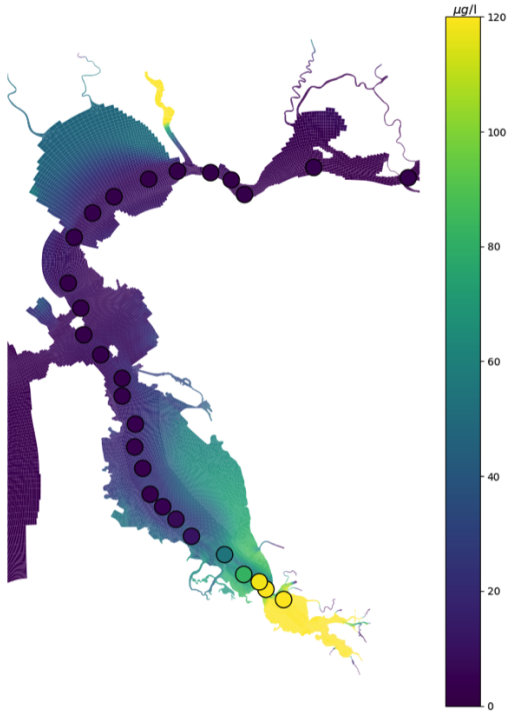

Figure 3.15: Modeled chl-a (colors) and Measured chl-a (colored circles) during the bloom, late February 2013

[25] https://doi.org/10.4319/lo.1990.35.2.0472

[26] https://doi.org/10.1016/j.jmarsys.2007.12.006

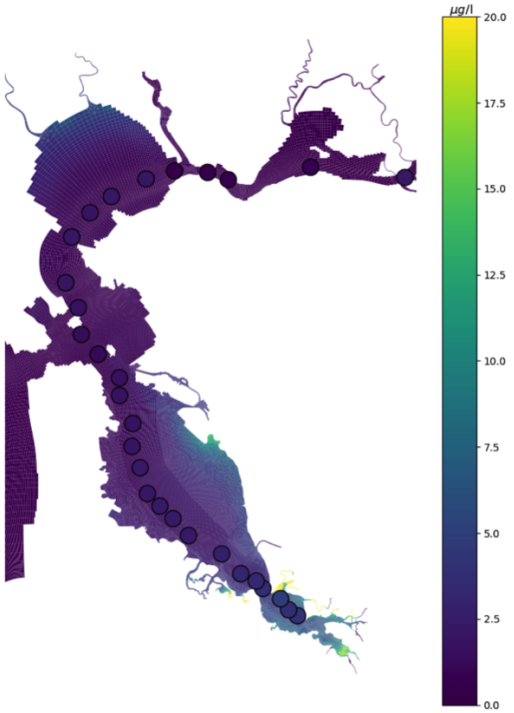

Figure 3.16: Modeled chl-a (colors) and Measured chl-a (colored circles) post-bloom, April 2013

3.4. Summary and Future Work

The current version of the SFB biogeochemical model incorporates a wide range of processes for simulating the loads, transport, and cycling of nutrients, and the influence of nutrients on phytoplankton and dissolved oxygen (see overview in Fig. 3.1). When applied to simulate biogeochemical conditions in WY2013, the model reproduced the major spatial and seasonal patterns of DIN and NO_3^- concentrations, suggesting that the magnitudes of, and balance among, a number of important processes (transport and transformations) are being approximated reasonably well. While the model also captured, in a broad and relative sense, the spatial differences in NH_4 abundance, the differences between modeled and measured NH_4 concentrations were often large on a percentage basis. In addition, the model predicted a large phytoplankton bloom in February - March 2013 in Lower South Bay that agreed well with the limited measured data available for this event, including peak chl-a magnitude and sharp decrease; increased DO concentrations during the event and a post-event DO minimum; and DIN drawdown during the event. Not surprisingly, there were also some important discrepancies between modeled and measured condition, for example: over-prediction of chl-a during the bloom period over a large area in South Bay; large relative overestimates of chl-a in San Pablo and Suisun Bays.
Work is continuing on model development, including the following underway or planned (next 1-2 years) activities:

1. Simulate additional time periods – with different physical forcings, different observed biogeochemical responses, and denser data availability – to develop an optimized calibration for a range of conditions. Work on model set-up for WY2017, WY2018, and WY2014 are currently underway.

2. Develop capability to run spatially-aggregated biogeochemical runs, to substantially reduce run times and allow for additional model tuning.

3. Incorporate additional field observational data or best available estimates based on literature: zooplankton grazing rate and biomass; sediment oxygen demand and sediment: water-column nutrient fluxes; nutrient concentrations at the coastal-ocean boundary; physical and chemical forcings from Delta; high frequency

4. Refine several important parameters or model components:
    a) Incorporate a spatially and temporally varying light extinction coefficient, through spatial/temporal interpolation of observational data and output from mechanistic sediment transport models.
    b) Add self-shading by phytoplankton (i.e., decreased light availability as chl-a increases)
    c) Add benthic grazer module
    d) Further tune sediment diagenesis model.

APPENDIX A ADDITIONAL FIGURES

A.1 HYDRODYNAMIC MODEL

A.1.1 VELOCITY

SOUTH BAY

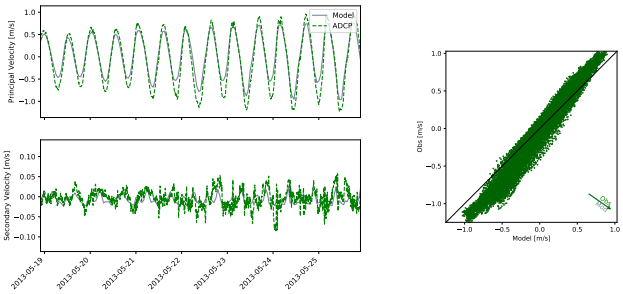

Figure A.1: SFB1302 Redwood Point, 1.7 nm E of

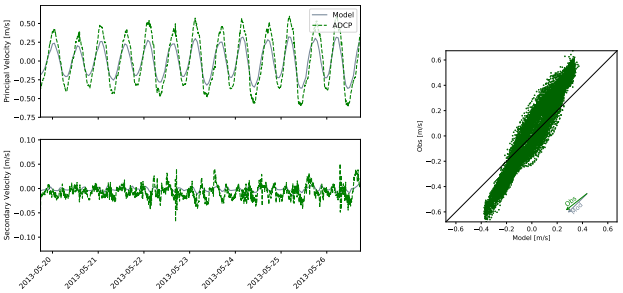

Figure A.2: SFB1304 Redwood Creek

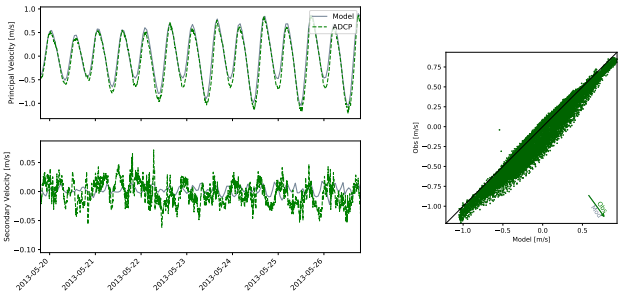

Figure A.3: SFB1306 Anchorage 138

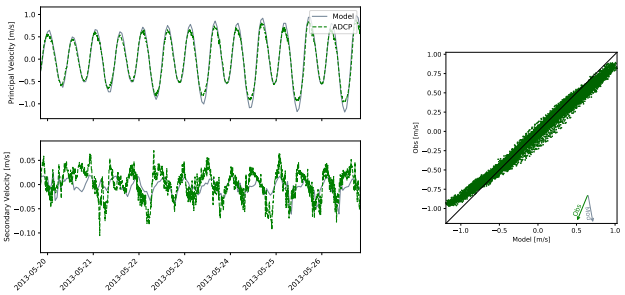

Figure A.4: SFB1308 Hunters Point, 1.6 nm SE of. Compass errors in the observations are likely the cause of the difference in principal direction.

Central Bay

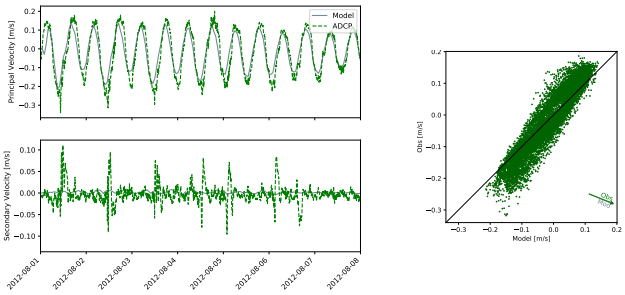

Figure A.5: SFB1215 Brooklyn Basin

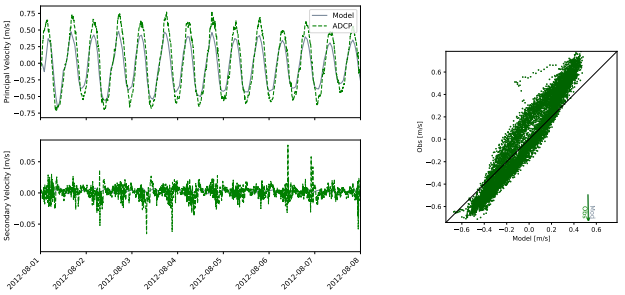

Figure A.6: SFB1216 Alameda Estuary, SE End

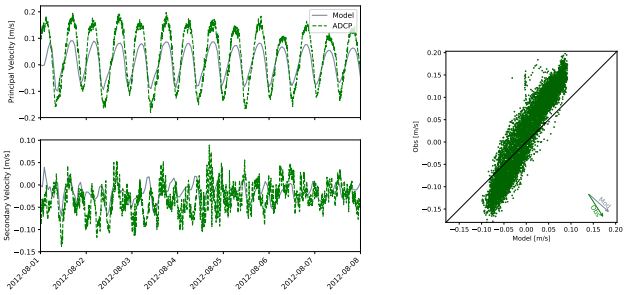

Figure A.7: SFB1218 Emmeryville Marina

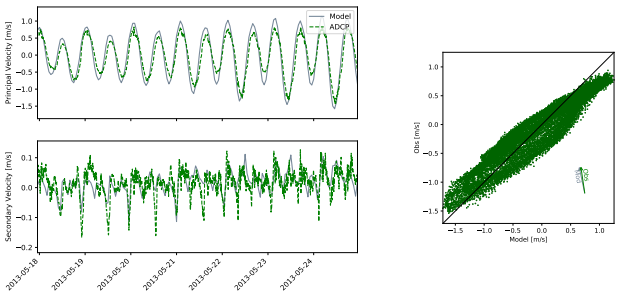

Figure A.8: SFB1310 Point Chauncey, 1.25 miles N of.

COASTAL

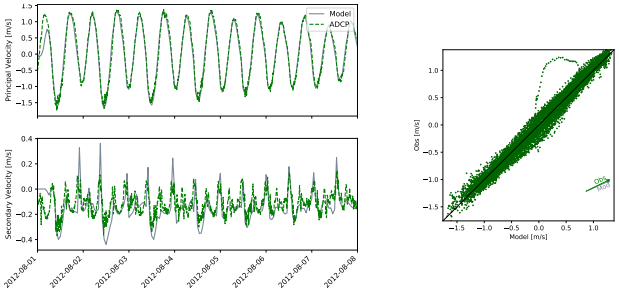

Figure A.9: SFB1220 Pt Bonita, 0.95 nm SSE

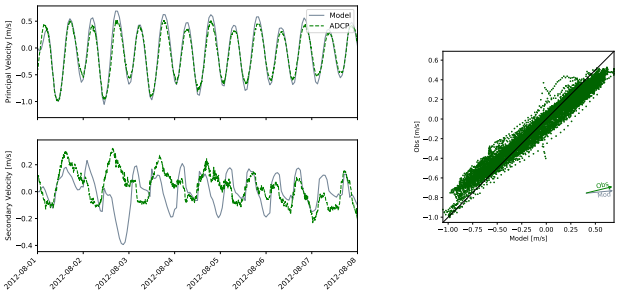

Figure A.10: SFB1221 SF Bar

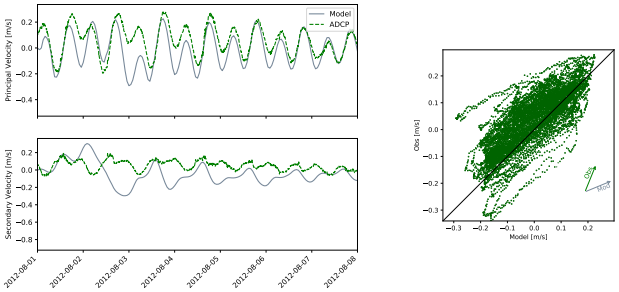

Figure A.11: SFB1222 SF Buoy

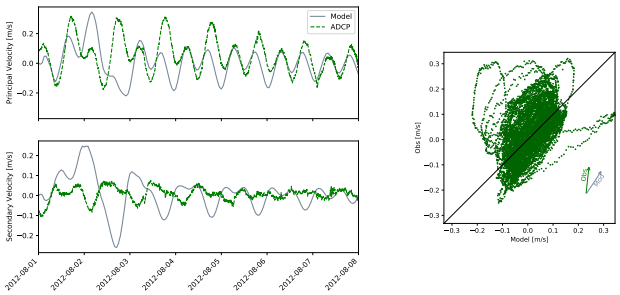

Figure A.12: SFB1223 Pt. San Pedro, 8.8 SSE of

NORTH BAY

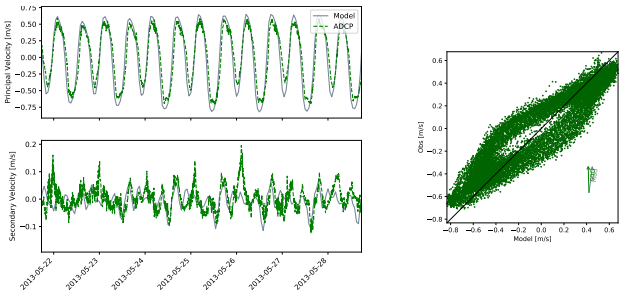

Figure A.13: SFB1313 Petaluma River approach (Buoys 3 and 4)

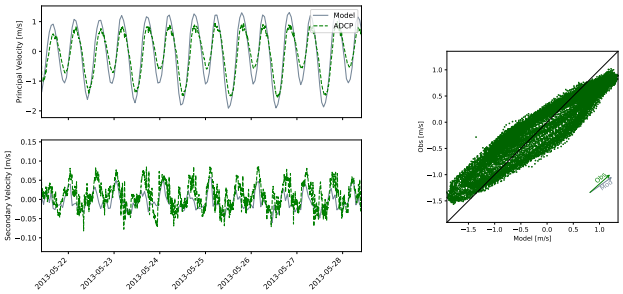

Figure A.14: SFB1314 Pinole Point, 1.27 nmi. NNW of

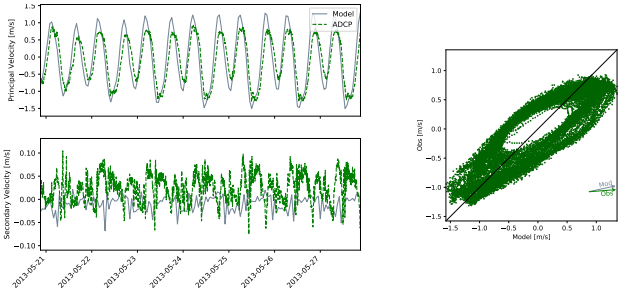

Figure A.15: SFB1316 Davis Point, 1.0 nmi. NW of

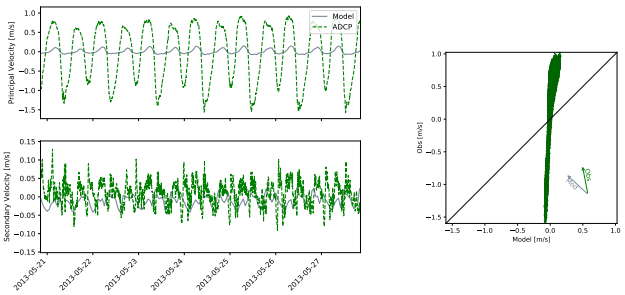

Figure A.16: SFB1317 Mare Island Strait, Pier 34, NE of

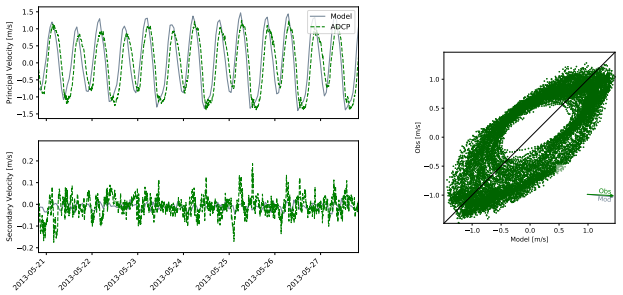

Figure A.17: SFB1318 I-80 Carquinez Bridge

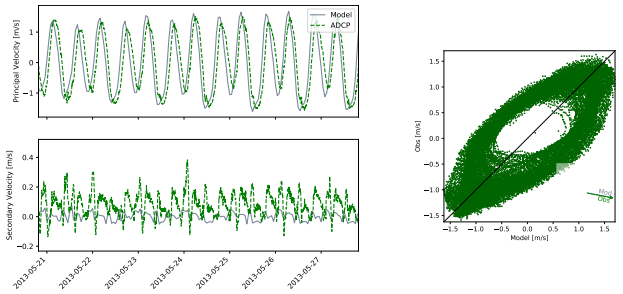

Figure A.18: SFB1319 Carquinez Strait

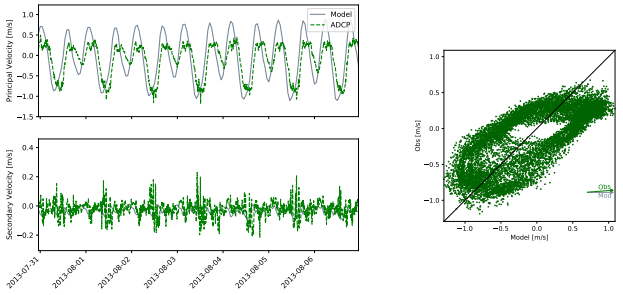

Figure A.19: SFB1320 Dillon Point

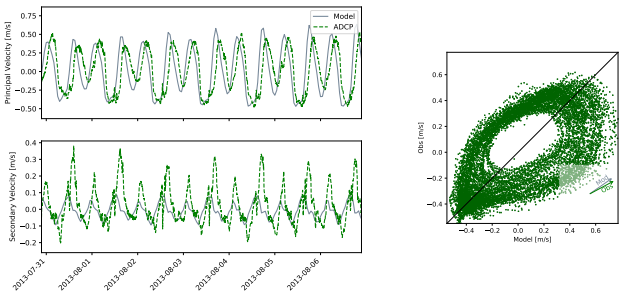

Figure A.20: SFB1322 Grizzly Bay, entrance

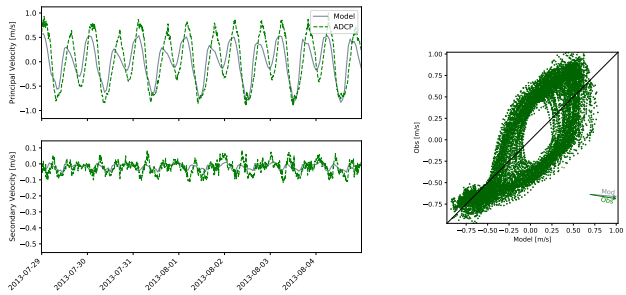

Figure A.21: SFB1324 Middle Point Lt., 0.18 nmi. NNW of

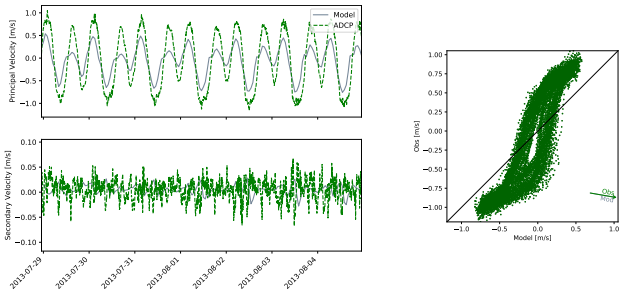

Figure A.22: SFB1325 Simmons Point 0.6 nm ESE of

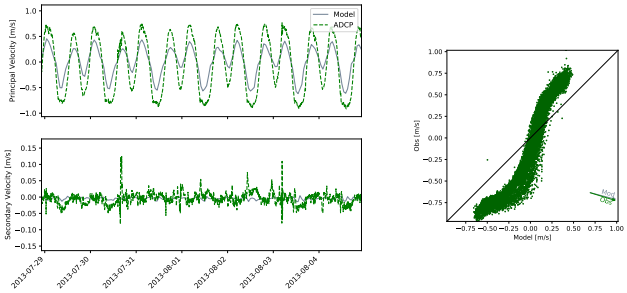

Figure A.23: SFB1326 New York Slough

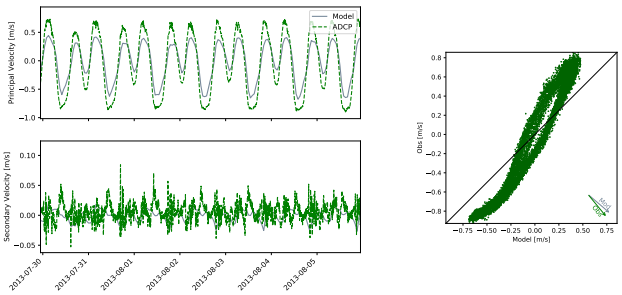

Figure A.24: SFB1327 Antioch Point

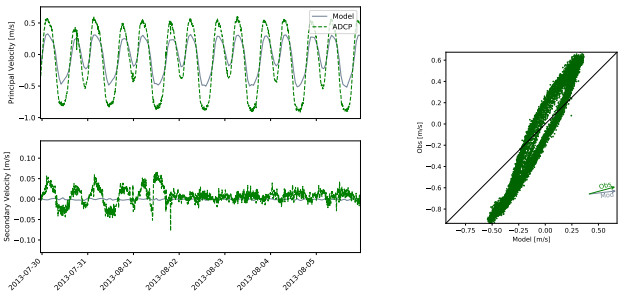

Figure A.25: SFB1328 West Island, N of

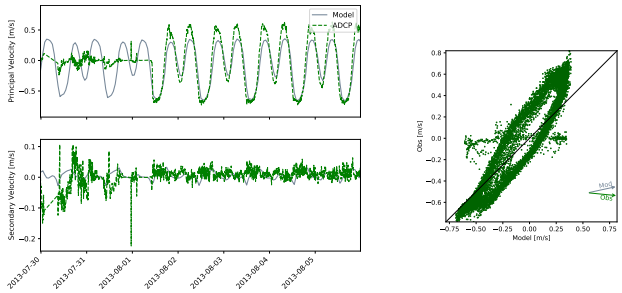

Figure A.26: SFB1329 Route 160 Bridge

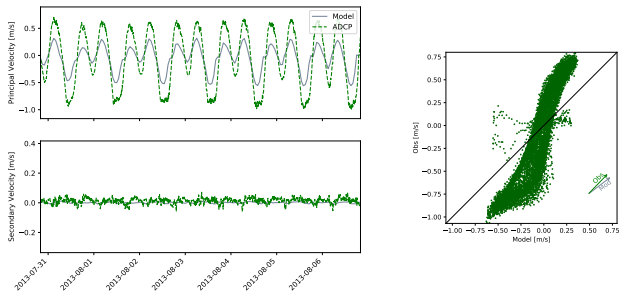

Figure A.27: SFB1330 Sacramento River Entrance, 0.7nm SW of Chain Island

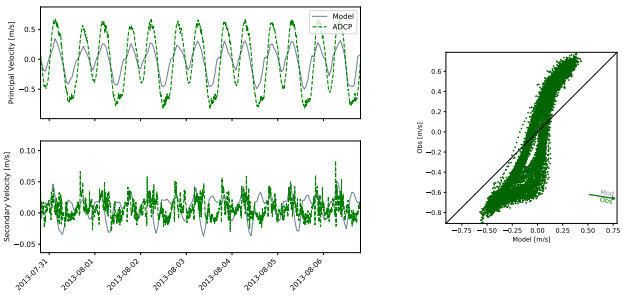

Figure A.28: SFB1331 Point Sacramento, 0.2 nm NE of

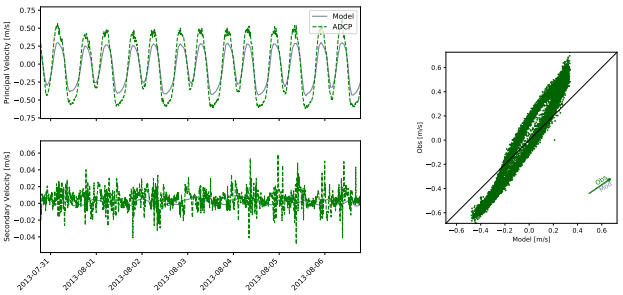

Figure A.29: SFB1332 Sacramento River, Light 14

A.1.2 SALINITY

TRANSECTS

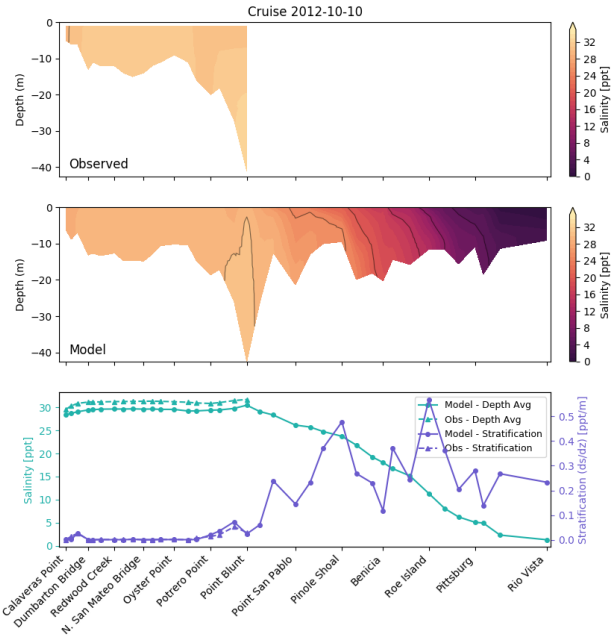

Figure A.30: USGS Transect, 2012-10-10

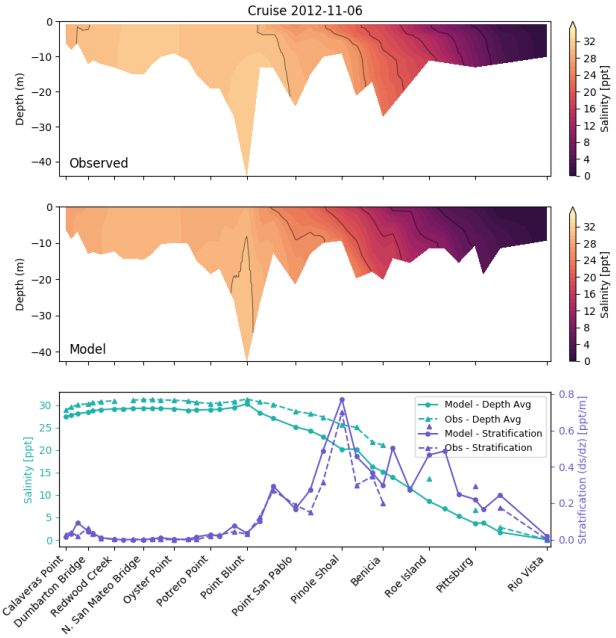

Figure A.31: USGS Transect, 2012-11-06

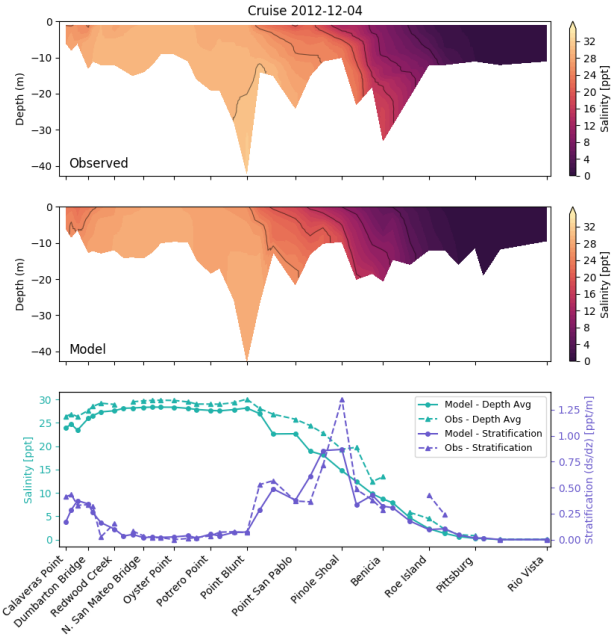

Figure A.32: USGS Transect, 2012-12-04

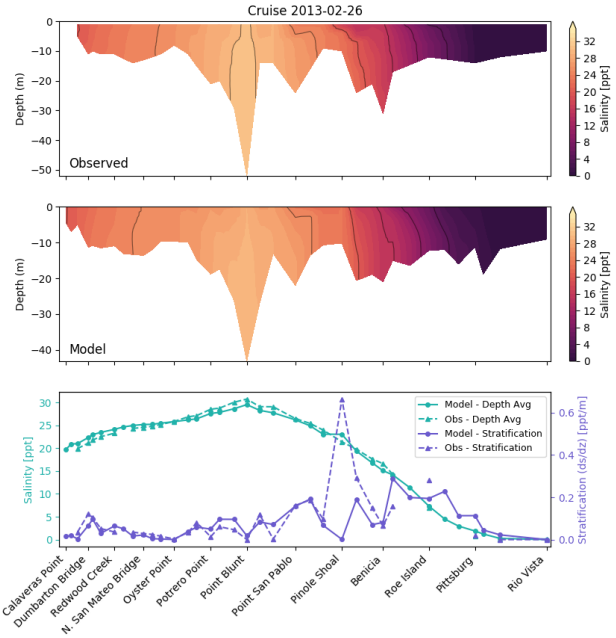

Figure A.33: USGS Transect, 2013-02-26

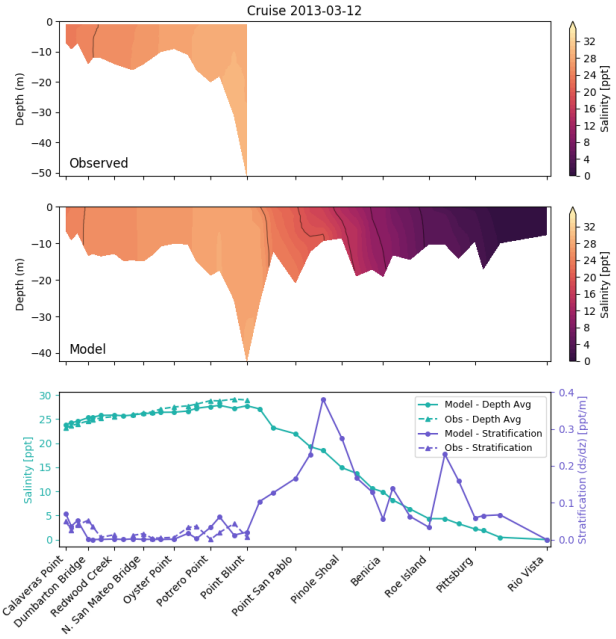

Figure A.34: USGS Transect, 2013-03-12

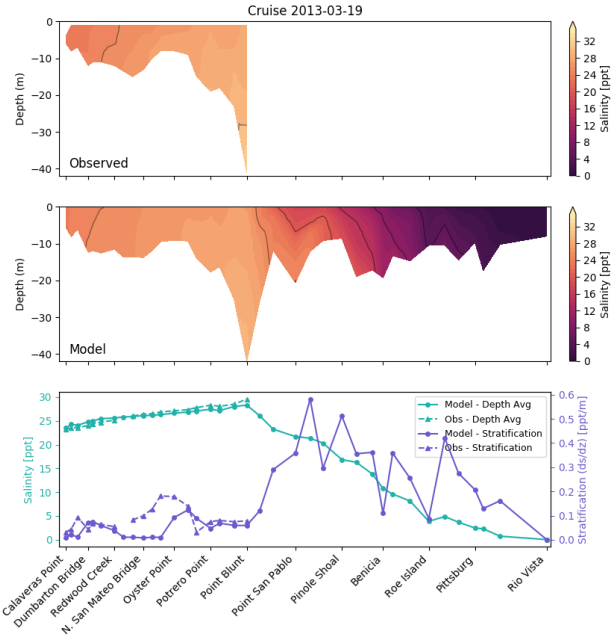

Figure A.35: USGS Transect, 2013-03-19

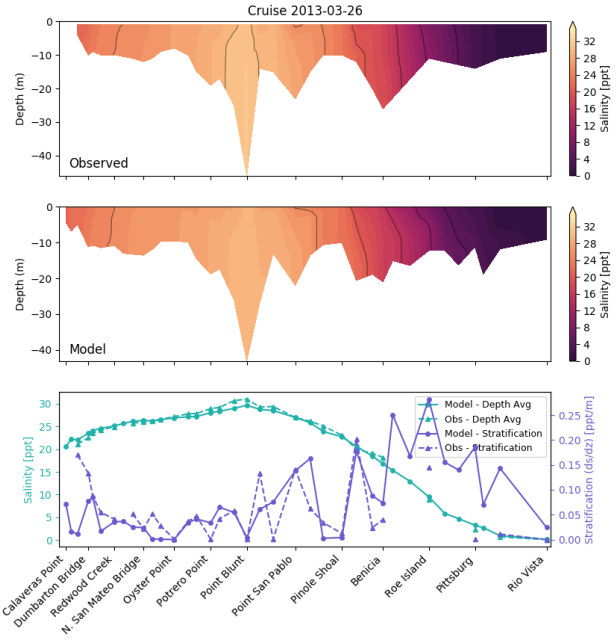

Figure A.36: USGS Transect, 2013-03-26

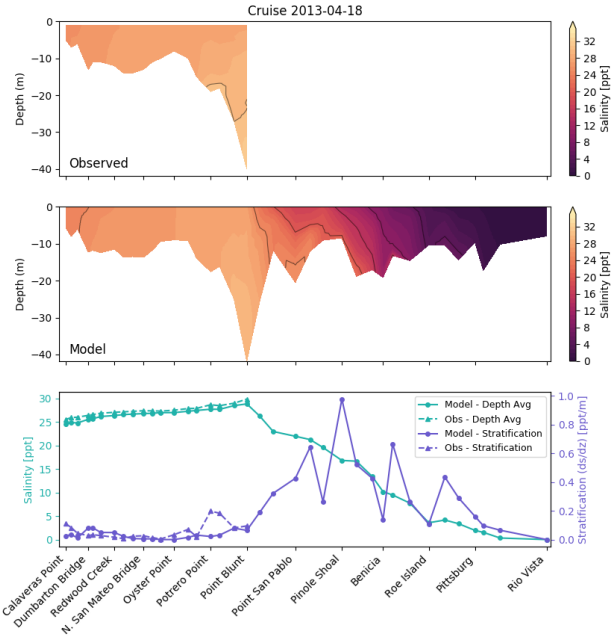

Figure A.37: USGS Transect, 2013-04-18

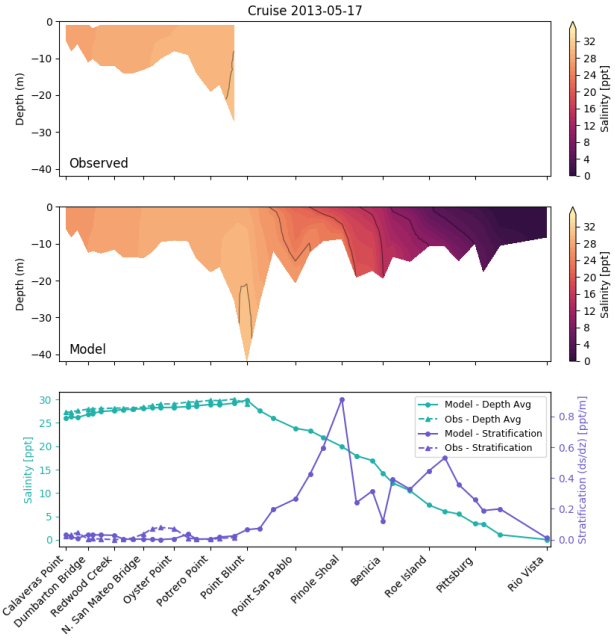

Figure A.38: USGS Transect, 2013-05-17

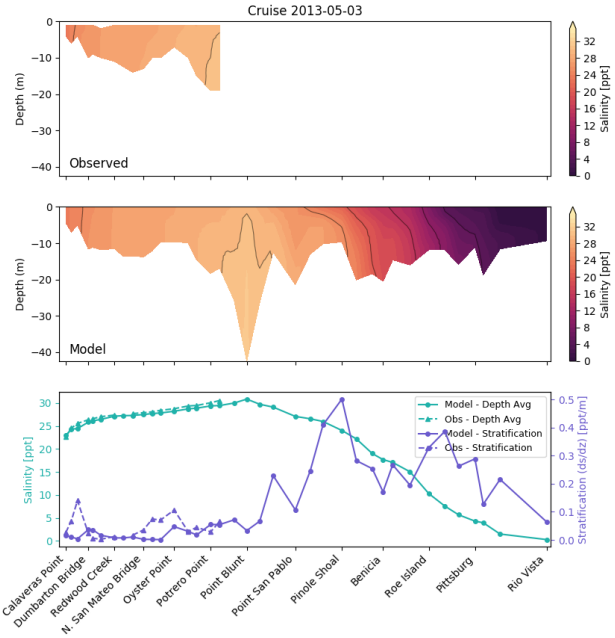

Figure A.39: USGS Transect, 2013-05-03

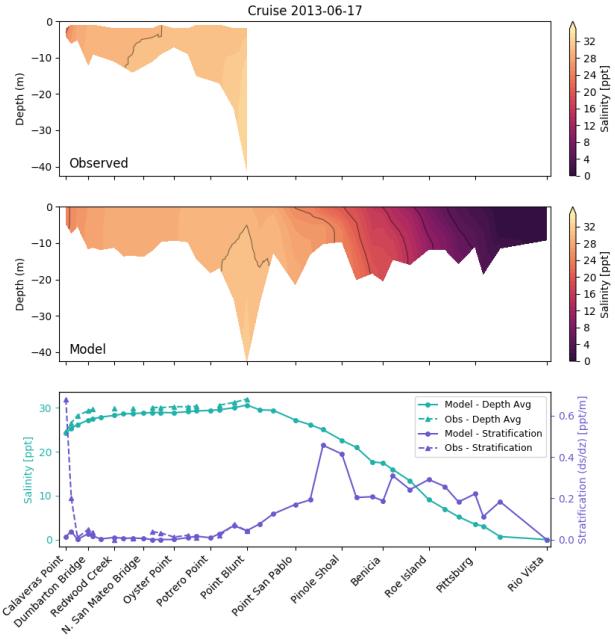

Figure A.40: USGS Transect, 2013-06-17

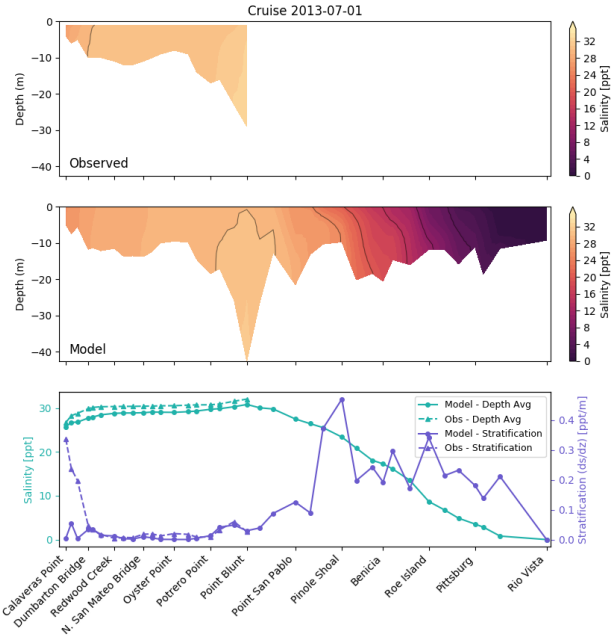

Figure A.41: USGS Transect, 2013-07-01

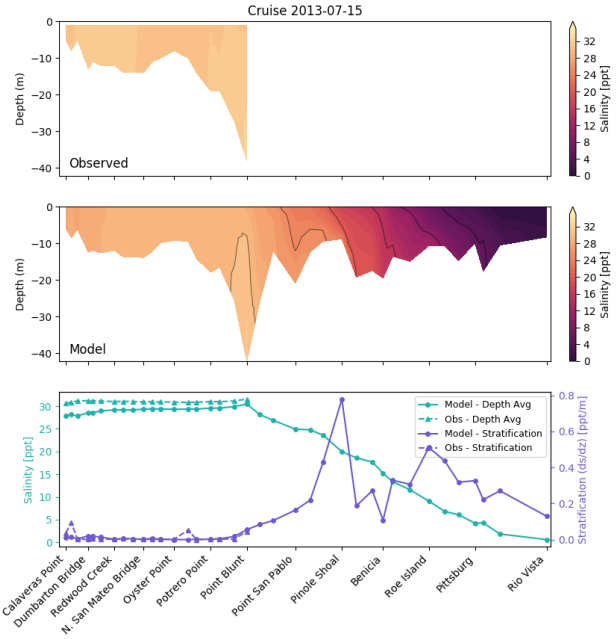

Figure A.42: USGS Transect, 2013-07-15

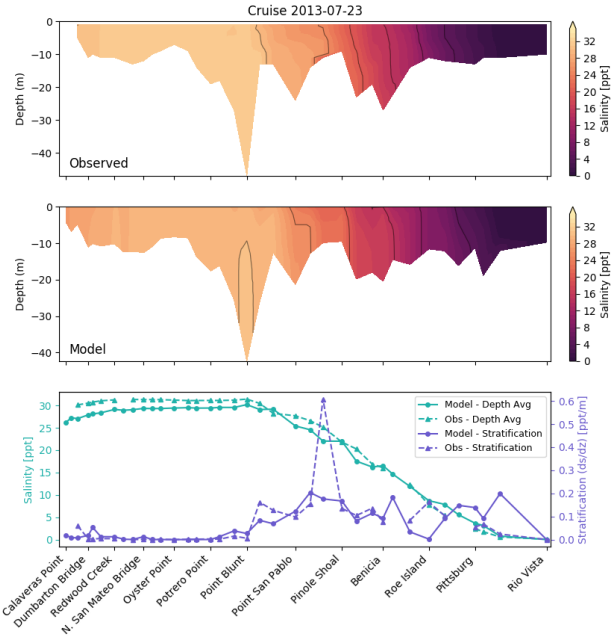

Figure A.43: USGS Transect, 2013-07-23

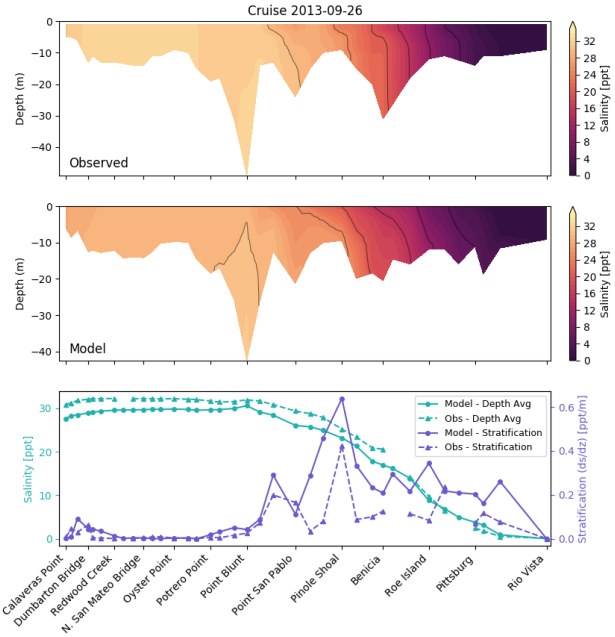

Figure A.44: USGS Transect, 2013-09-26

Time Series

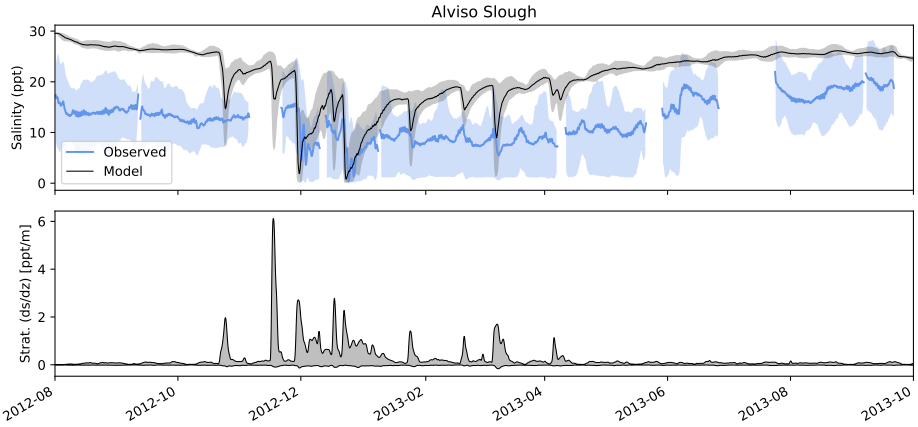

Figure A.45: Salinity time series: Alviso Slough, USGS 11169750

A.2 Biogeochemical Model

A.2.1 Chlorophyll

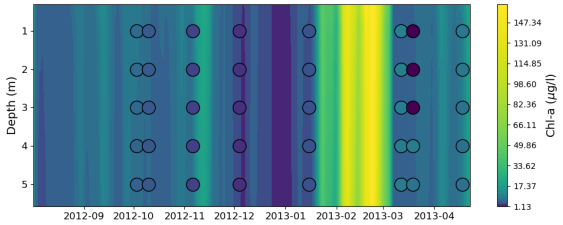

Figure A.46: Contours of modeled chlorophyll concentrations and observed chlorophyll concentrations in black circles through time at USGS Station 36

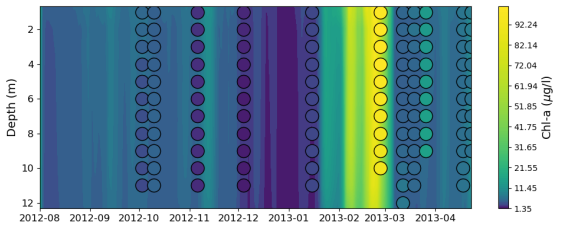

Figure A.47: Contours of modeled chlorophyll concentrations and observed chlorophyll concentrations in black circles through time at USGS Station 32

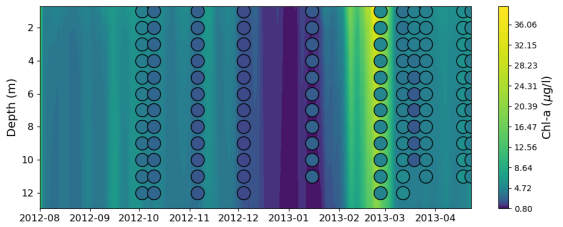

Figure A.48: Contours of modeled chlorophyll concentrations and observed chlorophyll concentrations in black circles through time at USGS Station 27

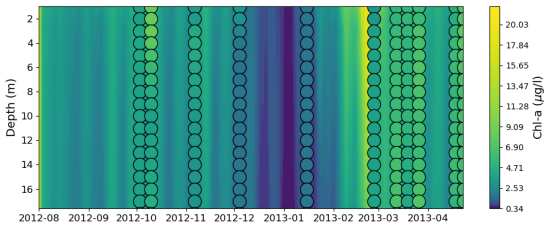

Figure A.49: Contours of modeled chlorophyll concentrations and observed chlorophyll concentrations in black circles through time at USGS Station 21

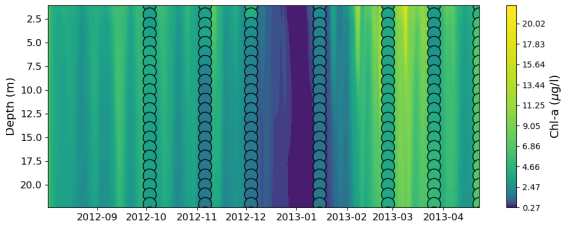

Figure A.50: Contours of modeled chlorophyll concentrations and observed chlorophyll concentrations in black circles through time at USGS Station 15

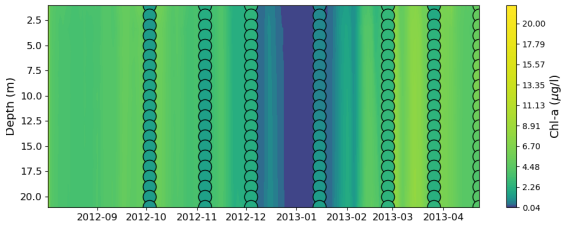

Figure A.51: Contours of modeled chlorophyll concentrations and observed chlorophyll concentrations in black circles through time at USGS Station 9

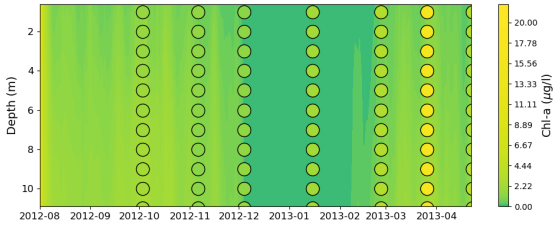

Figure A.52: Contours of modeled chlorophyll concentrations and observed chlorophyll concentrations in black circles through time at USGS Station 3

A.2.2 OXYGEN

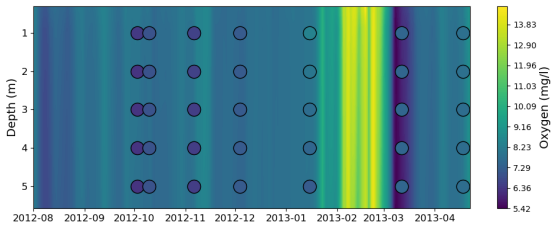

Figure A.53: Contours of modeled oxygen concentrations and observed chlorophyll concentrations in black circles through time at USGS Station 36

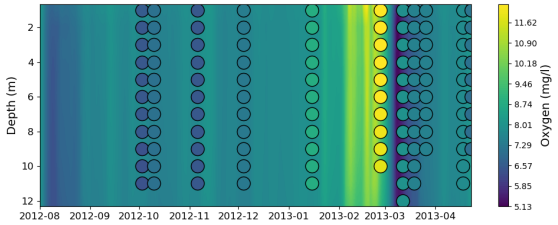

Figure A.54: Contours of modeled oxygen concentrations and observed chlorophyll concentrations in black circles through time at USGS Station 32

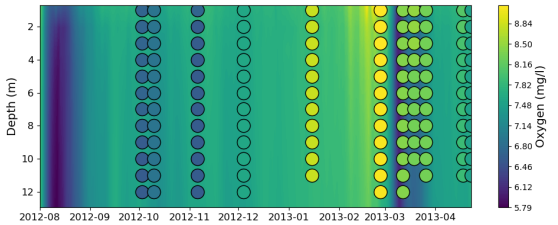

Figure A.55: Contours of modeled oxygen concentrations and observed chlorophyll concentrations in black circles through time at USGS Station 27

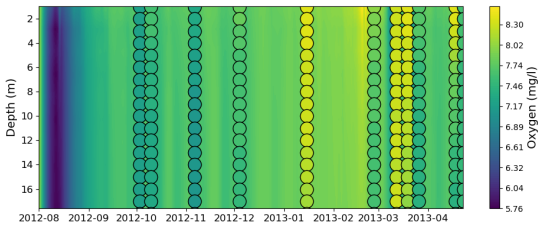

Figure A.56: Contours of modeled oxygen concentrations and observed chlorophyll concentrations in black circles through time at USGS Station 21

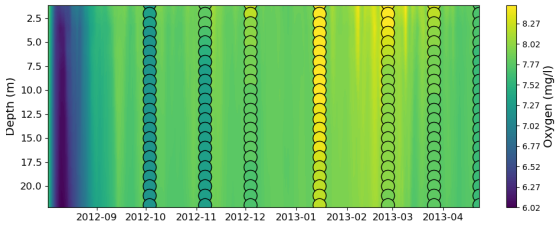

Figure A.57: Contours of modeled oxygen concentrations and observed chlorophyll concentrations in black circles through time at USGS Station 15

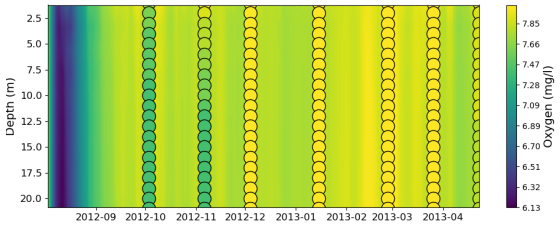

Figure A.58: Contours of modeled oxygen concentrations and observed chlorophyll concentrations in black circles through time at USGS Station 9

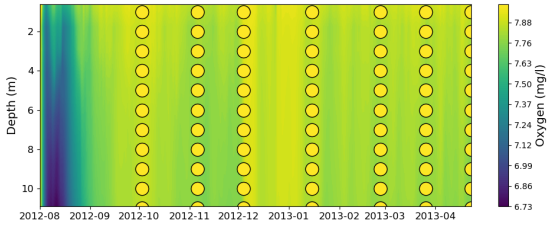

Figure A.59: Contours of modeled oxygen concentrations and observed chlorophyll concentrations in black circles through time at USGS Station 3

APPENDIX B BAY AREA HYDROLOGY MODEL

B.1 INTRODUCTION

Bay Area Hydrologic Model (BAHM) was originally developed by AQUA TERRA Consultants for Brake Pad Partnership (BPP) to estimate the copper from brake pad wear debris released to the Bay (Donigian and Bicknell, 2007). The model is built upon HSPF, a continuous simulation model capable of estimating flow and pollutant loads for mixed land use watersheds. The model delineated Bay area into 22 watersheds and simulated flow and sediment and copper loads from 1980 to 2005.
This modeling effort aims to update the model for broad use. Specially, the effort includes:

1. further delineated watershed into finer scale;
2. updated land use to most recent data;
3. extended model simulation period to 2017;
4. recalibrated model hydrology after the above changes were made;
5. produced flow time series as inputs to bay hydrodynamic model.

Below are the description of these efforts.

B.2 WATERSHED DELINEATION

The original model had the entire bay area delineated into 22 sub-basins. Current effort further delineated the areas directly draining into the bay into finer resolutions in order to meet the need of the Bay hydrodynamic model. The total sub-basins in the updated model are now 63.

B.3 LAND USE UPDATES

The 1992 National Land Cover Dataset (NLCD) was used in the original model, and grouped into six land use categories: Forest, Shrub/Wooded, Grass/Wetland, Developed Landscape, Impervious, and Agriculture. The land use data was updated to 2013 NLCD, classified in the same categories.

B.4 MODEL SIMULATION PERIOD

The model simulation period was updated from 1980-2005 to more recent period of 1999-2016 to be compatible with current needs. To do so, the model input data, including precipitation, evaporation, and urban irrigation, were collected and processed into model format. All model inputs are in English units.

B.4.1 PRECIPITATION

The HSPF model requires hourly precipitation. The precipitation from 20 NOAA weather stations across the Bay area were used in the model (Table B.1). Of these 20 stations, complete hourly data are available at only three stations and the rest of them have only daily data. The daily data were disaggregated into hourly data based on the rainfall patterns at nearby stations.

WEATHER STATIONS	LATITUDE	LONGITUDE	MAJOR SUB-BASINS
Berkeley	37.8744	-122.2589	East Bay North, Contra Costa West
Fairfield	38.2736	-122.0681	Solano West
Kentfield	37.9569	-122.5439	Upper Corte Madera, Marin South
Livermore	37.6947	-121.7778	Upper Alameda
Mount Hamilton	37.34361	-121.6425	Upper Alameda
Los Gatos	37.2319	-121.9592	Santa Clara Valley Central
Martinez Water Plant	38.0131	-122.1142	Contra Costa Central
Napa State Hospital	38.2775	-122.2642	Napa
Newark	37.5147	-122.0325	East Bay South
Palo Alto	37.4436	-122.1394	Santa Clara Valley West
Petaluma Airport	38.2578	-122.6078	Petaluma
Redwood City	37.47667	-122.23861	Peninsula Central
Saint Helena	38.5072	-122.4739	North Napa
San Jose*	37.3497	-121.9033	Coyote Creek
San Rafael Civic Center	37.9983	-122.5372	Marin North
SAN FRANCISCO DOWNTOWN*	37.7694	-122.4333	Upper Colma
SAN FRANCISCO WSO AP*	37.6581	-122.4378	Peninsula Central
Sonoma	38.2994	-122.4622	Sonoma, North Sonoma
Upper San Leandro Fltr	37.7719	-122.1675	East Bay Central, San Lorenzo Creek
WOODSIDE FIRE STN 1	37.4286	-122.2567	Upper San Francisquito

Table B.1: Weather stations and major sub-basins. * denotes hourly stations

Data Sources

All precipitation were downloaded from NOAA's weather data center website:
Hourly data: https://gis.ncdc.noaa.gov/maps/ncei/cdo/hourly
Daily data: https://gis.ncdc.noaa.gov/maps/ncei/cdo/daily

Missing Records

As common with weather data, there are missing records in most of weather stations (Table B.2). The missed data were filled by using data at nearby stations adjusted for average annual rainfall total. The annual rainfall for pertinent stations were obtained from PRISM. Table B.2 lists the stations with missing data, and the filling in stations, annual rainfall, and the adjusting factor.

Rain Gage	Data Gap?	Annual rain (in)	Fill in Gages	Annual rain (in)	Adjust factor
Berkeley	Y	27	Upper San Leandro Fltr	26	1.03
Fairfield	N	25		0	
Kentfield	N	40		0	
Livermore	N	15		0	
Mount Hamilton	Y	26	SAN JOSE 4.6 NE	17	1.51
Los Gatos	Y	22	San Jose	16	1.43
Martinez Water Plant	Y	20	MARTINEZ 0.8 SSE	21	0.98
Napa State Hospital	Y	27	Petaluma Airport	26.69286	1.01
Newark	Y	15	FREMONT	15.78737	0.98
Palo Alto	Y	16	Redwood City	20.23618	0.81
Petaluma Airport	N	27		0	
Redwood City	Y	20	Palo Alto	16.33855	1.24
Saint Helena	Y	37	SAINT HELENA 4 WSW	45.43298	0.82
San Jose	N	16		0	
San Rafael Civic Center	Y	34	Kentfield	40	0.85
SAN FRANCISCO DOWNTOWN	Y	24	SAN FRANCISCO 1.1 SW	24.21255	1.00
SAN FRANCISCO WSO AP	N	24		0	
Sonoma	Y	31	Petaluma Airport	26.69286	1.17
Upper San Leandro Fltr	N	26		0	
WOODSIDE FIRE STN 1	Y	30	Redwood City	20.23618	1.46

Table B.2: Weather stations and fill-in stations

2017 Daily Precipitation Daily precipitation data is downloaded from NCDC and then cleaned and filled in with the stations from the Table B.3. The data and the code for processing the data can be found in this github repository[27].

[27] `https://github.com/emmashie/Meteorology_Data_for_BAHM`

Station Name	Station Number	Fill Station Name	Fill Station Number	Fill Station Name 2	Fill Station Number 2	Fill Station Name 3	Fill Station Number 3	Adjust Factor (From Jing's prior work)
Berkeley	USC00040693	Upper San Leandro Fltr	USC00049185					1.03
Fairfield	USC00042934							
Kentfield	USC00044500							
Livermore	USC00044997	Livermore Municipal	USW00023285					1
Mount Hamilton	USC00045933	San Jose 4.6 NE	US1CASC0007	San Jose 3.5 ENE	US1CASC0012	Poverty California	USR0000CPOV	1.51
Los Gatos	USC00045123	San Jose 3.0 WSW	US1CASC0018	Cambrian Park 2.2	US1CASC0011	Saratoga 0.5 N	US1CASC0015	1.43
Martinez Water Plant	USC00045378	Martinez 0.8 SSE	US1CACC0001					0.98
Napa State Hospital	USC00046074	Petaluma Airport	USC00046826					1
Newark	USC00046144	Fremont	USC00043244					0.98
Palo Alto	USC00046646	Redwood City	USC00047339					0.81
Petaluma Airport	USC00046826	Petaluma 1.8 WSW	US1CASN0039					1
Redwood City	USC00047339	Palo Alto	USC00046646					1.24
Saint Helena	USC00047643	Saint Helena 4 WSW	USC00047646					0.82
San Jose	US1CASC0018	San Jose 6.2 W	US1CASC0032	San Jose 1.9 SW	US1CASC0052			1
San Rafael Civic Center	USC00047880	Kentfield	USC00044500					0.85
San Francisco Downtown	USW00023272	San Francisco 1.1 SW	US1CASF0004					1
San Francisco International Airport	USW00023234							
Sonoma	USC00048351	Petaluma	USC00046826					1.17
San Leandro	USC00049185	Oakland 1.2 ENE	US1CAAL0030					1
Woodside	US1CASM0022	Redwood City	USC00047339					1.46

Table B.3: Weather stations and fill-in stations for 2017

Data Disaggregation Since HSPF requires hourly meteorology data, the daily data need to be disaggregated into hourly data. To do so, hourly data were collected at additional stations that are not part of model stations (Table B.4). Given that the hourly data are available at different time periods for different stations and do not necessarily cover the full extent of a particular watershed, the disaggregation of most daily stations was based on the rainfall patterns at multiple nearby stations to improve accuracy. Table B.4 shows the daily stations and corresponding hourly stations that were used for disaggregation.

Daily Stations	Station Name	Hourly Stations		
CA040693	Berkeley	CA047772	WBAN:23230	
CA042934	Fairfield	CA042935	WBAN:93227	
CA044500	Kentfield	CA046826	CA047772	WBAN:93227
CA044997	Livermore	CA044995	WBAN:93228	
CA045933	Mount Hamilton	CA047821		
CA045123	Los Gatos	CA047821		
CA045378	Martinez Water Plant	CA042935	WBAN:23254	
CA046074	Napa State Hospital	CA046826	CA042935	WBAN:93227
CA046144	Newark	CA047821	WBAN:23244	WBAN:93228
CA046646	Palo Alto	CA047821	CA047769	WBAN:23244
CA046826	Petaluma Airport	CA046826	WBAN:93227	
CA047339	Redwood City	CA047769	WBAN:23244	
CA047643	Saint Helena	CA047646	CA046826	WBAN:93227
CA047821	San Jose	CA047821		
CA047880	San Rafael Civic Center	CA046826	CA047772	
CA047772	SAN FRANCISCO DOWNTOWN	CA047772	CA047769	
CA047769	SAN FRANCISCO WSO AP	CA047769		
CA048351	Sonoma	CA046826	CA047646	WBAN:93227
CA049185	Upper San Leandro Fltr	CA047772	WBAN:23230	WBAN:93228
CA049792	WOODSIDE FIRE STN 1	CA047769	CA047821	WBAN:23244

Table B.4: Daily stations and corresponding hourly stations for disaggregation

2017 Hourly Data Many of the CAXXXXXX stations stopped in 2013/2014, so hourly data at the WBANXXXXX stations is used. Table B.5 shows available hourly data corresponding to daily stations. This data and the code for processing the data can be found in this github repository[28].

USGS Station#	Name	Volume error%	Model Efficiency
11164500	San Francisquito Creek at Stanford University CA	5	0.45
11169000	Guadalupe River at San Jose CA	14	0.13
11172175	Coyote Creek above HWY 237 at Milpitas CA	64	-1.41
11179000	Alameda Creek near Niles, CA	8	0.72
11181040	San Lorenzo Creek at San Lorenzo CA	9	0.51
11458000	Napa River near Napa CA	1	0.76
11458500	Sonoma Creek at Agua Caliente CA	3	0.51
11460000	Corte Madera Creek at Ross CA	2	0.72

Table B.5: Daily stations and corresponding hourly stations for disaggregation for 2017

Evaporation Another key meteorologic input for HSPF is evaporation. For evaporation, HSPF

[28] https://github.com/emmashie/Meteorology_Data_for_BAHM

generally uses measured pan evaporation to derive an estimate of lake evaporation, which is considered equal to the potential evapotranspiration (PET) required by the model, i.e., PET = (pan evap) X (pan coefficient.) The actual simulated evapotranspiration is computed by the program based on the model algorithms that calculate dynamic soil moisture conditions, as a function of the rainfall, model ET (evapotranspiration) parameters, and the input PET data.
The original model used Pan evaporation data from the Los Alamitos gage in San Jose and adjusted it for using in other watersheds by the ratios of the CIMIS (Califronia Irrigation Management Information System[29]) values for the corresponding zones. However, it is concluded that using just one set of data for the entire bay area with very distinctive micro-climates zone created too much uncertainty in the estimated evaporation data. Therefore, a different approach was employed to derive evaporation data for current model, as described below.
Hourly evapotranspiration data from 1999 to 2015 at 5 CIMIS stations were downloaded from CIMIS website[30]. The evapotranspiration from CIMIS is considered equivalent to PET in HSPF model. These stations fall into 5 different (ETO) zones (Table B.6). For watersheds within these 5 zones, the hourly time series was directly used, and for those in different zones, the ratios of the CIMIS values for the corresponding ETO zones (ETO zones map[31]) was used to adjust the data set. In the end, each zone within the Bay area has its own hourly evapotranspiration data, which was then applied to each watershed within that zone.

Station ID	Station Name	CIMIS Region	Latitude	Longitude	Eto Zone
47	Brentwood	San Francisco Bay	37.928258	-121.6599	14
144	Petaluma East	North Coast Valleys	38.266428	-122.61646	5
149	Oakland Foothills	San Francisco Bay	37.780653	-122.18015	1
170	Concord	San Francisco Bay	38.015372	-122.02028	8
171	Union City	San Francisco Bay	37.598758	-122.05323	6

Table B.6: CIMIS stations for hourly evapotranspiration

Table B.6 comment: For 2017, Oakland Foothills (149) is no longer available, so El Cerrito (213) is used in place. This data and the code for processing the data can be found in this github repository[32] - Missing data was filled using the data from the other station scaled by the monthly ratios of Eto Zone from the CIMIS website.
As with precipitation, there were also missing data in CIMIS record. For each station, the data gap was filled by using monthly regression equation between evapotranspiration and temperature. The regression was carried out from all available data for each month, and the missed data were estimated using its monthly equation.
Urban Irrigation The developed urban and agricultural land use receives irrigation applications. With Bay Area's semi-arid climates, supplemental irrigation can and does have a significant impact on the hydrologic regime and stormwater runoff, potentially changing ephemeral streams into perennial ones. Often the irrigation applications will exceed annual rainfall by 50% to 100% or more (Donigian and Bicknell, 2007).

[29] http://wwwcimis.water.ca.gov/cimis/data.jsp
[30] http://www.cimis.water.ca.gov/Stations.aspx
[31] http://wwwcimis.water.ca.gov/App_Themes/images/etozonemap.jpg
[32] https://github.com/emmashie/Meteorology_Data_for_BAHM

Current model used the same approach as the original model to calculate urban and agricultural irrigation applications, which was based on prior modeling studies both in the Bay Area in Alameda County (AQUA TERRA Consultants, 2006) and in Ventura County of Southern California (AQUA TERRA Consultants, 2005). The approach assumes that irrigation systems would be used to make up monthly lawn and crop evapotranspiration (ET) demands that exceed available rainfall. The calculation requires rainfall, evapotranspiration, crop coefficient, and efficiency of irrigation system.
For calculating irrigation applications, the Bay area watersheds were lumped into six regions - Marin, East Bay, East Bay Inland, South Bay, Peninsula, and North Bay. The daily irrigation application was calculated for each region and applied to urban and agricultural land uses for every watershed within that region. Table B.7 lists the weather stations and CIMIS zone that were used for calculation for each region. The steps of calculating daily irrigation applications are:

1. Estimate mean rainfall region-wide
2. Use the CIMIS zones for ETo; use average when there are 2 zones
3. Use a crop coefficient, Kc= 0.70, as an average for urban and agriculture
4. Calculate the ratio of the rain gage mean (from the timeseries) to the region mean (Step 1)
5. Using the region rainfall, region Eto, and Kc, calculate the irrigation demand timeseries
6. Use an irrigation efficiency of 0.80 (account for loss), midway between the urban and agriculture values to calculate irrigation need
7. Estimate the amount of irrigation applied based on Irrigation needed while applying antecedent rain condition for previous 7 days. Within the model input file, a reduction factor of 0.65 for urban and 0.85 for agriculture was used to reduce the irrigation amount by the fraction of the area that was assumed to be irrigated.

Region/Group	Watersheds	Rain Gage	CIMIS Zones
Peninsula	Peninsula Central	Redwood City	2, 6
	Upper Colma		
	Upper San Francisquito		
South Bay	Santa Clara Valley West	San Jose	8
	Santa Clara Valley Central		
	Coyote Creek		
East Bay	Contra Costa West	Upper San Leandro	1, 6
	East Bay North		
	East Bay Central		
	Upper San Lorenzo		
	East Bay South		
East Bay Inland	Contra Costa Central	Martinez Water Plt	8, 14
	Upper Alameda		
North Bay	Solano West	Napa State Hospital	5, 8
	Napa/Napa North		
	Sonoma/North Sonoma		
	Petaluma		
Marin	Marin North	San Rafael Civic Center	5
	Upper Corte Madera		
	Marin South		

Table B.7: Irrigation groups, rain gages, and CIMIS zones

B.5 Model Calibration

The updated model was calibrated at 8 USGS stations where long-term flow data are available (Table B.8). The calibration period is 1999-2016. HSPF calibration procedure involved a âĂŸweight of evidenceâĂŹ approach with multiple graphical and statistical comparisons of observed and simulated flows. Overall, model calibration was fair to good for 6 of 8 stations, judged by two key statistics that measure model performance âĂŞerror in total volume and Nash model efficiency. The two stations - Guadalupe River at San Jose (discontinued at 2003) and Coyote Creek above highway 237 at Milpitas, CA, were not well calibrated. Both are large watersheds with reservoirs and complex water supply systems that intake and divert water in and out of the watersheds, which are not included and addressed in the current model. It is anticipated that model calibration will be improved if future updates take all important sources and sinks into account.

USGS Station#	Name	Volume error%	Model Efficiency
11164500	San Francisquito Creek at Stanford University CA	5	0.45
11169000	Guadalupe River at San Jose CA	14	0.13
11172175	Coyote Creek above HWY 237 at Milpitas CA	64	-1.41
11179000	Alameda Creek near Niles, CA	8	0.72
11181040	San Lorenzo Creek at San Lorenzo CA	9	0.51
11458000	Napa River near Napa CA	1	0.76
11458500	Sonoma Creek at Agua Caliente CA	3	0.51
11460000	Corte Madera Creek at Ross CA	2	0.72

Table B.8: Calibration stations and model statistics

After model calibration, the model parameters from calibration watersheds were assigned to the rest of watersheds that were not calibrated. The assignment was based on the principals of the paired watersheds should be fairly close to each other and generally in the same micro-climate. Table B.9 shows how the watersheds were paired for assigning model parameters.

Watersheds	Name	Use Parameter from...final
Contra Costa Central	CCOSTAC	Alameda Creek near Niles, CA
Contra Costa West	CCOSTAW	San Lorenzo Creek at San Lorenzo CA
Coyote Creek	COYOTE (a -d)	Alameda Creek near Niles, CA
East Bay Central	EBAYC (a-c)	San Lorenzo Creek at San Lorenzo CA
East Bay North	EBAYN	San Lorenzo Creek at San Lorenzo CA
East Bay South	EBAYS	Alameda Creek near Niles, CA
Marin North	MARINN	Sonoma Creek at Agua Caliente CA
Marin South	MARINS	Corte Madera Creek at Ross CA
Napa	NAPA	Napa River near Napa CA
North Napa	NNAPA	Napa River near Napa CA
North Sonoma	NSONOMA	Sonoma Creek at Agua Caliente CA
Peninsula Central	PENINSUL (a-b)	San Francisquito Creek at Stanford University CA
Petaluma	PETALUMA	Sonoma Creek at Agua Caliente CA
Santa Clara Valley Central	SCLARAVC (a-c)	Guadalupe River at San Jose CA
Santa Clara Valley West	SCLARAVW	San Francisquito Creek at Stanford University CA
Solano West	SOLANOW (a-c)	Napa River near Napa CA
Sonoma	SONOMA	Sonoma Creek at Agua Caliente CA
Upper Alameda	UALAMEDA (a-g)	Alameda Creek near Niles, CA
Upper Colma	UCOLMA	San Francisquito Creek at Stanford University CA
Upper Corte Madera	UCMADERA	Corte Madera Creek at Ross CA
Upper San Francisquito	USANFRAN	San Francisquito Creek at Stanford University CA
Upper San Lorenzo	USANLORZ	San Lorenzo Creek at San Lorenzo CA

Table B.9: Paired watersheds for assigning model parameters

B.6 Model Results

The daily timeseries of flow from 1999 to 2017 for each sub-watersheds that directly drains to the Bay were generated, to be used as an input to the Bay hydrodynamic model.

B.7 References

Donigian, Jr. A. S. and Bicknell, B. R., 2007. Modeling the Contribution of Copper from Brake Pad Wear Debris to the San Francisco Bay. Final Report. Prepared for Association of Bay Area Governments, Oakland, CA, and California Department of Transportation, Sacramento, CA. October 2, 2007.

AQUA TERRA Consultants, 2006. Hydrologic Modeling of the Castro Valley Creek and Alameda

Creek Watersheds with the U. S. EPA Hydrologic Simulation Program âĂŞ FORTRAN. Final Report. Prepared for the Alameda Countywide Clean Water Program, Hayward, CA. January 20, 2006.

AQUA TERRA Consultants, 2005. Hydrologic Modeling of the Calleguas Creek Watershed with the U.S. EPA Hydrologic Simulation Program âĂŞ FORTRAN. Final Report. Prepared for the Ventura County Watershed Protection District, Ventura CA. March 10, 2005.

APPENDIX C DISCHARGE AND NUTRIENT LOADS

Throughout the development of the hydrodynamic and biogeochemical models, intentional effort was put towards gathering data inputs to the model in a way that allows for other model years to be run with minimal effort. For example, during the process of gathering meteorology data for the hydrology model, data was gathered for the years 2000-2016. These 16 years of data were used in the hydrology model and freshwater flows were calculated for the whole time frame. Similarly for waste water treatment plant (WWTP) nutrient loads were compiled for the same years. The compiled 16 years of freshwater flow[33] and nutrient load[34] data can be found in two github repositories. This data compilation and the code[35] used to setup model runs are all a part of our emphasis on developing open access models that lend themselves to collaboration between different projects, as well, as science institutes and agencies.

[33] https://github.com/rustychris/sfbay_freshwater
[34] https://github.com/rustychris/sfbay_potw
[35] https://github.com/rustychris/sfb_dfm

APPENDIX D LIGHT FIELD

D.1 INTRODUCTION

The goal of this project was to develop a daily, space-varying light field (light extinction coefficient) throughout the San Francisco Bay for use in DELWAQ model runs. The light extinction coefficient (K_{ext}) is a key parameter in the development of phytoplankton blooms, and thus we hoped to improve bloom predictability through implementing an improved light field input to the model. We developed this light field via stitching together a high-frequency suspended sediment concentration (SSC) dataset collected by the USGS, as well as discrete SSC and K_{ext} samples collected by the USGS Polaris/Peterson cruise.

This product was developed knowing that it would be far from perfect, but that any daily light field dataset complete in time and space would be an improvement on the current lack of availability of a light-field product for SF Bay. The main goal was to develop a product that approximately captures the correct K_{ext} magnitude range and seasonal variability throughout SF Bay.

D.2 DATASET

The primary dataset used to develop the daily light field is from a collection of 15 USGS high-frequency water quality sondes throughout SF Bay (Figure D.1). The sondes collect 15-minute, high-frequency optical turbidity data, which has been converted to SSC estimates using regressions developed through discrete SSC sample collection at the instrument locations. In our development of this product, we averaged the 15-minute SSC data into daily averages.

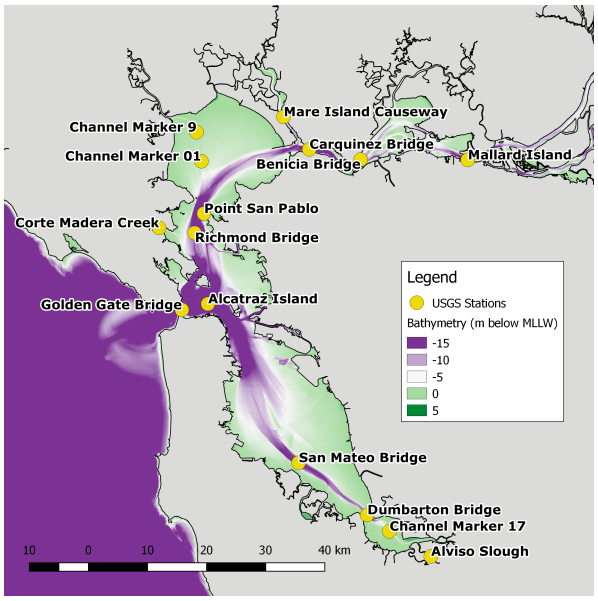

Figure D.1: Map of USGS high frequency stations used in developing the SF Bay light field

The dates of data collected ranges from February 26th, 1992 (Channel Marker 17) to the present, although the date range of each station varies. For the purposes of developing this daily product, we used the date range of 02/26/1992 âĂŤ 12/31/2017. Table D.1 displays the date range of data produced by each station, along with the total days that each station logged measurements and the depth of the instrument.

Figure D.2 displays the instrument measured, daily averaged SSC data for each station. As shown, there are data time gaps at each station, with some more extensive than others. Through inter and intra-station interpolation efforts described in section three, we were able to 1) estimate SSC values at each station for all days with missing data, 2) convert the resulting SSC values to Kext, and 3) spatially extrapolate the station values to polygons that cover the extent of the open bay and the DELWAQ model grid.

Station	Year Start	Year End	# Days With Instrument Measurements	Depth/Height of Instrument
Alcatraz Island	2003	Present	3606	Unknown
Alviso Slough	2010	2017	2025	Unkown
Benicia Bridge	1996	Present	5283	71 ft from bed
Carquinez Bridge	1998	2005	1718	48 ft from bed
3/1/01	2003	2005	423	Unknown
3/9/01	1998	2003	1302	Unknown
3/17/01	1992	2005	2941	Designated as ÂŚUpperÂŠ instrument
Corte Madera Creek	2010	2013	855	Unknown
Dumbarton Bridge	1992	Present	5007	25 ft from bed
Golden Gate Bridge	1996	1997	336	Unknown
Mallard Island	1994	Present	7562	3.3 ft from water surface
Mare Island Causeway	1998	2005	1920	Designated as ÂŚUpperÂŠ instrument
Point San Pablo	1992	2005	3078	Designated as ÂŚUpperÂŠ instrument
Richmond Bridge	2006	Present	2951	30 ft from bed
San Mateo Bridge	1992	2005	1796	44 ft from bed

Table D.1: USGS High Frequency Station Information

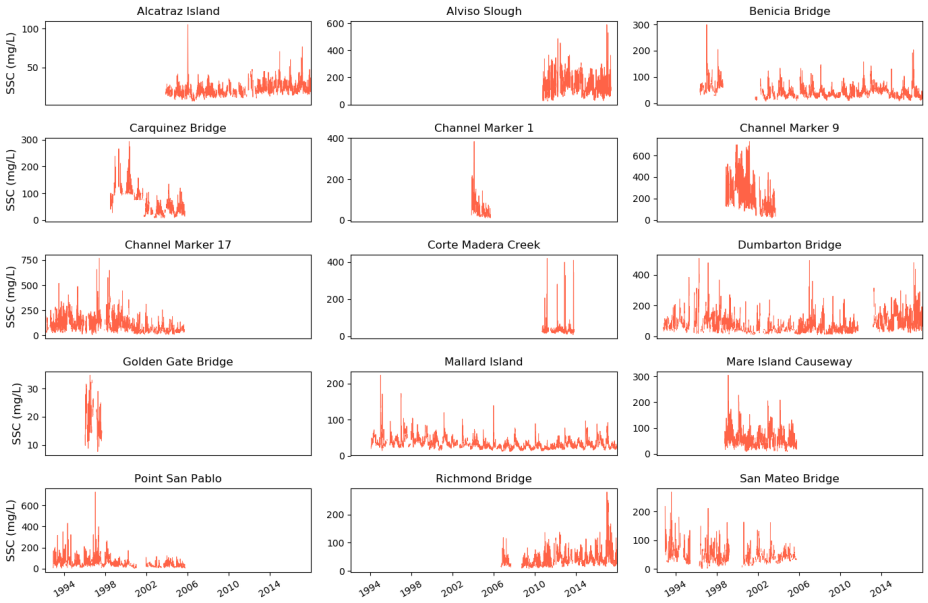

Figure D.2: Time-series of the instrument measured, daily averaged SSC data available from each USGS high frequency stations.

In order to convert from SSC to Kext, we use discrete data collected by the USGS Polaris/Peterson cruises. Dating back to 1977, the Polaris/Peterson cruises have collected discrete suspended particulate matter (SPM) samples together with measured Kext values. This has resulted in 900 samples directly comparing the two measurements. We use these 900 samples to generate a linear regression equation to convert SSC data into estimated Kext values (see section D.3.6).

D.3 Station Data Temporal Interpolation

We employ three techniques, in the order seen below, for estimating missing daily SSC data at each station:

1. Log-linear regression estimation across stations
2. Within-station linear interpolation
3. Station monthly mean

Importantly, we note that if there is instrument measured data in the original dataset, this is automatically left in the final dataset. We only estimate values for days with missing data. The steps below describe our methods for estimating missing data points.

D.3.1 Log-Linear Regression Estimation

The first level of data filling is through the use of a log-linear regression approach to estimate days of missing SSC data. After first taking the natural logarithm of the entire dataset of instrument measured daily averages, the approach then has the following steps:

1. Locate a day of missing data at a specific station.
2. Find all stations throughout the bay on that same day that have instrument measured data, and select those stations. For example, on a day of missing data at Richmond Bridge, there might be recorded data on that day at Alcatraz Island, Benicia Bridge, and Dumbarton Bridge.
3. For each overlapping selected station (Alcatraz Island, Benicia Bridge, Dumbarton Bridge), we look throughout the entire dataset to find how many days of instrument measured data overlap each station has with the data-gap station (Richmond Bridge). We only keep stations for the regression estimation that have at least 100 days of measured data overlap with the data-gap station. For example, if Alcatraz Island only has 5 days of overlap with Richmond Bridge, we drop Alcatraz Island. Whereas if Benicia Bridge and Dumbarton Bridge each have 100 and 900 days, respectively, of overlap with Richmond Bridge, we will keep those stations for the log-linear regression estimation.
4. Once we have selected all stations which have at least 100 days of measured data overlap with the data-gap station, we then select across time the days when all of those stations have overlapping instrument data. For example, there may be 77 days throughout the entire time frame (1992-2017) that Richmond Bridge, Dumbarton Bridge, and Benicia Bridge have all recorded instrument measured data. These 77 days will be the dataset used to develop the linear regression equation to estimate this specific day of missing data at Richmond Bridge. We only proceed with this method if the total number of overlapping data days is greater than 50 days.
5. With this final qualifying dataset, we develop a linear regression equation (e.g. Richmond = a + b*Benicia + c*Dumbarton), and use this equation to estimate the missing data point. We note that this method of regression estimation entails that a different equation can be developed for each day of missing data at each station (since the specific regression equation is dependent on which other stations have available data on the day of missing data). Due to the fact that the stations come on and offline so frequently (thus creating many combinations of overlapping station data), it would be difficult to have a generalized regression equation for each station.

6. Exponentiate the estimated SSC value ($e^{estimated\ SSC\ value}$) to return the final SSC estimate (since the regression estimation was performed on the natural log of the original dataset).

D.3.2 Within-Station Linear Interpolation

For missing data points that do not qualify for the log-linear interpolation method, the next level of data filling is to use within-station linear interpolation. For this method, if there is a data gap at a station that is less than or equal to 30 days, we linearly interpolate that data gap using the two surrounding data points (before and after the gap) from that station to generate the linear equation. We do not discriminate on whether the before/after points used to generate the linear equation are instrument data or log-linear filled data.

D.3.3 Station Monthly Mean

The final step is to fill in any data gaps that are longer than 30 days. For this step, we use the station SSC monthly mean (of real instrument data, i.e. not including interpolated data) as the estimated value.

D.3.4 'Ocean' Station

We include an 'Ocean' station in order to represent the zone outside of the Golden Gate. There is no instrument data for our 'Ocean' station, and thus we define our estimates for this station as being 0.75*('Golden Gate Bridge'). Having an ocean zone that is proportionally less than the golden gate bridge station data is useful for modeling purposes, but it should be recognized that this is not an official station based off of its own data.

D.3.5 Data Flags

After completing the above steps, we are left with a complete dataset at daily intervals for each of the 16 station locations (including the 'Ocean' station) for 02/26/2017 to 12/31/2017. We assign the following flags to the types of data included in the dataset:

1. Daily Averaged Instrument Data
2. Log-Linear Interpolated Data
3. Within-Station Linear Interpolation
4. Station Monthly Mean
5. 0.75*'Golden Gate Bridge'

Table D.2 provides a per station breakdown of the percentage of data represented by each data type over the 1992-2017 timeframe, and Figure D.3 presents a time series of the completed daily SSC dataset for each station, with each color corresponding to the data flags indicated above (note that the 'Ocean' station is not plotted). Enlarged time series plots for each station are presented in Light Field Appendix 1.

Station	1 - Instrument Data (%)	2- Log-Linear (%)	3 - Within Station Linear (%)	4 - Monthly Mean (%)	5 - 0.75*Golden_Gate_Bridge (%)
Alcatraz Island	38.2	51.8	4.7	2.5	0
Alviso Slough	21.4	48.8	13.3	13.9	0
Benicia Bridge	56	28.7	8.7	5.1	0
Carquinez Bridge	18.2	69.3	6.3	2.5	0
Channel Marker 1	4.5	82.3	6.3	2.5	0
Channel Marker 9	13.8	60.6	14.3	8.1	0
Channel Marker 17	31.2	58	7	0.1	0
Corte Madera Creek	9.1	60.5	13.3	13.9	0
Dumbarton Bridge	53	35.8	6.4	2.9	0
Golden Gate Bridge	3.6	47.3	28.2	18.4	0
Mallard Island	80.1	12.7	4	2.5	0
Mare Island Causeway	20.3	67.7	5.5	2.9	0
Point San Pablo	32.6	55.5	6.1	2.9	0
Ocean	0	0	0	0	100
Richmond Bridge	31.3	39.5	13.3	13.9	0
San Mateo Bridge	19	67	7.9	2.5	0

Table D.2: Percentage of data assigned to each flag (per station).

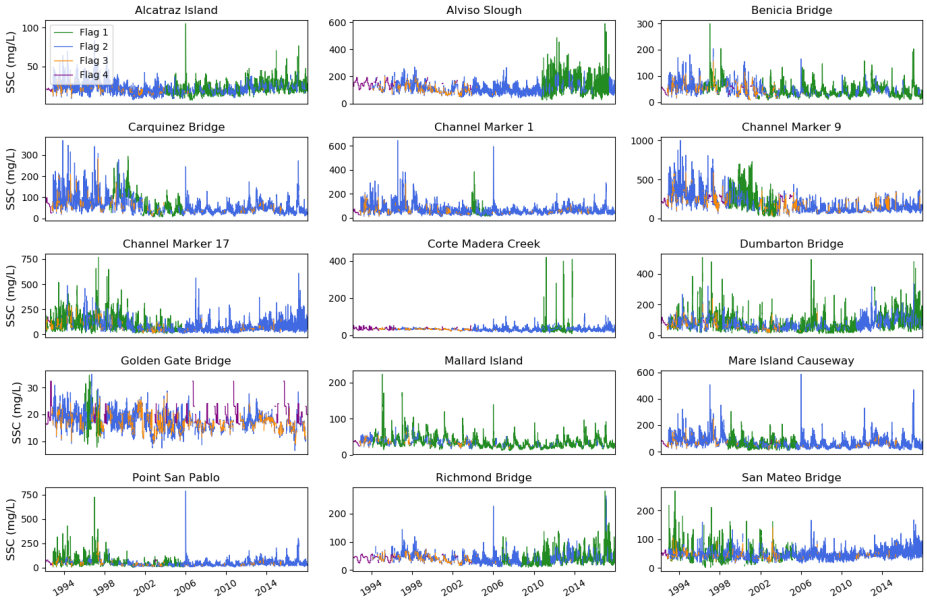

Figure D.3: Time series of the completed daily SSC dataset for each station. The colors correspond to the different data flags (Green: instrument measured data; Blue: Log-linear estimated data; Orange: Within-station linear interpolation; Purple: Station monthly average). Zoomed-in time series for each station can be found in Light Field Appendix 1

D.3.6 SSC to Light Extinction Coefficient (K_{ext})

As mentioned in Section 2, we utilize a collection of 900 simultaneous measured samples of SPM and K_{ext} in order to estimate K_{ext} values from the complete SSC dataset (K_{ext} values are used as the direct input to the DELWAQ model). Figure 4 displays the resulting linear relationship between SPM and K_{ext} (R2 = 0.83, P-Value < 0.01). We use SPM as a proxy for SSC, and thus convert our daily SSC data to K_{ext}.

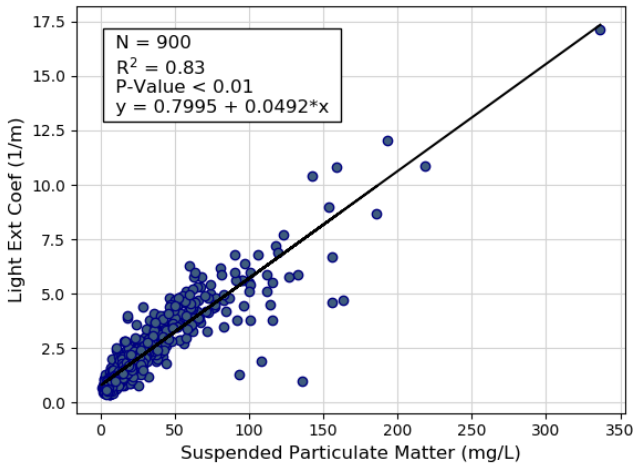

Figure D.4: Discrete SPM vs measured light extinction coefficient data from USGS Polaris/Peterson cruises. This measured regression relationship is used to convert SSC data to light extinction coefficient in generating our light field.

D.3.7 Spatial Interpolation to DelWAQ Grid

In order for the completed daily dataset to be useful as a DELWAQ Model input, we spatially interpolate the individual station data over the cells of the model grid. For this process, we first designate the polygonal coverage represented by each station. Figure D.5 presents the polygons assigned to each station, along with the underlying DELWAQ grid. These polygons were determined based off of institutional knowledge and visual inspection of satellite imagery.

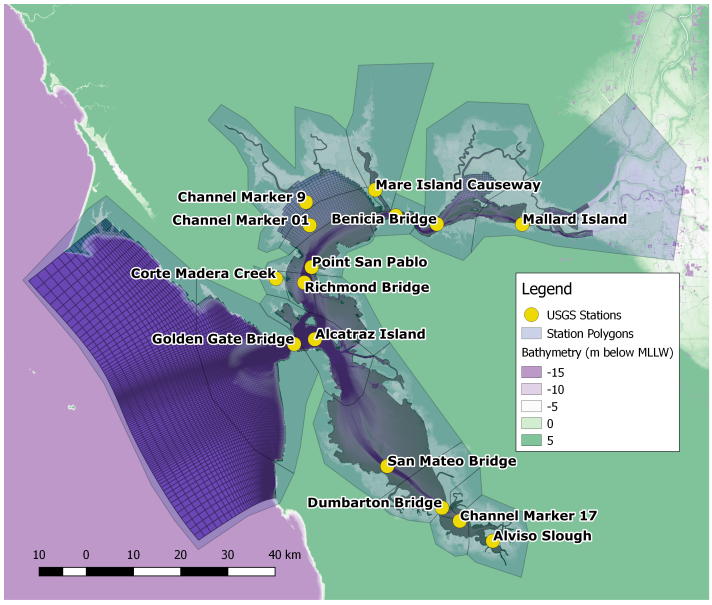

Figure D.5

Next, we determine which cells of the DELWAQ grid lie within each stationâĂŹs polygon

(determined by the centroid of each DELWAQ grid cell), and assign the respective station data to all cells that lie within each stationâĂŹs polygon. In order to avoid harsh spatial gradients in K_{ext}, we then perform a smoothing method across the DELWAQ cells. To smooth the data, we take the average of each cell with its neighboring cells, for a total of 75 rounds of averaging. Figure D.6 provides a before and after of the initial DELWAQ grid data assignment with the final smoothed version (for one day of data).

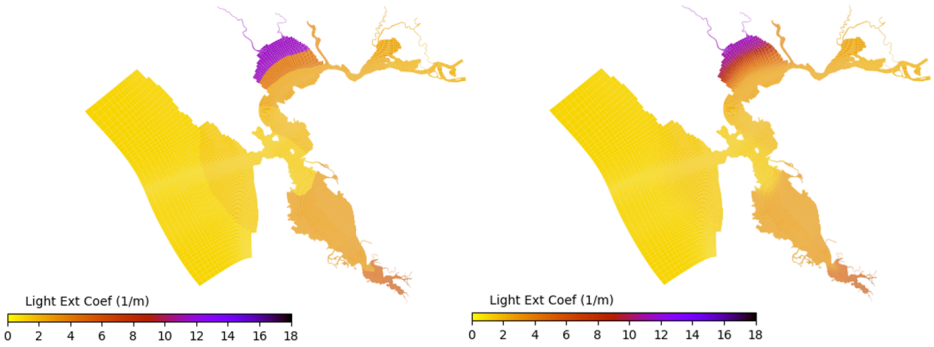

Figure D.6

D.3.8 Final Data Format

The complete station data is stored in netCDF format, and contains the following variables:

1. Suspended Sediment Concentration (mg/L)
2. Light Extinction Coefficient (1/m)
3. Flag

Along with the following coordinates:

1. Time (day)
2. Station
3. UTM east
4. UTM north
5. Latitude
6. Longitude

The station data is additionally stored in CSV format, with each variable stored in a separate file. The data is not stored as a DELWAQ text file, as the format of the model input changes depending on the characteristics of the model run. Once the specifics of the model run are determined, the station data can be merged and smoothed onto the DELWAQ grid for the specified model run.

D.4 Interpolation Sucess Metrics

We tested our log-linear regression estimation method on the measured instrument data in order to get a metric of the success of our method. To do this, we ran through the entire dataset of instrument measured values and tested the log-linear estimation approach against those real values (i.e. treating the real values the same as if they were missing values, and comparing the estimated result from the log-linear regression approach to the real value).
In the original dataset, there are 40,803 days with instrument measured values. Through our developed overlap filtering methods, we were able to test the log-linear approach against 37,295 instrument measured values (the regression approach is not used if there are less than 50 total overlapping days of data between the stations).
The median of the absolute difference between measured and estimated values is 8.22 mg/L. The median percent error between measured and estimated values is 19.98 % [(abs(estimated âĂŞ real)/real) * 100]. The median R2 of the log-linear regression equations is 0.49. Figure D.7 shows the results of the testing plotted as histograms, and Table 3 presents the median regression statistics per station.

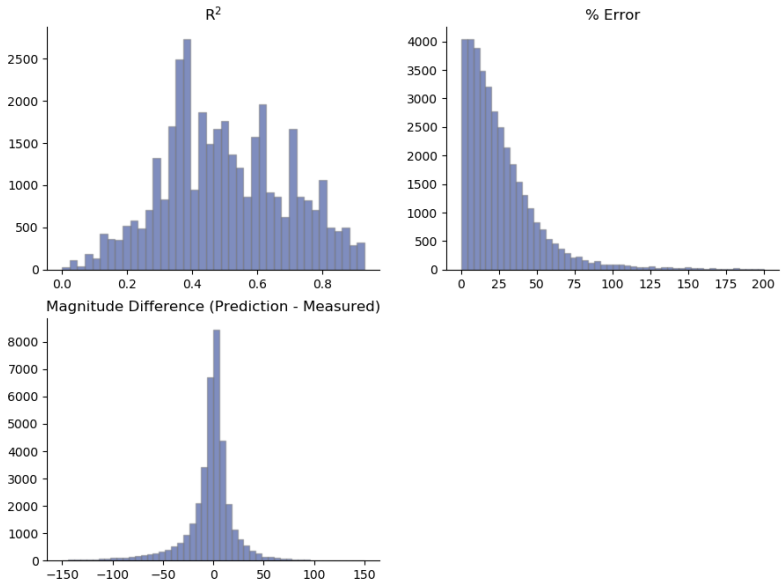

Figure D.7: Summary histograms from testing the log-linear regression estimation method on the measured instrument data. The histograms represent the results of 37,295 tests of the method (although a small number of test results are excluded for visual purposes, explained below).

Station	Median Percent Error	Median Absolute Difference (Estimated - Real)	Median R2
Alcatraz Island	13.9	2.84	0.5
Alviso Slough	25.5	31.4	0.37
Benicia Bridge	18.2	7.06	0.59
Carquinez Bridge	16.9	8.01	0.68
3/1/01	20.6	10.28	0.7
3/9/01	28.3	61.6	0.45
3/17/01	26	23.3	0.65
Corte Madera Creek	20.9	6	0.24
Dumbarton Bridge	27.6	18	0.44
Golden Gate Bridge	17.5	3.5	0.18
Mallard Island	16.7	4.9	0.38
Mare Island Causeway	19.2	10.9	0.62
Point San Pablo	22.4	10.8	0.56
Richmond Bridge	20.5	7.4	0.63
San Mateo Bridge	24	10.4	0.36

Table D.3: Median regression statistics per station in testing the log-linear estimation approach on instrument measured data.

We note that the histogram for percent error is capped at 200% for visual purposes, and the magnitude difference is capped at -150 and 150 for the same reason, but there are values that exceed these limits. As can be seen in the tailing off nature of the histograms, however, there are only a small quantity of values beyond these limits. For example, the highest percent error is 2,316%. In this case, the measured value was 1.61 mg/L, and the estimated value was 38.86 mg/L. This is likely to be either an anomalous event not captured in the scope of the log-linear regression, or a measurement error.

While the log-linear regression approach is certainly not perfect, it is important to remember that the guiding light of this project was to develop a daily sediment/light field in SF Bay that is better than the current lack of a similar accessible product. We also note that the log-regression approach performs quite well overall, with a low median absolute magnitude difference between measured and estimated values, and a relatively low median percent error. The most important metric of this product is whether the magnitudes of the predicted values are close to the range of where they should be for the specific station and time of year, as the relative magnitudes of SSC are what determine the K_{ext}. A median magnitude difference between measured and estimated values of only 8.22 mg/L gives us confidence in the quality of the light field product and its ability to capture spatial and temporal variations throughout SF Bay.

Figure D.8 presents a few examples of time-series results of the measured instrument data plotted together with the corresponding regression estimated values. A five-year and one-year window are displayed for Mallard Island, Point San Pablo, and Dumbarton Bridge. These plots present examples of both the strengths and weaknesses of the regression estimation approach.

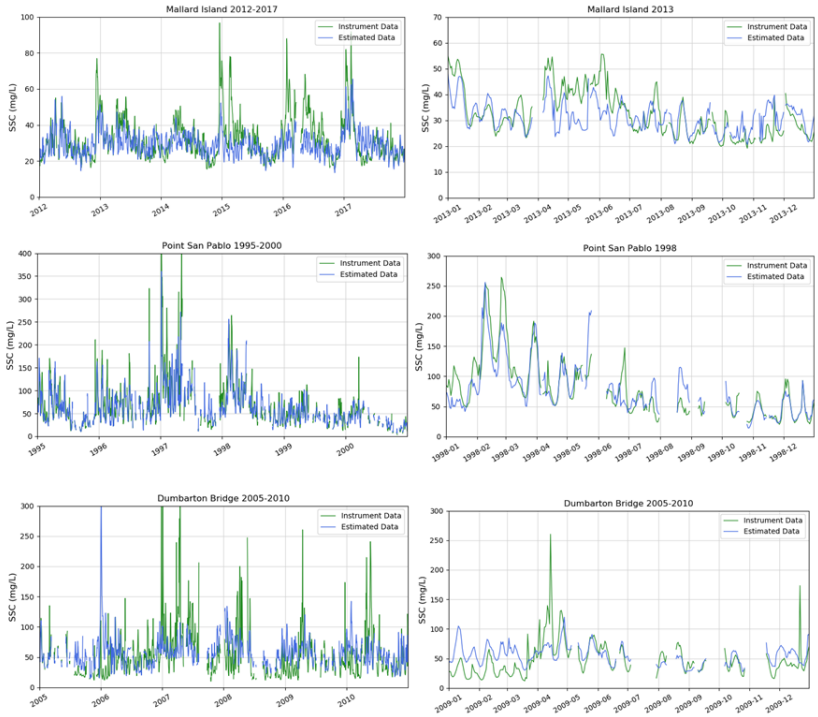

Figure D.8: Time-series plots for three stations comparing instrument measured data together with the corresponding regression estimated values. For each station, a five-year plot and one-year plot are presented.

D.5 Light Field Appendix 1

The first two sets of plots in the appendix show yearly summary boxplots of the data. The first set contains yearly summary boxplots of the complete daily dataset, and the second set contains yearly summary boxplots of the instrument measured dataset (i.e. does not include the estimated values for missing days of data).
The rest of the plots show the complete dataset (instrument measured + estimated data) for each station. The flags correspond to the following data types:

1. Daily Averaged Instrument Data
2. Log-Linear Interpolated Data
3. Within-Station Linear Interpolation
4. Station Monthly Mean

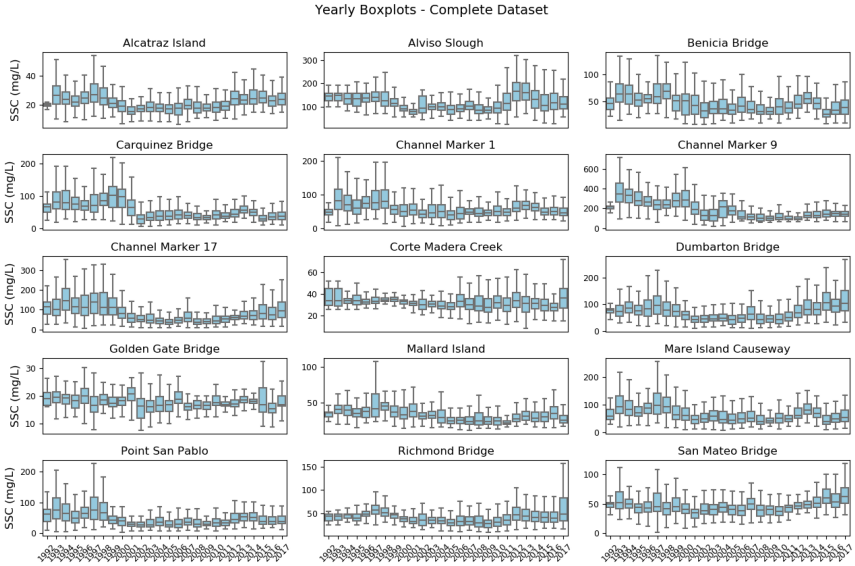

Figure D.9

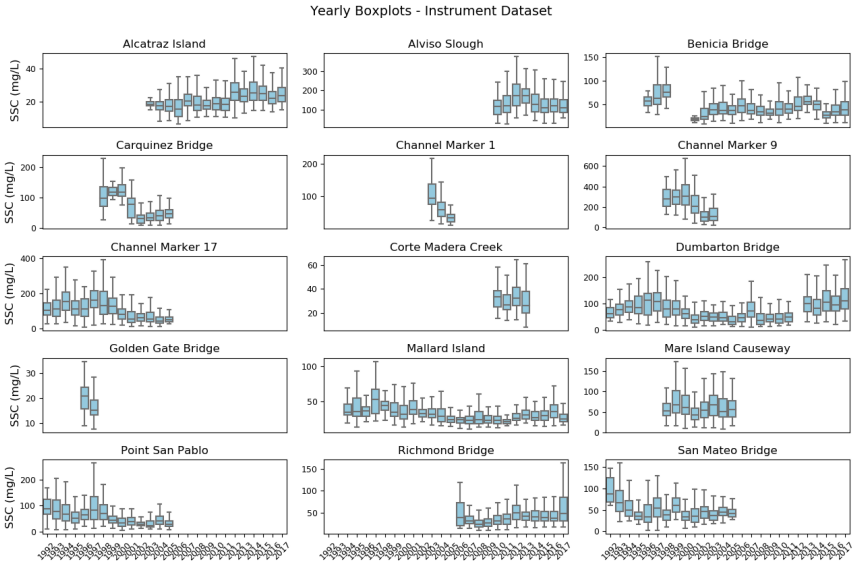

Figure D.10

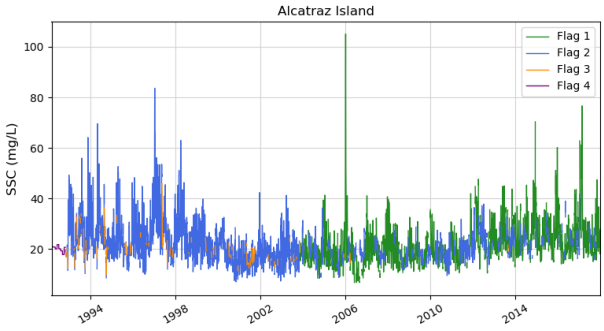

Figure D.11

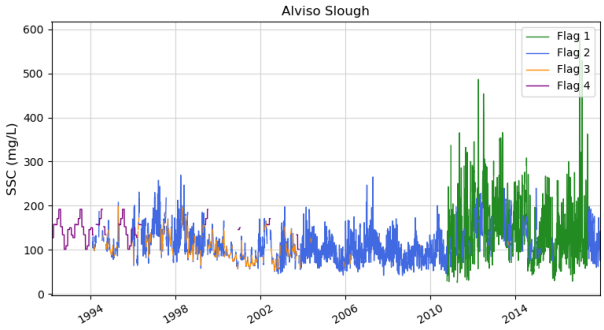

Figure D.12

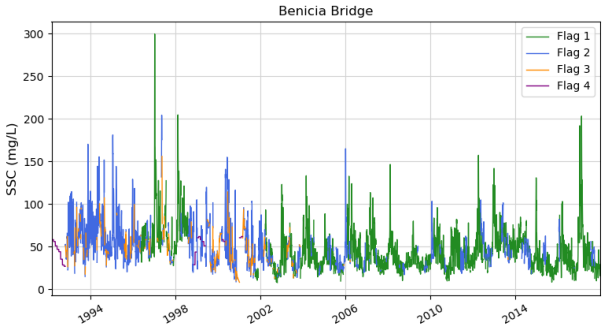

Figure D.13

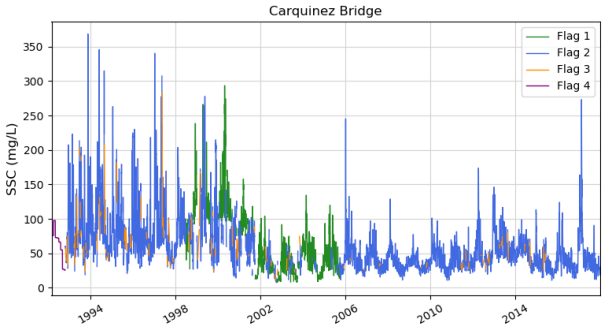

Figure D.14

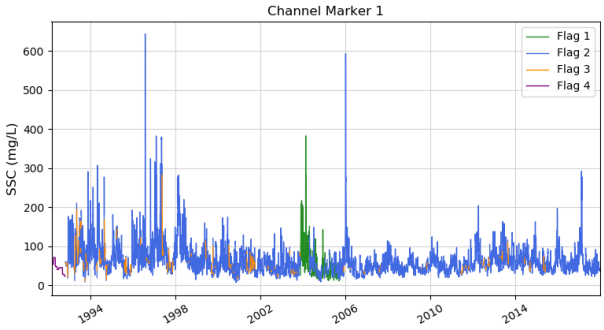

Figure D.15

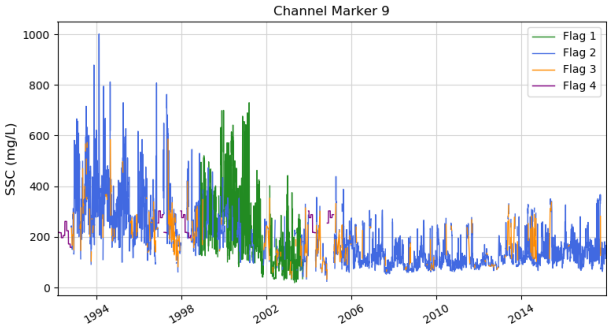

Figure D.16

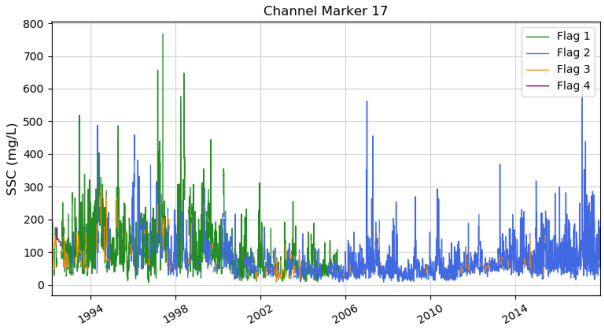

Figure D.17

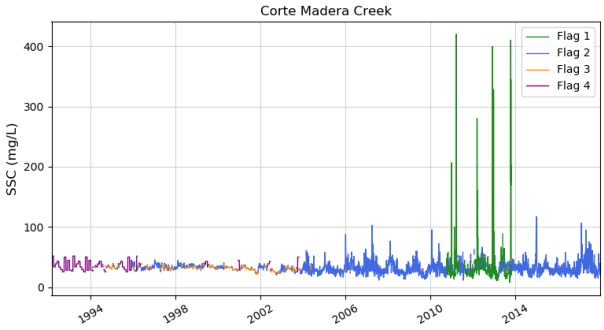

Figure D.18

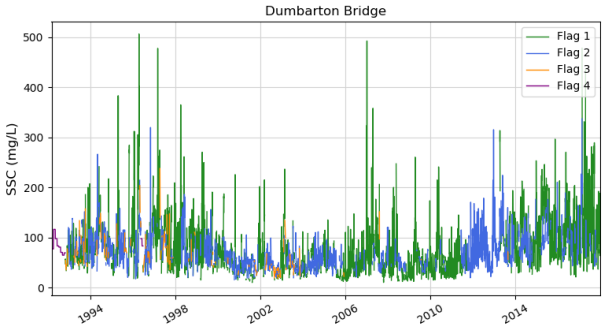

Figure D.19

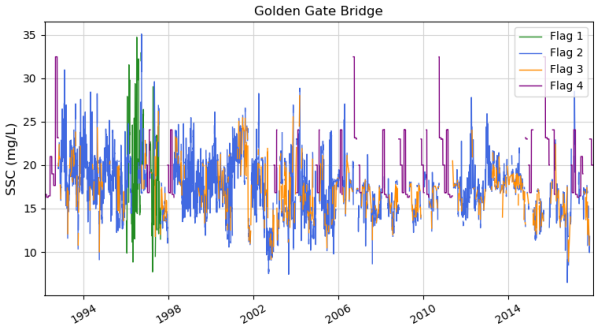

Figure D.20

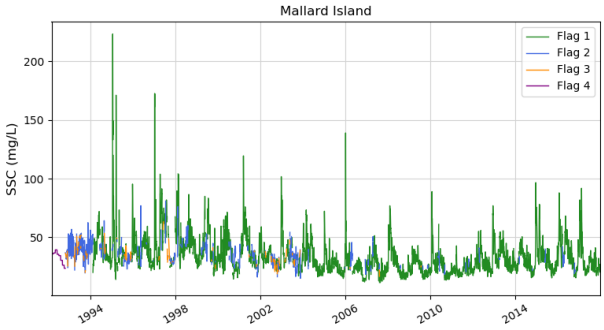

Figure D.21

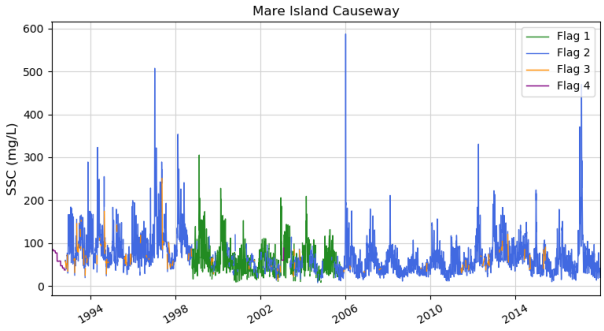

Figure D.22

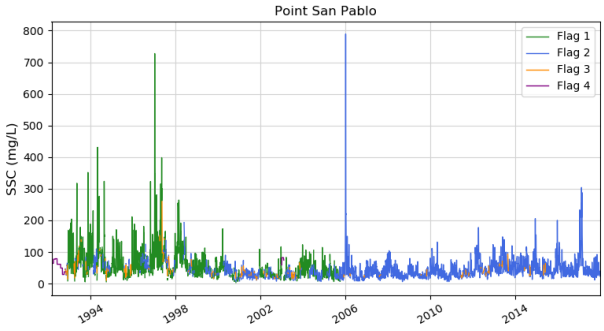

Figure D.23

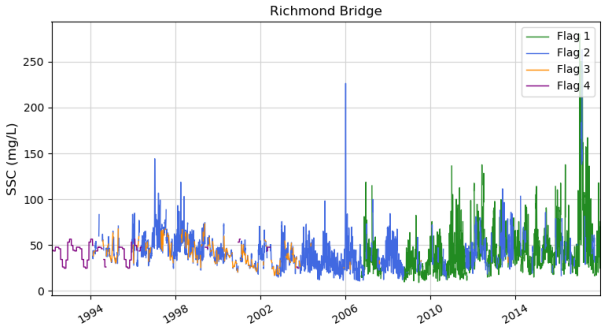

Figure D.24

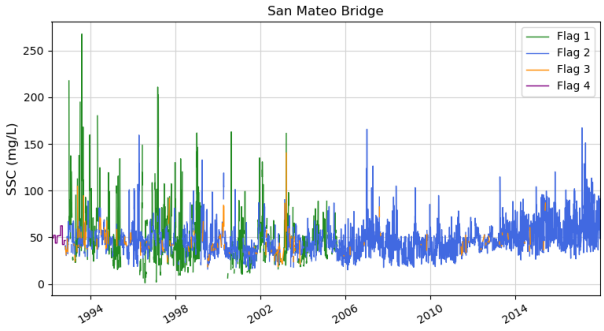

Figure D.25

APPENDIX E SAN FRANCISCO BAY AND DELTA WATER QUALITY MODEL SEDIMENT FLUX SUBMODEL WORK PLAN

FOUR PEAKS
ENVIRONMENTAL
Science & Data Solutions

SAN FRANCISCO BAY AND DELTA WATER QUALITY MODEL: SEDIMENT FLUX SUBMODEL WORK PLAN

DRAFT REPORT

DECEMBER 2018

SAN FRANCISCO BAY AND DELTA WATER QUALITY MODEL: SEDIMENT FLUX SUBMODEL WORK PLAN

P. Mugunthan[1]
Z. Zhang[2]
D. Senn[2]
A. Chelsky[2]
December 2018

Prepared for
Aquatic Science Center
San Francisco Estuary Institute
Richmond, California

[1] Four Peaks Environmental Science & Data Solutions
[2] San Francisco Estuary Institute

TABLE OF CONTENTS

FIGURES

TABLES

ACRONYMS AND ABBREVIATIONS

Acronyms or Abbreviation	Defined
AAP	Adsorbed Orthophosphate
CD3	Contaminant Data Display & Download
DELWAQ	Delft3D-Based Water Quality
DFM	D-Flow Flexible Mesh
DIN	Dissolved Inorganic Nitrogen
DO	Dissolved Oxygen
MERL	Mesocosm Experimental Research Laboratory
NNE	Nutrient Numeric Endpoint
RMP	Regional Monitoring Program
SFB	San Francisco Bay
SFEI	San Francisco Estuary Institute
TOC	Total Organic Carbon
UGEMS	University of Maryland – Gust Erosion Microcosm System
USGS	U.S. Geological Survey

1. INTRODUCTION

1.1 Background

San Francisco Estuary Institute (SFEI) has developed a biogeochemical model of the San Francisco Bay (SFB) and the Sacramento-San Joaquin River Delta (Delta) using DELWAQ, a Delft3D-based water quality model (Holleman et al. 2017). This model is being developed as a tool to support the SFB and Delta Nutrient Numeric Endpoint (NNE) framework that is being developed by the California State Water Resources Control Board to meet water quality objectives in the estuary.

Although the Bay and the Delta receive substantial point source nutrient loads, modeling work to date and analysis of observational data have both suggested that benthic nutrient fluxes may be important during some times of the year. Compared to many estuaries in which nutrient modeling has been/is being undertaken (for example, Chesapeake Bay), there are few SFB- or Delta-specific observations on sediment diagenesis, nutrient fluxes, or basic biogeochemical characterization of sediments (e.g., organic matter content, reactivity of sediment organic matter, sediment oxygen demand, carbon to nitrogen to phosphorus [C:N:P] ratio, etc.).

The DELWAQ model of the SFB and the Delta presently employs a basic sediment diagenesis module with essentially default settings recommended in the DELWAQ model user's manual. The water column and sediment processes are simulated at the same spatial resolution as the hydrodynamic model, which results in long run times. This makes it challenging to 'experiment' with different sediment diagenesis configurations such as differing spatial and temporal resolution of the sediment sub-model, differing process levels, different numbers of state variables (for example, organic matter G classes), and different combinations of sediment initial conditions. A concerted effort to calibrate the model has not been undertaken yet.

1.2 Objectives

This work plan aims to optimize the model development and calibration process by reviewing existing data from San Francisco Bay and estuarine sites to prioritize processes and parameters that are likely to be important in SFB. Specifically, this work plan will develop the following:

- An approach for specifying the initial concentration of model state variables in the sediments
- Identify important processes to include in the model
- Develop calibration metrics that reconcile overarching modeling goals, spatial and temporal scales, and key processes
- Identify potentially sensitive parameters and range for calibrating those parameters

2. REVIEW OF SEDIMENT FLUX MODELING FRAMEWORK

2.1 Estuarine Sediment Flux Models

Representation of feedback between water column and sediments is central to modeling the aquatic biogeochemistry. Several papers and books discuss available sediment flux modeling approaches (Paraska et al. 2014; DiToro 2001; Boudreau 2000, 1997; Wang and Van Cappellen 1996; Berner 1980). Regardless of whether the models are developed for an estuarine or a freshwater setting, there are several fundamental processes that affect water column-nutrient exchanges. These include deposition and resuspension of organic matter at the sediment-water interface, biogeochemical (re)mineralization of organic matter, diffusive exchange within and between sediment porewater and water column, mixing of particulates in the sediments stimulated by activity of benthic fauna, burial and eventual sequestration of organic matter within deep sediments, and redox processes within sediments that affect the production sequence and fate of reduced solutes within the sediments.

Common approaches to representing sediments include the use of the two-layered model typically segmented as a thin surface aerobic layer and a thicker anaerobic layer (DiToro 2001; Brady et al. 2013) or as multi-layered models that provide a finer discretization of the sediments over many layers (for example, Chapra et al. 2015). Another common feature of most models is the use of different numbers of reactive classes or 'G'-classes (first introduced by Berner [1980]) to reflect the labile and refractory components of organic matter. Organic matter is typically represented in a few different pools each with a different mineralization rate (Paraska et al. [2014] provides a summary of the multi-G models).

For the purpose of this report, the Chesapeake Bay sediment flux model (Cerco and Noel, 2017; Brady et al. 2013; Testa et al. 2013; Cerco et al. 2010) is used as a representative estuarine sediment flux model for comparison to SFB DELWAQ model because of the long history of development and similar objectives (i.e. evaluate water quality improvement strategies and nutrient load allocations) for which the model was developed, and the framework under which it was applied (coupling to three-dimensional water column model of a tidally-driven large estuary). The Chesapeake Bay sediment flux model uses the two-layered approach developed by DiToro (2001) and represents nearly all the major benthic and biogeochemical processes affecting sediment-water column nutrient exchange (Brady et al. 2013). While parameter ranges from literature compilations (for example, Paraska et al. 2014) will also be used for constraining calibration, the Chesapeake Bay Model would be used as a primary source for process comparisons and developing parameter ranges. Furthermore, results of the benthic flux studies conducted in Chesapeake Bay will also be reviewed to estimate possible correlations that are transferable to SFB model parameterization.

2.2 Overview of SFB DELWAQ Model Capabilities

The SFB model uses the Deltares suite of models that includes D-Flow Flexible Mesh (DFM) for hydrodynamics and D-Water Quality (DELWAQ) for simulating water column and sediment biogeochemistry (Holleman et al. 2017). The SFB model has nearly 50,000 cells in the horizontal with

a nominal grid resolution of 250 m in South Bay and 350–500 m in North Bay and 10 layers based on a sigma coordinate system. Additional details on the model grid, and hydrodynamic model development and calibration are available in Hollemen et al. (2017). Based on current computational resources used, the DFM model of SFB requires approximately 7 days of wall clock time for running a 426-day simulation that includes one full year of simulation with a 2-month spin up (Holleman et al. 2017).

The DELWAQ model is coupled at the same resolution as the overall hydrodynamic model grid, with externally coupled hydrodynamics and sediment transport providing the velocities, water levels, deposition and erosion fluxes. The water quality model runs at a time step of 20 minutes and takes approximately 10 days to complete an 8-month simulation. SFEI is presently working on aggregating the spatial grid to develop a coarser scale water quality model that would have a significantly lower run time (~1-2 days).

The DELWAQ model provides two sediment flux model options: a 2-layer model and a multi-layer model. The 2-layer model formulation is the one that is presently employed in the SFB model. A schematic of the processes represented in this model is shown in Figure 1. The 2-layer model is a simplified version that is intended to primarily simulate particulate organic matter transport and decomposition within the sediments. It includes two reactive classes ("G" classes) to represent differing mineralization/decomposition rates of autochthonous and allochthonous particulate organic matter. It does not have sediment porewater and releases nutrients, dissolved organic carbon, and dissolved silica that result from the decomposition and dissolution (for opal silica) directly into the water column. Settling of particulate organic matter and algae are the sources, and burial is a sink. The model includes a deep sediment layer boundary that can also serve as a source of particulate organic matter through "digging", which is a particulate upwelling rate that is intended to represent the activity of benthic macroinvertebrates. Nutrient and electron donor limitation on decomposition are included in the model but use the water column concentrations in place of the sediment porewater concentrations. Similarly, sediment denitrification is simulated as an additional loss of nitrate in the water column which is released from the particulate organic matter mineralization. Particulate inorganic phosphorus is included in the form of adsorbed orthophosphate (AAP), which upon desorption is simulated as a dissolved orthophosphate source in the water column. Primary production from microphytobenthos can be simulated through two algal groups, and grazing can also be included from a single zoobenthos group.

The multi-layer sediment flux model is equipped with nearly all the processes simulated in the water column. It provides a more realistic simulation through inclusion of sediment porewater phase, and simulating the sediment reactions therein rather than in the water column. Moreover, bioturbation is simulated as a dispersion process as in most sediment flux models. The multi-layer sediment will require more wall clock time to complete the same simulation, but is likely a more accurate representation of the sediment processes.

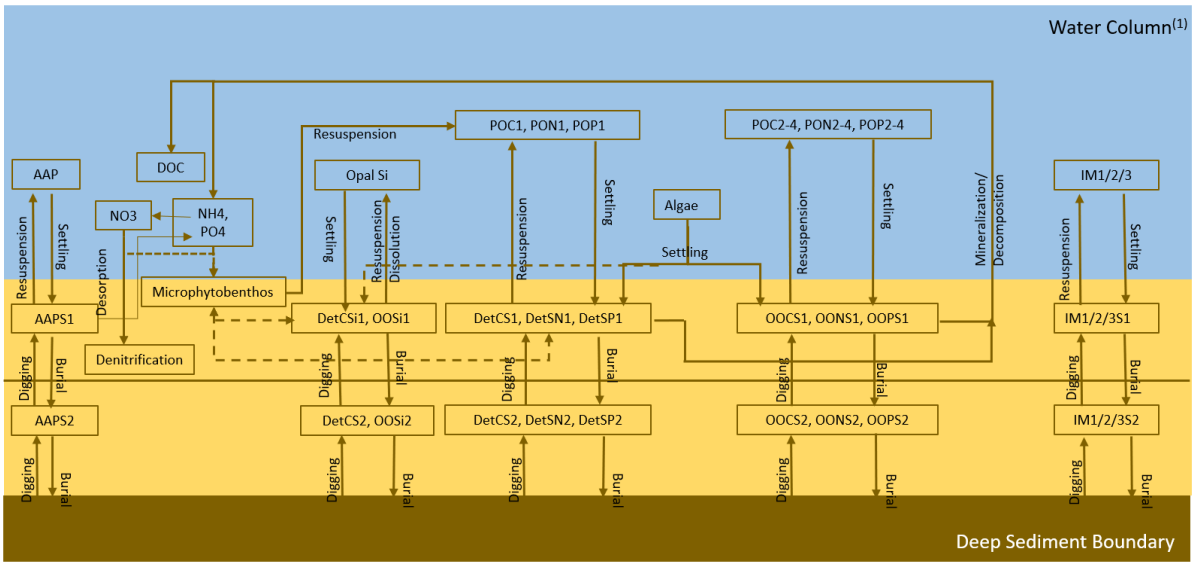

Notes:

1. Only water column processes that directly interact with the sediment layer are shown (see also Note 4 below)
2. Direct resuspension from Sediment Layer 2 can occur if Layer 1 is completely depleted
3. Particulate iron in water column also undergoes settling and resuspension
4. Electron acceptors other than dissolved oxygen that are simulated in the model include nitrate, iron(III), sulfate, methane, and carbon dioxide. These are used during decomposition of detrital organic matter only under anoxic conditions. In the 2-layer sediment model, redox reactions are not explicitly simulated in the sediments but use the water column concentrations of the electron donors to estimate limitation terms.

Abbreviations: AAP = adsorbed orthophosphate; DOC = dissolved organic carbon; POC/N/P = particulate organic carbon, nitrogen, phosphorus, IM = inorganic matter; OO[C/N/P]S = slow decomposing organic carbon/nitrogen/phosphorus in sediments; Det[[C/N/P]S= slow decomposing organic carbon/nitrogen/phosphorus in sediments; OOSi = fast dissolving opal silicon in sediments; Opal Si = opal silicon in water column; NH4 = ammonium; NO3 = nitrate; PO4 = phosphate; suffixes S1/S2 refer to sediment layers 1 and 2; suffixes 1/2/3 (for IM) or 1-4 (for POC/N/P) in the water column – refer to different particulate matter classes.

Figure 2-1. Major Processes Represented in SFB Sediment Flux Model

2.2.1 Findings from Preliminary Water Column Model Application to South Bay

A simplified version of the SFB model was applied to simulate the effects of nitrogen load reductions to San Francisco Bay (Holleman and Senn 2017 - unpublished).[3] A baseline (i.e., current conditions) and scenarios with lower nitrogen loads were simulated for the 2013 water year. The study concluded that external nutrient load reductions would result in significant reduction in nutrient export to coastal ocean and in the dissolved inorganic nitrogen (DIN) concentration within the Bay. More importantly, the study showed that the extent of these reductions depends on location within the Bay (i.e. proximity to sources versus coastal ocean) and the time of the year (winter vs. summer). Reductions in winter were predicted to be lower presumably due to lower denitrification loss within the Bay.

Recognizing that the SFB model is still work in progress, these findings nonetheless provide useful insight. Denitrification is a predominantly sediment-driven process. The relative magnitude of denitrification loss predicted in the model simulations compared to external sources (see Table 2-1) indicates the importance of sediments. The change in storage (calculated from the reported loss, transport and external loading components) indicates that throughout the Bay there is a net loss of nutrients from the sediments in July (Table 2-1). Considering that historical data has shown a consistent spring algal bloom in the Bay (Crauder et al. 2016), and sediment bacterial activity in late fall through early spring is likely minimal due to the lower water temperature, this probably points to the importance of the benthic-pelagic coupling in regulating nutrients within the Bay. The modeling results were limited to one year which precluded from assessing long-term memory in the system. Considering the change in the primary production in the Bay it is possible that there may be a nutrient build up, but without a longer-term model simulation or multi-year sediment flux studies this would be difficult to determine. A sediment flux model that provides a reasonable representation of the benthic-pelagic coupling and that can be simulated over a longer time frame (several years to a decade) can provide more meaningful insights on the role sediments could play under different nutrient reduction scenarios that are contemplated in the overall nutrient management strategy for the Bay.

A preliminary SFB model simulation was used to assess the factors controlling the 2013 spring phytoplankton bloom in the Bay (Zhang et al. 2018). Sensitivity analysis indicated that simulation of light and nutrient limitation alone was insufficient to reproduce the observed chlorophyll-a pattern in South Bay. Simulation of top-down control (grazing) was also necessary to explain the observed timing of the chlorophyll-a peak and subsequent decline. Plankton (primary producers and grazers) mortality enriches the sediments with nutrients. When viewed in light of the earlier modeling results on effects of nutrient reductions in the Bay (Holleman and Senn 2017 – unpublished), which showed a net loss of nutrients from storage in July 2013 (Table 2-1), these findings support the hypothesis that the sediments are acting as a reservoir of labile

organic matter deposited during the spring event, releasing a significant portion back to the water column in summer.

Table 2-1. Predicted Dissolved Inorganic Nitrogen Mass Balance in San Francisco Bay in 2013

Embayment	External Loads (kg N/ day)	Transport (kg N/ day)	Denitrification Loss (kg N/ day)	Change in Storage (kg N/ day)[1,2]
Lower South Bay	6533	-2695	-3927	-89
South Bay	3043	4507	-9110	-1560
Central Bay	27920	-22567	-9593	-4240
San Pablo Bay	624	4349	-6486	-1513
Suisun Bay	6684	-3442	-5210	-1968

Notes:
1. Change in storage was not reported in Holleman and Senn (2017 - unpublished) but was calculated as the difference needed to conserve mass.
2. A positive change in storage indicates nutrients are stored within the Bay (presumably in the sediments), and a negative value indicates nutrients are released from storage.

2.3 Comparison to Chesapeake Bay Model

Table 2-2 provides a comparison of the SFB model as it is currently developed using the two-layer sediment flux model, and the Chesapeake Bay model. The hydrodynamics, sediment transport, and water column models for both are comparable in technical rigor. The most notable difference between the two models is the lack of sediment porewater and the direct release and uptake of solutes from the water column in the SFB model. Other processes such as benthic stress to hypoxic/anoxic conditions do not appear to be included in the DELWAQ model. Considering that the existing dissolved oxygen (DO) data from SFB does not show extended hypoxic conditions, not including benthic stress to DO may not be as severe a limitation (DO data from South Bay indicate that margins and sloughs are likely more affected than the open bay [Crauder et al. 2016]). The SFB model is more advanced in some processes – for example, limiting the organic matter mineralization rates to nutrient levels, simulation of microphytobenthos and zoobenthos are not directly included in the Chesapeake Bay model. To what extent these processes control the sediment-water column nutrient cycling is unclear.

Table 2-2 also shows a comparison of the capabilities of the full multi-layer sediment flux model in DELWAQ. The multi-layer sediment flux model is equipped with nearly all the processes employed in the Chesapeake Bay model. As indicated earlier, the multi-layer sediment flux model provides a more realistic simulation of sediment nutrient cycling by including sediment porewater and representing bioturbation as dispersion processes. Including sediment porewater will allow a more gradient-based transfer at the sediment-water interface. Considering the use of a more finely resolved sediment bed,

its ability to include a range of microphytobenthos and zoobenthos, and nutrient and electron donor limitations, the multi-layer sediment flux model in DELWAQ can be considered a more advanced version of the sediment flux model used in the Chesapeake Bay model.

At this stage, it is unclear whether the capabilities of the multi-layer sediment flux model will be required for SFB. During initial explorations, it is recommended that the simpler, two-layer sediment flux model be used in conjunction the full suite of water column processes to assess whether such a framework is capable of providing a useful representation of observed water quality processes. If the model simulations are inadequate in capturing water quality and/or if preliminary modeling assessments and site-specific data indicate substantial sediment contributions in one or more embayments then it may be useful to consider developing a multi-layer model.

Table 2-2. Process Comparison between Chesapeake Bay and SFB Sediment Flux Models

Process	SFB Model (as Developed Currently – Two-layer Sediment Flux Model)	Additional Options Available in DELWAQ Model with Multi-layer Sediment Flux Model	Chesapeake Bay Model
Spatial and Temporal Representation: Integration with Water Column			
Sediment Discretization	1-D (vertical) with 2 layers	Multiple layers possible	2-layer model (1 thin aerobic layer and a thicker anaerobic layer)
Hydrodynamics	Full 3D hydrodynamics drives sediment and water column transport	Full 3D hydrodynamics drives sediment and water column transport	Full 3D hydrodynamics drives water column transport
Suspended Sediment Transport	Inorganic sediments only; Deposition and resuspension fluxes to represent particulate matter exchanges	Organic matter can be added to sediment transport	Only inorganic solids are resuspended; Organic matter is modeled on a net deposition basis using a settling rate
Water Column Coupling	Instantaneous transfer of dissolved components; particulates transferred through deposition or resuspension	Gradient-based diffusive transfer possible in multi-layer model	Sediment flux model was integrated into the water column model; A separate decoupled sediment flux model was also used for calibration and long-term simulations – this was driven by observed and synthetic data
Time Steps	Same as water column model	Same as water column	Water column model time steps are 5

Process	SFB Model (as Developed Currently – Two-layer Sediment Flux Model)	Additional Options Available in DELWAQ Model with Multi-layer Sediment Flux Model	Chesapeake Bay Model
			minutes; likely the same time step for coupled sediment flux model
Run Time	2 weeks for 1-year run	Likely > 2 weeks for 1-year run	Decoupled version [1] runs in seconds for a 25-year simulation
Transport within Sediments			
Porewater Advection	Not simulated	Available in multi-layer model	Not simulated
Porewater Diffusion/Dispersion	Not simulated	Available in multi-layer model	Simulated as a dispersion process
Bioturbation/Particulate Dispersion	Zero- or first-order "digging"; benthic stress to DO not represented	Can be simulated as a dispersion process; benthic stress to DO not represented	Simulated as dispersion; benthic stress to low/no DO is simulated
Burial/Particulate Advection	Zero- or first-order process	Zero- or first-order process	First-order burial rate
Transformation Processes/Sediment Reactions			
Organic C/N/P Diagenesis	First-order process with reduced solutes directly transported to water column	First-order process	First-order process
Silica Dissolution	Dissolution process with a pseudo-second-order dissolution rate; uses the dissolved silica over saturation to model dissolution	Same as 2-layer model	Dissolution process with a first-order rate and M-M limitation term; uses the dissolved silica over saturation to model dissolution
Methanogenesis [2]	Not simulated in sediments; simulated through methane and DO removal in water column; methane bubble formation can be simulated as an option	First order with M-M-based kinetics for competition with other electron acceptors (O2, SO4, CO2); Methane bubble formation is simulated	First-order process with M-M limitation on CH4 and DO; methane bubble formation is simulated
Sulfate Reduction [2]	Not simulated in sediments	First order with M-M-based kinetics for competition with other electron acceptors (O2, SO4, CO2)	First-order process with M-M limitation on SO4 and DO

Process	SFB Model (as Developed Currently – Two-layer Sediment Flux Model)	Additional Options Available in DELWAQ Model with Multi-layer Sediment Flux Model	Chesapeake Bay Model
Iron Reduction [2]	Not simulated in sediments	First order with M-M-based kinetics for competition with other electron acceptors (O2, SO4, CO2)	Not simulated
Nitrification [2]	Not simulated in sediments; mineralization releases ammonia to water column with nitrification simulated through ammonia and DO removal from water column	First-order process with M-M or linear limitation on NH4 and DO	First-order process with M-M limitation on NH4 and DO
Denitrification [2]	Not simulated in sediments; simulated through nitrate removal in water column	First-order rate with M-M limitation on nitrate; optionally additional limitation for consumption of other electron acceptors can be included	First-order process
Benthic primary production/respiration	2 algal classes	Up to 30 classes	Not simulated
Orthophosphate/Ammonium Partitioning to Iron/Inorganic Matter	Simulated as adsorbed orthophosphate; desorbed ortho P is directly released to water column	Simulated for ortho P (sorbs to inorganic matter); capacity is estimated based on pH and iron concentrations, and presence of DO	Simulated

Notes:

1. Decoupled version runs on a single box, two-layered model that is not linked to the full model grid. This simplification allows for short run times, but also requires an extensive water column and sediment data set to properly constrain the model.
2. These processes do not appear to be simulated in the sediments in the 2-layer model, although information in the D-Water Quality user's manual is ambiguous.

3. DATA FOR MODEL DEVELOPMENT AND CALIBRATION

3.1 Data Needs for Model Development

The primary sediment state variables in the two-layer DELWAQ model that represent nutrient cycling are components of particulate organic matter (C, N, P) and their corresponding inorganic state variables (carbon dioxide, ammonia, orthophosphate). Silica associated with diatoms and externally derived watershed solids undergo dissolution to release dissolved silica back to the water column. Another key state variable in the model is nitrate, which is denitrified in the sediments (representing a loss of the nutrient from the system). Inorganic solids are important for adsorbed orthophosphate and also for establishing the overall burial rate of solids within the sediments. For a reasonable simulation of these state variables, the model requires several inputs that are discussed below.

3.1.1 Initial Conditions

The initial composition of state variables (particularly particulate organic matter) in the sediments is an important input in the model. This is determined from surface sediment cores analyzed for nutrient and organic matter content. The spatial distribution of sediment state variables is likely highly variable for a system like San Francisco Bay because of the highly varying levels of watershed and point source inputs between the sub-embayments that are subject to variable depositional and erosional environments within the system. It can be anticipated that over the long term, surficial sediments would reach a quasi-steady-state condition with the water column if external inputs and internal trophic controls remain relatively consistent between the years. The time period over which such an equilibrium establishes in San Francisco Bay is unknown. Coming up with reasonable initial conditions for the model will require an assessment of the available surface sediment data within the Bay, and an assessment of the long-term changes simulated within the model. Under a quasi-steady-state condition, surface sediment levels would show seasonal changes without a significant long-term trend. Establishing sediment initial concentrations that reflect these patterns will be important, particularly for short-term simulations to avoid inaccurate sediment feedback.

3.1.2 Boundary Conditions

An accurate simulation of benthic-pelagic coupling will essentially require accurate specification of nutrient loading to the water column, and an accurate representation of the particulate organic and inorganic solid fluxes between the sediments and water column. If the sediment model is viewed in isolation (i.e., if the water column is treated as a boundary condition), then nutrient cycling within the sediments will require the specification of organic matter loading from water column and concentrations of dissolved solutes in the water column. For the two-layer DELWAQ sediment flux model, isolating the sediments can be a challenge because of its dependency on water column for

direct cycling of nutrients from diagenesis to the water column and direct use of water column state variables for sediment processes (for example nitrate).

In addition, the model will also require the specification of concentration of state variables at the bottom sediment boundary to which state variables can be lost through burial, and from which state variables can re-enter the active sediment layer through digging. In general, sediments lost to deep sediment layer are largely recalcitrant because majority of the labile organic matter is converted into nutrients within the active layer. Nonetheless, the state variable levels in the deep sediments should be specified with due consideration to local conditions (depositional conditions, known zones of high productivity, proximity to external sources etc.).

3.1.3 Model Parameterization

The DELWAQ model requires specification of numerous sediment parameters for simulating the sediment processes. Even the "simpler" two-layer sediment model is parameter rich. The parameters that control the transport within the sediments include burial and digging rates of particulate matter. The key parameters required for simulation of fate of sediment model state variables include diagenesis rates for each reactive class of carbon, nitrogen, and phosphorus, parameters controlling dissolution of silica, parameters controlling denitrification, parameters controlling adsorption of orthophosphate, and parameters for simulating phytobenthos and zoobenthos. The multi-layer DELWAQ model requires a suite of additional parameters for simulation of bioturbation, nitrification, organic carbon oxidation, sulfate reduction, methanogenesis and methane oxidation, and iron reduction. A literature summary of range for most of these parameters are provided in Section 3.3.1 to serve as a meaningful starting point for model development and calibration.

3.2 Available Data from SFB and Delta

3.2.1 Review of Sediment and Water Column Data

Crauder et al. (2016) provide a synthesis of existing water column and sediment data in the Lower South Bay. The data reported in the synthesis that are relevant for sediment flux modeling are the following:

- Nutrient loads from point sources (major wastewater treatment plants) from 1980 to present
- Estimated nutrient loads from stormwater
- U.S. Geological Survey (USGS) monitoring data provides salinity, temperature, turbidity, suspended sediments, nutrients, DO, and chlorophyll-a data at a monthly frequency from 1970 to present (except for 1981–1987) along the channel from Lower South Bay to lower Sacramento River; in addition, ambient nutrient data are also available from other sources in

the lower South Bay sloughs at varying frequency (often monthly) and years

- Continuous DO data from a near-surface sensor are available at Dumbarton Bridge (2013-present), and bi-weekly DO depth profiles along the axis are available from the USGS dataset (period of record as noted above); DO data are also available in the sloughs and shallow margin habitats
- Settling velocity and depositional fluxes of suspended sediments estimated from floc populations sampled at 10 locations in South Bay; sediment bed erosion rate estimates based on Sedflume study (four sites in South Bay) and surface erodibility study (University of Maryland – Gust Erosion Microcosm System [UGEMS]) on one site (two cores); overall sediment budget for South Bay based on three different (wet, dry, and normal) water years
- Estimates of grazing rates from benthic organisms but this appears to be predominated by bivalves (filter feeders) and therefore, not directly useful for specifying a grazing rate for benthic feeders (zoobenthos) that consume microphytobenthos; nonetheless these grazing rates provide an estimate of phytoplankton-based organic matter fluxes (DetSC/N/P) to the sediments (beyond those directly settling to sediments)

Novak et al. (2015) developed a similar synthesis of water column and sediment data for the Sacramento-San Joaquin River Delta. The following data and analyses reported by Novak et al. (2015) are relevant to sediment flux modeling:

- Water column nutrient concentration and point source loading data from the Delta from 2000–2011
- Mass balance evaluations on nitrogen loading from Delta to Suisun Bay, and evaluations that provide a conceptual model for nitrogen transformation within the Delta
- Denitrification rates synthesized from sediment incubation studies of Cornwell et al. (2014)
- Estimates of burial loss for allochthonous organic matter

Benthic flux studies from cores collected in the South Bay channel and shoals in the 1980s and from 1992 to 1994 provide estimates of sediment oxygen demand, dissolved organic carbon, ammonium, nitrate, dissolved inorganic phosphorus and dissolved silica fluxes (Caffrey et al. 1996). Paired estimates of sediment chlorophyll-a, phaeopigment, and macrofaunal biomass are also available from these studies. Nutrient flux and sediment oxygen flux estimates were also developed based on benthic cores collected at two South Bay sites centered on the spring 1996 phytoplankton bloom (Grenz et al. 2000). Benthic flux estimates were developed using in-situ flux chambers at a channel and a shoal station in South San Francisco Bay from February 1980 through February 1981 (Hammond et al. 1985).

Sediment cores from South Bay were analyzed to assess the role of nitrification inhibitors (Caffrey and Miller 1995). From this study sediment chlorophyll and phaeopigment concentrations are available at three locations. This study also provided

sediment oxygen demand, ammonium and nitrate fluxes, and benthic macroinvertebrate biomass estimates. Another estimate of oxygen demand from benthic respiration is available from a study conducted at two South Bay sites (Caffrey et al. 1998).

Figure 3-1. Locations of Surface Sediment Samples Collected from 1993-2017

Flux estimates, benthic microalgae primary production, and denitrification rates were developed for Suisun Bay and Sacramento-San Joaquin Delta based on sediment incubation studies at 12 sites in September 2011 and March 2012 (Cornwell et al. 2014). Nutrient and trace metal fluxes were also estimated based on porewater profilers deployed at six Suisun Bay and Delta sites in July and August 2008 (Kuwabara et al. 2009).

Estimates of long-term sedimentation rates for the Bay were developed based on radioisotope depth profiles at two locations (Fueller et al. 1999). This work also provided long-term sediment accumulation rates and surface mixing coefficients.

Surface sediment data collected in the Bay including total organic carbon (TOC), total nitrogen, and total phosphorus are available from SFEI's Contaminant Data Display & Download[3] (CD3) web-based visualization tool. Based on the data downloaded from this tool we identified over 1000 surface sediment samples for TOC, over 700 samples for total nitrogen, and 27 samples for total phosphorus, majority of which were collected as part of the SFB Regional Monitoring Program (RMP). Sediment concentrations were predominantly reported for surficial sediments (presumably surface grabs) from different sub-embayments with samples scattered over both the shoals and deeper portions of the Bay (Figure 3-1). All sediment phosphorus data are from February 2010.

Majority of the data were collected in the first and third quarters, although some data are available in the second quarter. Box plots showing the TOC, total nitrogen, and C:N ratios are shown in Figure 3-2 to 3-4, respectively. The box plots show several interesting patterns:

- TOC and total nitrogen increase in the third quarter (relative to first quarter) in several sub-embayments, notably in South Bay and Lower South Bay reflecting freshly deposited organic matter generated in the spring bloom and generally appear to be migrating towards the channel
- Overall sediment nitrogen levels in South Bay and Lower South Bay are greater than elsewhere in the Bay
- The carbon to nitrogen ratio (Figure 3-4) appears to be lower on average in the third quarter reflecting more labile organic matter produced within the Bay in spring; a notable exception is the Lower South Bay channel where the average ratio increases in the third quarter– considering that both the TOC and total nitrogen showed increases in the channel in the

[3] https://cd3.sfei.org/

third quarter this suggests that nitrogen may be potentially mineralized at a greater rate in the Lower South Bay channel compared to other locations

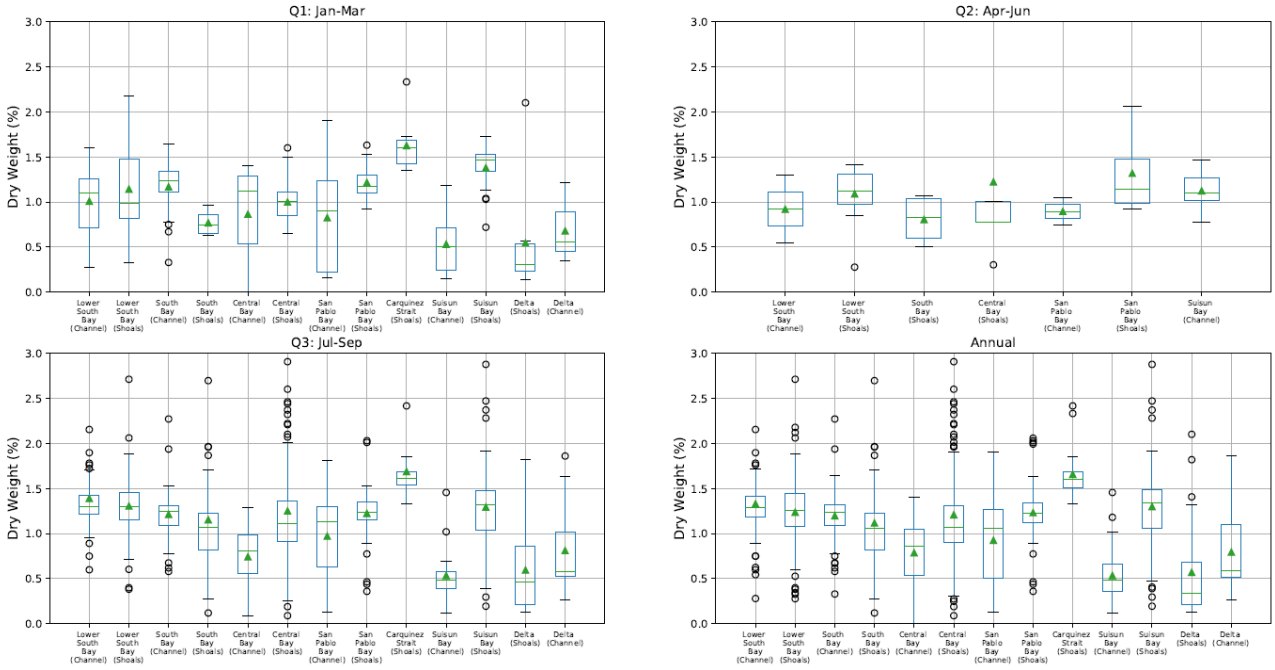

Notes: Values are grouped by sub-embayment and area (Channel or Shoals). Green triangles represent means; bars show the median; edge of the boxes extend from the first to the third quartile (inter-quartile range [IQR]) and whiskers extend to 1.5 x IQR; circles represent outliers beyond the whiskers.

Figure 3-2. Total Organic Carbon Concentrations in Surface Sediment Samples Collected from 1993-2017

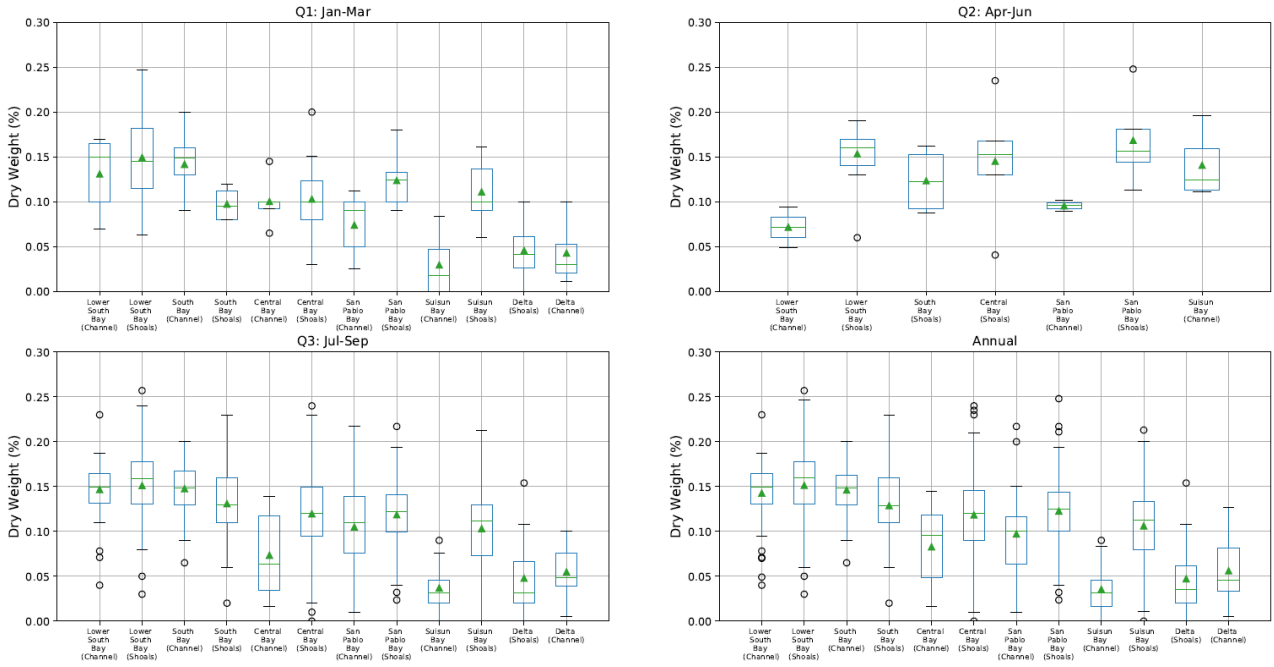

Notes: Values are grouped by sub-embayment and area (Channel or Shoals). Green triangles represent means; bars show the median; edge of the boxes extend from the first to the third quartile (inter-quartile range [IQR]) and whiskers extend to 1.5 x IQR; circles represent outliers beyond the whiskers.

Figure 3-3. Total Nitrogen Concentrations in Surface Sediment Samples Collected from 1993-2017

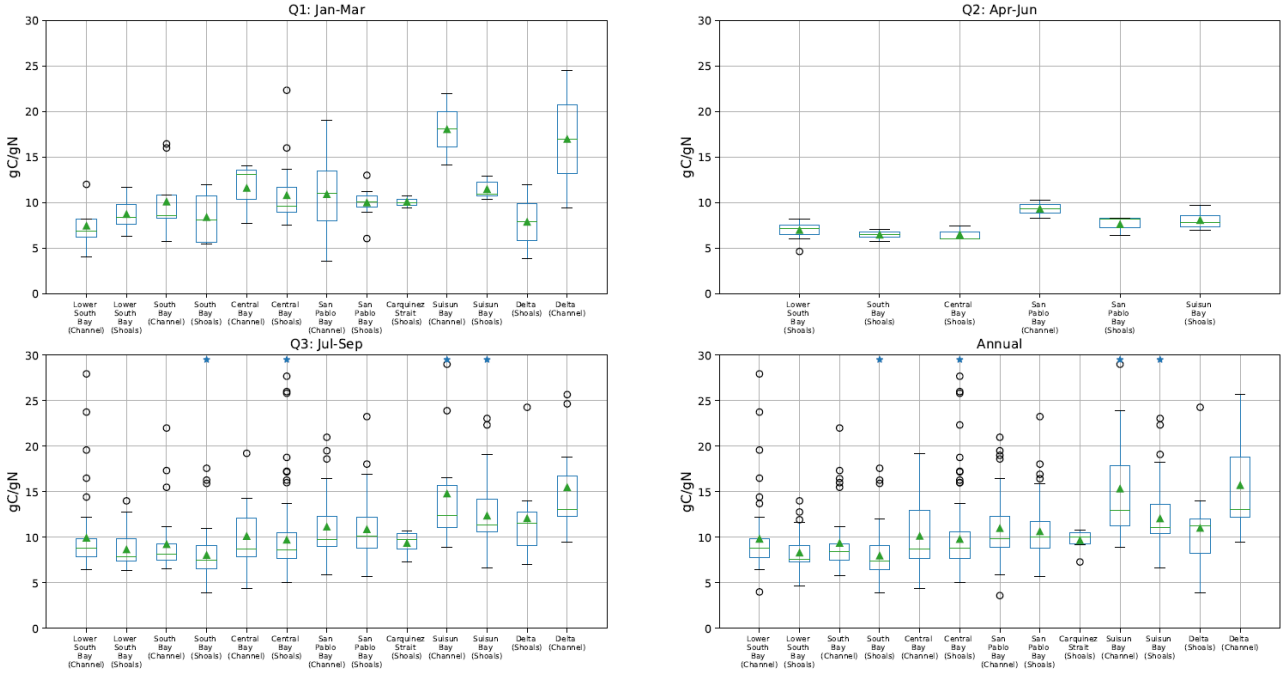

Notes: Values are grouped by sub-embayment and area (Channel or Shoals). Green triangles represent means; bars show the median; edge of the boxes extend from the first to the third quartile (inter-quartile range [IQR]) and whiskers extend to 1.5 x IQR; circles represent outliers beyond the whiskers. Outliers falling beyond the plot panels are shown with a blue star.

Figure 3-4. Carbon to Nitrogen Ratio in Surface Sediment Samples Collected from 1993-2017

The preliminary findings from modeling discussed in Section 2.2.1 that suggested a potential loss of nitrogen from sediments in summer is supported by the data above which show sediment enrichment through spring that progressively gets depleted over summer and fall (as evidenced by the lower nitrogen levels in spring). The data above further support the conclusions drawn on benthic-pelagic interactions in San Francisco Bay from a study based on sediment and water column data collected between the end of 1999 and the end of 2001 (Lesen 2006). This study concluded that sediment organic matter levels showed seasonal cycles with sediment peak levels that follow the water column spring-time chlorophyll-a levels.

Figure 3-5 shows the total phosphorus levels in the surface sediments. All phosphorus data are from February 2010, and are limited in spatial extent compared to the carbon and nitrogen dataset.

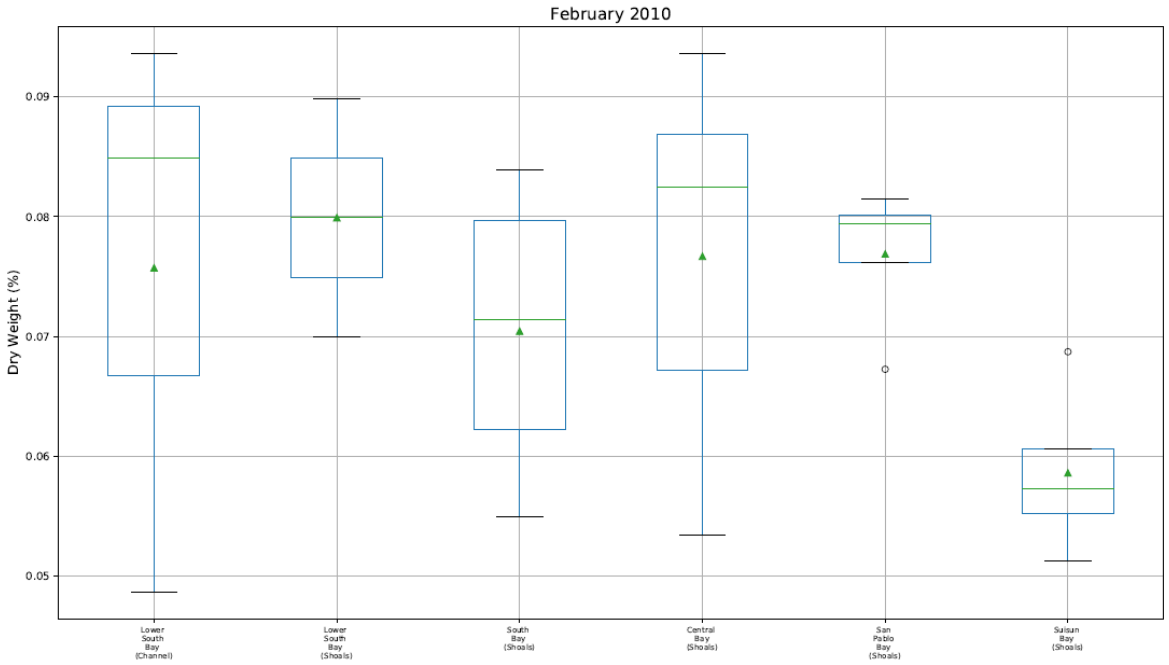

Notes: Values are grouped by sub-embayment and area (Channel or Shoals). Green triangles represent means; bars show the median; edge of the boxes extend from the first to the third quartile (inter-quartile range [IQR]) and whiskers extend to 1.5 x IQR; circles represent outliers beyond the whiskers.

Figure 3-5. Total Phosphorus Concentration in Surface Sediment Samples Collected in 2010

3.2.2 Data Gaps

For a spatially expansive and complex system such a San Francisco Bay estuary, it is a challenge to obtain a comprehensive dataset to constrain a sediment flux model for the entire system. Most notably there are critical data gaps for developing model initial conditions, and to properly constrain model calibration. When coupled with the inherent difficulty in estimating key parameters such as

depositional flux of organic matter, this presents a formidable challenge in developing a robust modeling framework for the Bay.

The Chesapeake Bay model was developed initially using data from eight sites collected over a three-year period and was subsequently refined to a long-term (25-year) data set. Such a phased approach would be prudent to address the data gaps for SFB. The sediment flux studies identified in Section 3.2.1 provide a data set for a preliminary model. Additional data collection guided by existing observations, predictions from the preliminary model and parallels from other sites (most notably Chesapeake Bay) can be used to develop a long-term monitoring plan for SFB that would provide a more comprehensive dataset.

The overall nutrient fluxes in any estuarine system are a product of both external (point sources, watershed, marine) and internal sources (sediments). Even if the Bay is generally enriched in nutrients for a majority of the year, data and preliminary modeling findings have both shown that nutrient limiting conditions can occur, particularly in the South Bay (Crauder et al. 2016). During such times the role of internal sources in triggering or sustaining a bloom can be important. As summarized in Section 3.2.1 existing data for external sources extends over 25 years, which is typically adequate. However, the limited sediment data that exists is insufficient to provide a characterization of the internal sources.

Even for a preliminary model, the following critical data gaps will need to be addressed:

- Measurements of organic matter content of suspended sediments entering SFB from freshwater inflows, point sources, key sub embayment boundaries, and restored salt ponds will be necessary to assess overall mass budgets for organic matter and nutrients; these measurements will need to cover key hydrological events (winter runoff), and must be conducted over multiple spring and neap tidal cycles to provide a robust mass budget.
- Sediment incubation studies from cores collected over a broader range of locations than those presently available to assess sediment oxygen consumption and nutrient fluxes and provide calibration targets for a model. Part of the issue with existing sediment flux data identified in Section 3.2.1 is that much of it was collected during a different productivity regime (greater grazing pressure and lower phytoplankton levels compared to present). Therefore, it is essential to characterize the present depositional conditions ideally over multiple growing seasons to capture inter-annual variability in hydrology, external sediment inputs, and variability in plankton and benthic macroinvertebrate diversity within SFB.
- Sediment trap studies will provide vital information on organic (and inorganic) matter deposition (and hence nutrient fluxes) to the sediments that can be used to calibrate settling speeds for water column solids and burial rate in the sediments. Sediment traps are difficult and expensive to implement on a large scale. Therefore, it is desirable to use historical observations to identify a subset of the locations with moderate to high primary production, pairing these with the sediment incubation studies identified earlier to the extent feasible.

Sediment trap studies conducted in Chesapeake Bay concluded that a mid-depth deployment is most representative of the deposition flux to sediments (Hagy III et al. 2005 and references therein). A similar approach can be adopted for SFB. Sediment phaeopigments can also serve as a useful indicator of autochthonous deposition (Hagy III et al. 2005).

Existing sediment TOC and total nitrogen data discussed in Section 3.2.1 are likely adequate to provide a reasonable starting condition for the model simulations, particularly for the "spin up" approach discussed in Section 4.2. However, there is only limited data on sediment phosphorus levels in the Bay. Considering that phosphorus has not been identified as a limiting nutrient in the Bay, and that overall nitrogen and carbon levels can serve as a useful proxy for sediment phosphorus levels, this is likely not a critical data gap. Nonetheless, sediment cores collected for the flux studies proposed above should consider including a joint estimation of C, N, P (and silica) levels in the surficial sediments to provide a more robust dataset for model development and calibration. Existing data on sediment phaeopigment and chlorophyll-a are also limited. Future data collection should also include these parameters. The areas chosen should be representative of the range of conditions in the Bay. These areas can be identified using the existing sediment transport model predictions of depositional and erosional areas, and historical observations.

The data above will not only help develop a sediment flux model but also provide a more robust constraint for the water column model. Considerations for translating field data to develop model parameters and constrain model calibration are discussed in Section 3.4.

3.3 Available Data from Other Estuarine Sites

3.3.1 Parameter Ranges from Other Models

Sediment model parameter ranges derived from literature are summarized in Table 3-1. The literature range was compiled from the following sources:

- Paraska et al. (2014) developed a comprehensive summary of sediment diagenesis rates based on a review of 83 sediment flux models published since 1996; in addition, this work also provided useful information on first-order reaction rates for denitrification, sulfate reduction and methanogenesis
- DiToro (2001) developed a summary of the two-layer sediment flux model parameters based on application of the model to six different data sets including Mesocosm Experimental Research Laboratory (MERL) studies in Narragansett Bay, Chesapeake Bay, Long Island Sound, Jamaica Bay, Lake Champlain, and Massachusetts Bay. This largely overlapped with the final parameters used in the Chesapeake Bay Model. Nonetheless, this provides a useful

range and validates the usefulness of the two-layer approach for a relatively large range of freshwater, estuarine and coastal conditions

- Testa et al. (2013) provided a comparison of literature-derived parameter ranges to those used in the final Chesapeake Bay Model. These have been included where available in addition to those from the sources above

The compilation in Table 3-1 is intended to provide useful starting values and calibration ranges for target parameters. The studies cited in the references above can be consulted for additional details on the parameter ranges. The final values used in the most recent Chesapeake Bay Model is also provided in Table 3-1 for reference (Brady et al. 2013; Testa et al. 2013).

Table 3-1. Parameter Ranges from Literature and Chesapeake Bay Model

Parameter	Literature Range[1]	Chesapeake Bay Model[2]	Chesapeake Bay Model Remarks
Diagenesis			
G1(rate, theta)[3]	0 – 0.822 d^{-1} (mean = 0.07 d^{-1}); from Testa et al. [2013]: rate = 0.019 – 0.066 d^{-1}; theta = 1.052 – 1.166	0.01-0.035 d^{-1}, 1.1	Range reflects use in current (0.01) and original (0.035) calibrations
G2(rate, theta) [3]	0 – 0.003 d^{-1} (mean = 0.0007 d^{-1}); from Testa et al. [2013]: 0.0012 – 0.0088 d^{-1}	0.0018 d^{-1}, 1.15	
G3(rate, theta) [3]	0 – 1.2e-05 d^{-1} (mean = 1.5e-06 d^{-1})	0 (non-reactive)	
Silica[1] (dissolution rate, theta)	0.5 – 0.75 d^{-1}, 1.1; from Testa et al. [2013]: rate = 0.02 – 0.2 d^{-1}; theta = 1.059 – 1.084	0.5 d^{-1}, 1.1	Silica is modeled through dissolution rather than bacterially-mediated diagenesis; DELWAQ model uses a pseudo-second order process to model dissolution (see Table 2-2)
Silica saturation for dissolution, theta	946 – 1560 mmol Si/ m^3 (from Testa et al. [2013])	1390 mmol Si/ m^3, 1.023	
Silica half-saturation for Michaelis-Menten limitation term	707 - 3571 mmol Si/ m^3 (from Testa et al. [2013]);	3560 mmol Si/ m^3	
Advection and Mixing			

Parameter	Literature Range[1]	Chesapeake Bay Model[2]	Chesapeake Bay Model Remarks
Burial[1]	0.2 – 0.75 cm/yr in DiToro (2001); 0.02 to 1 cm/yr in Testa et al. [2013]	0.25 cm/yr	Units reported in Brady et al. (2013) is incorrect – correct unit is cm/yr
Bioturbation	0.001 – 0.5 cm^2/d reported in Testa et al. [2013]	0.6 cm^2/d	
Diffusion[1]	5.0 – 50.0 cm^2/d; from Testa et al. (2013): 0.6 – 8.64 cm^2/d	5.0 cm^2/d	Diffusion is converted to a mass transfer rate (m/d) based on aerobic and anaerobic layer thicknesses. The anaerobic layer mass transfer is temperature dependent.
Active Layer Thickness[1]	10 cm	10 cm	
Benthic Stress[1] (first-order rate, half-saturation constant for DO)	0.03 d^{-1}, 125 µM O2	0.03 d^{-1}, 62.5 µM O_2	
Nitrification			
Rate[1,4], theta[1]	0.131 m/d, 1.123	0.131 m/d, 1.123	
Half-saturation for ammonium[1], theta[1]	52.0 µM N, 1.125	52.0 µM N, 1.125	
Half-saturation for DO[1]	11.5 – 23.1 µM O_2	11.5 µM O_2	
Denitrification			
Rate[4] (aerobic layer)	N/A	0.1 – 0.3 m/d	Denitrification is assumed to occur in anoxic microsites even in aerobic layer; reaction velocity range reflects values used for freshwater (0.1) and saltwater (0.3
Rate[4,6] (anaerobic layer)	1.6 e-06 – 2.1 d^{-1}, (mean = 0.24 d^{-1})	0.25 m/d	

Parameter	Literature Range[1]	Chesapeake Bay Model[2]	Chesapeake Bay Model Remarks
Theta[1]	1.08	1.08	Same temperature correction factor is used for both layers
Sulfide/Sulfate[5]			
Sulfide Oxidation Rate[1,4,5,7]	0.2 m/d (dissolved – H2S), 0.4 m/d (particulate – iron-bound)	0.2 m/d (dissolved – H2S), 0.4 m/d (particulate – iron-bound)	Sulfide oxidation is simulated in the aerobic layer for both dissolved and particulate phases
Theta[1]	1.08	1.08	Same temperature correction factor is used for both layers
Partitioning Coefficient[1]	100 L/kg	100 L/kg	Same value used in both layers
Half-saturation for DO for sulfide oxidation[1]	125 µM O2	62.5 µM O_2	
Half-saturation for sulfate for sulfide oxidation[1]	N/A	0.1 µM O_2	Sulfate is expressed in O_2 equivalent
Sulfate Diffusion[5]	N/A	1.0 cm^2/d	This is used in the estimation of sulfate penetration depth
Sulfate Reduction[6]	1e-04 – 0.04 d^{-1} (mean = 0.007 d^{-1})	-	Same as POC G1/2 diagenesis rate[5]
Methane[8]			
Oxidation Rate, theta	N/A	0.2 m/d, 1.08	
Half-saturation constant for methane oxidation	N/A	3.125 µM O_2	
Methane saturation, theta	N/A	3125 µM O_2, 0.976	Methane saturation value at STP; methane saturation is used for calculating aqueous to gaseous phase methane

Parameter	Literature Range[1]	Chesapeake Bay Model[2]	Chesapeake Bay Model Remarks
Methanogenesis rate[6]	1.6 e-05 to 4.0 e-04 d^{-1}(mean = 1.5 e-04 d^{-1})	-	Same as G1/2 diagenesis rate[7]
Phosphate			
Partitioning Coefficient (anaerobic conditions – linear sorption)	20 – 1000 L/kg	50 – 100 L/kg	For the aerobic layer, a multiplier is employed to account for increased sorption to iron

Notes:

1. Literature range derived from Paraska et al. (2014) except those parameters superscripted with 1, which were obtained from DiToro (2001); other references that were used are cited in the table.
2. Chesapeake Bay Model parameter values from Brady et al. (2013); phosphorus and silica parameters are from Testa et al. (2013).
3. Diagenesis rates corresponding to 3 G classes from Figure 3 in Paraska et al. (2014); for G-3, range and average were estimated from values reported for studies with 3 G classes in Table 2 in Paraska et al. (2014)
4. First-order reaction rate is treated as a reaction velocity which is defined as the product of the rate and aerobic/anaerobic layer thickness; aerobic layer thickness (typically a few millimeters) is calculated dynamically depending on extent of DO available in sediment porewater.
5. In the Chesapeake Bay Model sulfate reduction in the anaerobic layer is tracked through sediment organic carbon diagenesis rate. A sulfate penetration depth is used to scale the mass transfer of sulfate between the aerobic and anaerobic layers.
6. Literature range and mean reflects the organic matter diagenesis rates reported in Table 2 in Paraska et al. (2014) for the corresponding electron donor.
7. In the Chesapeake Bay Model methanogenesis is calculated simultaneously with carbon diagenesis and sulfate reduction; methanogenesis takes over as sulfate is depleted in the anaerobic layer. In the aerobic layer, methane undergoes oxidation. Methane saturation is used to compute gaseous methane formation in the anaerobic layer.
8. Values shown as N/A indicate a literature range was not available from the references reviewed

3.3.2 Chesapeake Bay Benthic Flux Study

An extensive set of benthic flux studies have been conducted in the Chesapeake Bay and its tributaries since 1978. Findings from these studies were synthesized into a report and compiled into a large publicly available database (Boynton and Bailey 2008). The report provides a comprehensive comparison of the sediment oxygen consumption and nutrient fluxes throughout Chesapeake Bay. Flux measurements grouped by bottom water temperature, salinity, redox conditions, and depth provide a range of conditions that can be used to derive similarities to San Francisco Bay and potentially develop constraints on predicted fluxes during SFB model calibration.

Estimates of sediment oxygen consumption and nutrient fluxes from all sediment data collected in Chesapeake Bay are shown in Figure 3-6 (adapted from Boynton and Bailey 2008). The figure shows a clear seasonal pattern in the sediment oxygen consumption and ammonium and dissolved

inorganic phosphorus fluxes. Sediment fluxes of ammonium showed a strong correlation with surface sediment chlorophyll-a concentrations (evidence of recent deposition) across Chesapeake Bay providing evidence for benthic-pelagic coupling (Boynton and Bailey 2008).

The average sediment oxygen consumption at a channel and a shoal location in San Francisco South Bay from 1991-1993 was reported to be 49 mmol O_2 m^{-2} d^{-1} and 47 mmol O_2 m^{-2} d^{-1} respectively (or 1.56 and 1.50 g m^{-2} d^{-1}) Caffrey et al. (1998). This is comparable to the average sediment oxygen consumption in Chesapeake Bay from May through August (see Figure 3-6). This would seem to indicate some applicability of Chesapeake Bay fluxes to SFB. However, Caffrey et al. (1998) concluded that there is no consistent seasonal pattern in either sediment oxygen consumption or ammonium fluxes measured in 1980s and 1990s based on data collected from South Bay sites, which seems to be different compared to observations in Chesapeake Bay, where a clear seasonal pattern is evident (Figure 3-6). The lack of seasonality in the 1990s SFB data is somewhat confounding given that historical (Caffrey et al 1998) and more recent water column data (2008–2013) has shown a distinct spring bloom at most South Bay stations (Crauder et al. 2016). Sediment Oxygen Consumption at Suisun Bay was reported to be in the range of (approximately) 0.35 to 1.1 g m^{-2} d^{-1} in September and 0.08 to 0.5 g m^{-2} d^{-1} in March respectively (Cornwell et al. 2014). This shows there is a seasonal variability at some locations in SFB.

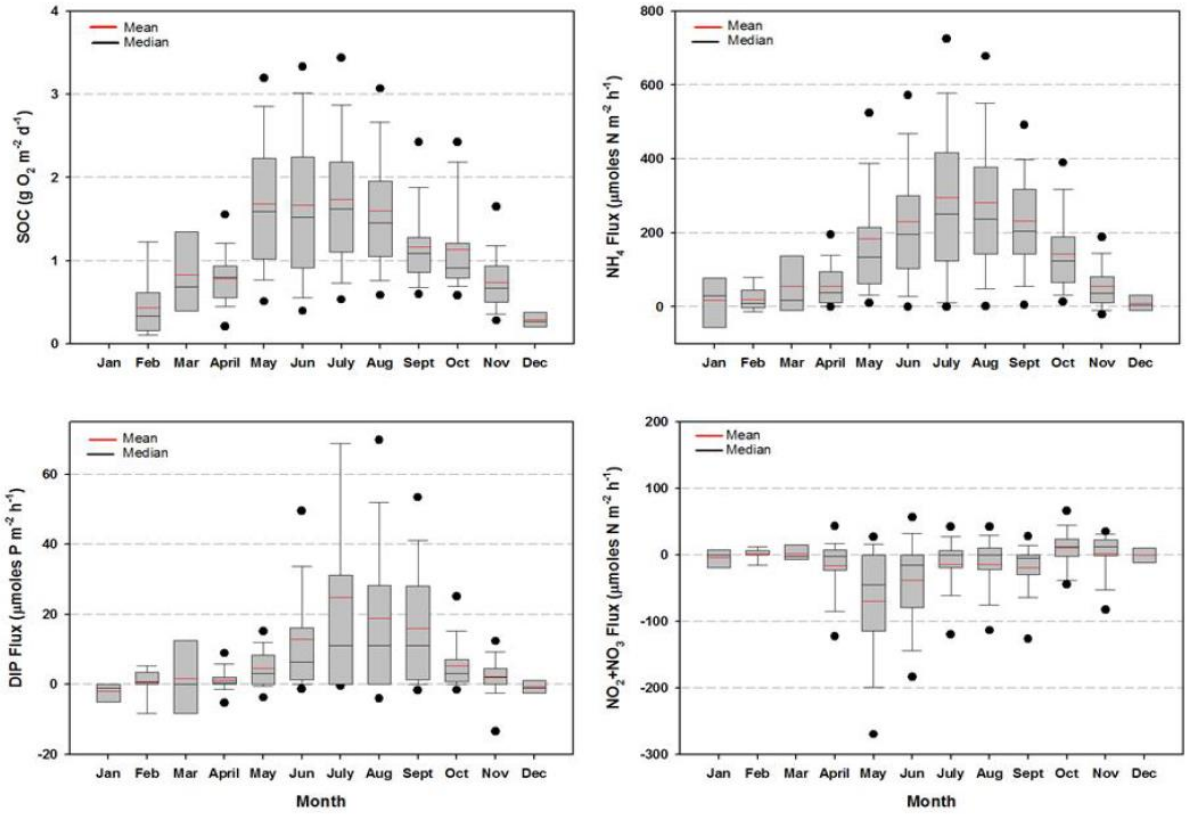

Note: This box plot was presented as Figure 6-2 in Boynton and Bailey (2008)

Figure 3-6. A Compilation of Sediment Oxygen Consumption and Nutrient Flux from Chesapeake Bay Benthic Flux Studies

These differences indicate that there is insufficient data at this time to develop a more robust comparison between the SFB and Chesapeake Bay. If additional sediment incubation studies are conducted under contemporary conditions (as recommended in Section 3.2.2) then it will provide more representative data that can be compared to Chesapeake Bay fluxes. These comparisons should be made based on regions with comparable physical, chemical, and biological conditions (depth, salinity, temperature, turbidity, DO, and other water column conditions such as chlorophyll-a levels) between the two locations. If similarities are indicated in the two datasets then the data from Chesapeake Bay can be used to supplement the SFB-specific data through extrapolations to potentially other seasons and hydrologic conditions for which SFB data are not available. The extrapolations will aim to develop bounds for SFB model calibration based on observed sediment oxygen demand and nutrient fluxes and decomposition/mineralization rates used in the corresponding locations in the Chesapeake Bay model.

Findings from the Chesapeake Bay benthic flux studies and insights gained from preliminary SFB model simulation runs can be used to guide additional data collection from SFB sediments. For example, preliminary SFB model predictions can be used to assess potential depositional areas, which can then be compared against the Chesapeake Bay benthic flux studies to assess whether the physical (depth, turbidity, temperature) and chemical (salinity, bottom DO) conditions indicated in the candidate depositional areas from the SFB model are likely to result in high nutrient turnover that can possibly trigger phytoplankton blooms.

3.4 Translating Field Data and Literature-based Parameters to DELWAQ Model Inputs

While DELWAQ simulates the fundamental diagenesis processes similar to most models, there are some considerations in translating field data and parameters derived from other models/literature into DELWAQ model inputs.

3.4.1 Using Flux Measurements to Estimate Model Parameters

Depositional fluxes determined from sediment trap studies can be used to estimate burial rate. DELWAQ uses a zero or first-order burial (and digging) rate to model particulate matter transport within the sediment bed. Because sediment benthic activity is limited to the top few centimeters (cm), and majority of the mineralization occurs within this region it is useful to consider the “active” sediment bed to have a fixed thickness that represents the top several cm (typically 10 cm), effectively passing particulate matter through the “active” bed at a net burial rate (in the absence of any transformation). Since majority of the particulate matter (predominantly inorganic solids) will

not undergo transformation, a useful bound on the net burial rate (burial – digging) can be estimated from the depositional flux of suspended solids as follows (DiToro 2001):

$$w = \frac{J_{SS}}{\rho_s(1-\varphi)} \qquad (3\text{-}1)$$

where:

w is the net burial rate

J_{SS} is the (net) sedimentation flux of suspended solids

$\rho_s$is the dry bulk density (typically 2.6 g/cm^3)

φ is the porosity of the surficial sediments (typically 0.7 – 0.9)

Loss (diagenesis) of particulate organic matter can be modeled using zero- and first-order process terms in DELWAQ. Typically, a first-order process is assumed for diagenesis (DiToro 2001). If this approach is adopted then a first-order diagenesis rate can be estimated from sediment incubation studies by recognizing that the loss terms in the overall mass balance equation ultimately produce the changes in concentration of solutes in the water column (in this case the filtrate from the incubation chamber). For a first-order diagenesis process, the loss terms can be linked to fluxes observed in a sediment incubation experiment as follows (DiToro 2001):

$$[c(t)] = c[0] + mG(0)(1 - e^{-kt}) \qquad (3\text{-}2)$$

where:

$c(t)$ is the concentration of solute observed in the filtrate at time t

m is the solids concentration in the incubation slurry

$G(0)$ is the reactive organic matter on a dry weight basis

k is the diagenesis rate

In Equation 3-2, c(t) are the observed concentration of reduced solutes (i.e. CO_2, NH_4^+, PO_4^{3-}) over time. Equation 3-2 can also be used with a minus sign on the right-hand side to represent SO_4^{2-} consumption during diagenesis after applying a suitable stoichiometric conversion factor. $G(0)$ and k are unknown and can be estimated through a curve fitting exercise with the two unknowns fitted to the concentration versus time data. Details on solution methods for estimating these parameters can be found in Burdige (1991).

The simplified approach above does not provide parameter estimates of multiple reactive classes. It is possible to formulate Equation 3-2 with multiple reactive classes. For example, with two G-classes Equation 3-2 can be written as follows:

$$[c(t)] = c[0] + mG_1(0)(1 - e^{-k_1 t}) + mG_2(0)(1 - e^{-k_2 t}) \qquad (3\text{-}3)$$

where:

$G_1(0)$, $G_2(0)$ are the labile and refractory reactive organic matter on a dry weight basis

k_1, k_2 are the diagenesis rates for labile and refractory organic matter, respectively

In this case four parameters will need to be estimated with the same data. Hence, the curve fitting problem is likely to yield parameters that are relatively uncertain compared to the scenario with just two. Burdige (1991) provides additional details on the relative merits of each approach. Regardless of which approach is used these estimates can provide a useful check and a useful starting estimate towards the final calibrated parameters for each reactive class (fraction and diagenesis rate). If the single G-fraction approach is used (Equation 3-2) it can still provide useful insights for a multi-G model because the total reactive organic matter (G(0)) is the sum of the individual reactive classes, and the range in diagenesis rates estimated from the observed data would reflect the different reactive classes (the higher values of the diagenesis rates would be indicative of freshly deposited, labile organic matter, and the lower values will be indicative of refractory organic matter).

3.4.2 Considerations in Using Literature-based Parameters

Parameters used in other models may not directly apply to DELWAQ. For example, reaction rates used in the Chesapeake Bay model are expressed as a reaction velocity (as length per unit time). An equivalent first-order rate can be derived by dividing by the respective length scale depending on the process. For reaction rates in the anaerobic layer the depth of the anaerobic layer (typically ~10 cm) can be used. The depth of the aerobic layer is typically only the top few millimeters and is calculated dynamically within the Chesapeake Bay model (DiToro 2001), which presents a greater challenge in incorporating this directly into DELWAQ. Because the aerobic layer thickness is determined by the extent to which DO diffuses down from the water column, DiToro (2001) provides a relationship between diffusion coefficient of DO and other reaction velocities employed in the aerobic layer as follows:

$$k = \frac{\kappa^2}{D} \qquad (3\text{-}4)$$

where:

k is the first order reaction rate, T^{-1}

κ is the reaction velocity, $L\ T^{-1}$

D is the diffusion coefficient, $L^2\ T^{-1}$

As is evident from Table 3-1, literature-based diagenesis rates provide a rather broad range for calibration, particularly for labile organic matter (G1). The general approach for calibration of the different reactive classes should reconcile the importance of seasonal (freshly deposited) versus long-term (refractory) diagenesis. It is recommended that the model be calibrated to two reactive

classes with the third G-class considered completely non-reactive. Calibration of G2 diagenesis is likely meaningful only when using multi-year simulations. Therefore, it may be useful to initially fix G2 and refine it subsequently during long-term simulations.

4. MODEL CALIBRATION APPROACH

4.1 Calibration Metrics

Model calibration can be targeted to simulate a range of water column and sediment observations. The suggested model metrics are based on the following:

- Observed sediment fluxes in sediment incubation studies from past (Caffrey et al. 1996; Caffrey and Miller 1995) can be used for the "simplified" model described under Section 4.2. When/if the sediment flux measurements proposed in Section 3.2.2 are available, these can provide a more robust constraint on both the "simplified" and the "full" models described in Section 4.2. In addition, as discussed in Section 3.3.2 there is a potential to use Chesapeake Bay benthic flux data in conjunction with SFB-specific measurements to potentially provide a larger suite of comparisons under different locations in SFB.
- Observed water column concentrations of DO, nutrients, and reduced solutes such as H2S and methane provide additional constraints on sediment fluxes. If excessive or inadequate sediment fluxes are predicted or the timing of fluxes are incorrect, then these can have impacts on the water column parameters; therefore, if adjustment of water column parameters does not provide a satisfactory result, then it may indicate inaccurate benthic-pelagic coupling in the model.
- Timing of predicted algal blooms–if sediment fluxes become a significant source of nutrients under nutrient limiting conditions it can result in algal blooms, particularly later in the year when the nutrients deposited from the spring bloom are released back into the water column. Late summer/fall blooms including nuisance algal blooms observed in SFB can be indicative of internal sources later in the year.
- Sediment trap measurements and water column particulate organic matter data can provide a suite of useful calibration targets:
    - Estimated depositional fluxes of organic and inorganic matter from the water column model must be comparable to the observations in the sediment traps.
- The ratio of labile to refractory organic matter in depositing sediments can be adjusted to reflect laboratory measurements of water column suspended solids using 5-day versus the ultimate biochemical oxygen demand (i.e. BOD-5 versus BOD-u) to make the distinction between labile and refractory matter. As discussed in Section 3.4.1, sediment deposition and burial rates can be compared to sedimentation rates

estimated from sediment trap data; in addition, these rates can also be compared to radioisotope data (for example, Fueller et al. 1999).

4.2 Model Calibration Strategy

Considering the paucity of key data needed to properly constrain a sediment flux model, the calibration strategy will need to be explorative and iterative. To enable this strategy, it will be essential to develop a "simplified" model that can run at a relatively short time interval (minutes to hours for a multi-year simulation). This model will then be refined iteratively until an acceptable set of parameters are identified for use in a more detailed, "full" model of SFB. The overall strategy is illustrated in Figure 4-1.

The objective of the "simplified" model is to provide a reasonable simulation of seasonally-averaged, long-term fluxes and inter-annual water column trends on an embayment (or a large, well-defined subembayment) level. To achieve this objective, it will be necessary to first spin up the model (i.e. identify a stable sediment initial condition). A key consideration is the selection of hydrological and boundary conditions that are reflective of the modeling objectives. Recognizing that the productivity has changed from the 1990s to present, it may be necessary to assess which of those conditions (historical or present) have a greater influence in controlling the internal source. One might anticipate that the higher productivity in recent years would result in greater enrichment of the sediments until a new equilibrium is reached with the water column. Furthermore, considering the overall hydrological and sea level changes resulting from global climate change, the recent past (post-2000) conditions are probably more reflective of the conditions anticipated in the near- and medium-term.

Following spin-up, exploratory sensitivity analysis can help identify a preliminary set of parameters for calibration. Model metrics selected for sensitivity analysis should include long-term fluxes and seasonal/inter-annual trends. Parameter ranges can be (largely) literature-based, including those used for the Chesapeake Bay model. It is recommended that the initial set of parameters be restricted to decomposition rate constants and benthic mixing coefficients that affect long-term nutrient fluxes and sediment concentrations. There may be opportunities for parsimonious parameterization. For example, rather than calibrating a burial rate and a digging rate, an effective burial rate (burial – digging) may be used as a calibration parameter.

The preliminary set of parameters can be refined as necessary within the ranges identified during sensitivity analysis to develop a calibration of the "simplified" model. Quality of the calibration will be assessed after sediment concentrations stabilize. It may be necessary to perform multiple iterations of the long-term simulation for each parameter set. Conclusion of this step will provide a "base case" set of model parameters and representative initial sediment concentrations for use in the "full" model calibration.

To limit the number of parameters in the "base case" parameter set that are calibrated during the "full" model calibration a sensitivity analysis may be useful, but the lengthy simulation time for the "full" model may preclude this step. Therefore, this is listed as an optional step in Figure 4-1.

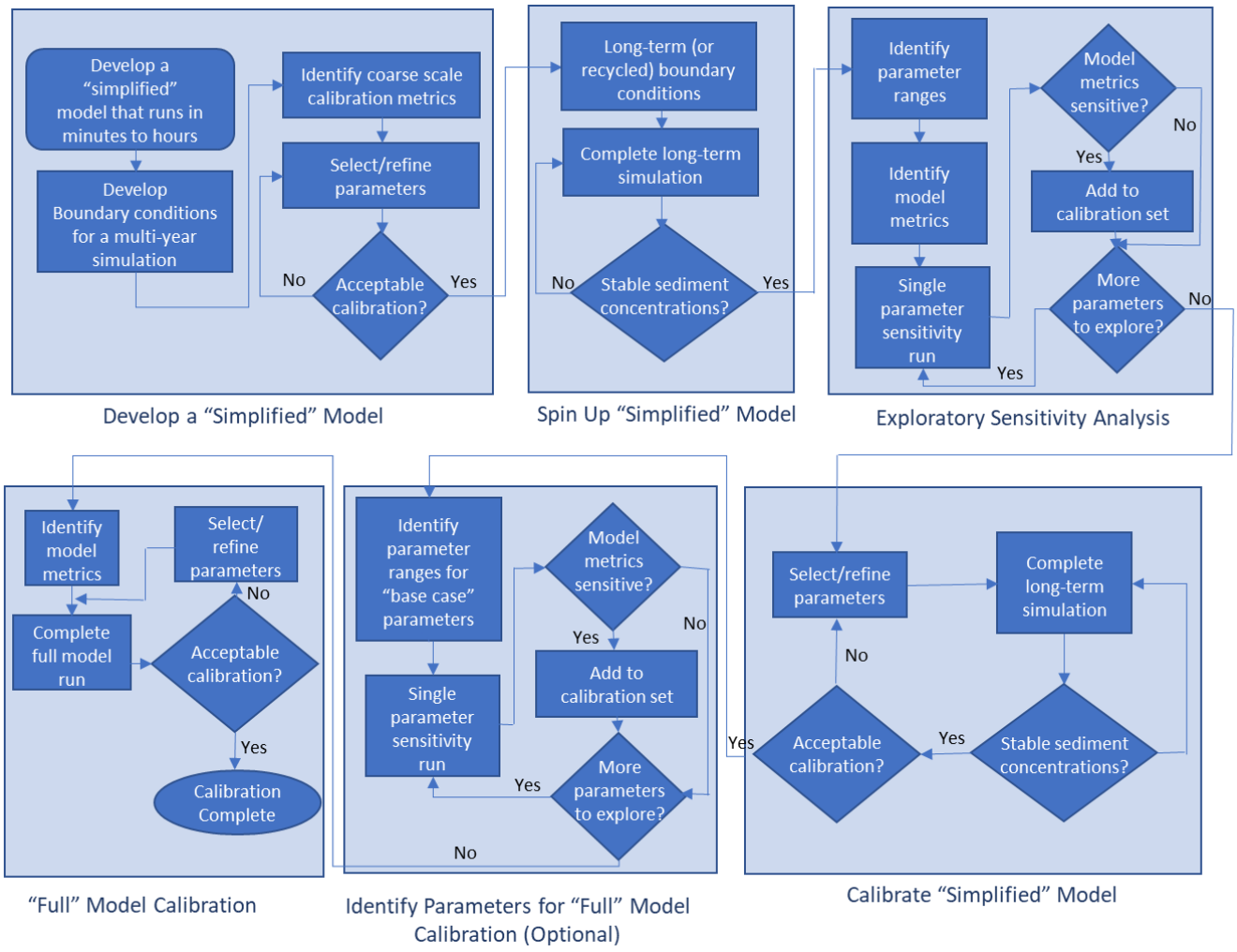

Figure 4-1. Proposed Calibration Approach for SFB Sediment Flux Model

"Full" model calibration will employ model metrics aimed at seasonal and local-scale processes. In addition to overall fluxes, observed water column concentrations will also provide useful calibration targets. Considering that the full model will be more sensitive to short-term changes and water column feedback, parameter refinements may require the inclusion of water column model parameters to reproduce model calibration targets.

4.3 Optimizing Model Utility for Long-term Simulations

Based on sensitivity of water column metrics, it is possible to introduce different levels of complexity for the sediment flux submodel as follows:

- If the observed sediment fluxes are minor relative to the external loads, then the sediment flux submodel simulations can be simplified greatly to include only the bare minimum processes or none at all.
- If the observed benthic-pelagic feedback is slow (i.e. turnaround of nutrients from sediments does not significantly affect productivity or water column DO within a growing season) then a decoupled sediment model can be run that provides approximate long-term fluxes for use in the water column model.
- If the sediment-water column model feedback is more apparent within a season, then spatial aggregation with a decoupled sediment model that provides fluxes as distributed sources to the water column model can help in cutting down run times; however, the numerical stability of such representations will require careful evaluation

Spatial variability of sediment and water column processes can provide additional opportunities to optimize model simulations. Sub-embayments that have stronger benthic-pelagic coupling can be simulated as stand-alone models with a larger suite of sediment flux processes. A full model of SFB encompassing all sub-embayments can subsequently be simulated that can use the benthic fluxes from the stand-alone model thereby avoiding the need to simulate a large suite of sediment flux processes over the entire Bay.

The recommendations above are intended as broad guidelines. Other options may become apparent once detailed data collection and modeling efforts get underway, and the conceptual model for SFB is refined based on those findings. Therefore, it is important to adopt an adaptive approach to model refinements and long-term application.

5. REFERENCES

Berner, R., 1980. Early Diagenesis: A Theoretical Approach, Princeton University Press, New Jersey.

Boudreau, B.P., 2000. The mathematics of early diagenesis: from worms to waves. *Reviews of Geophysics*, 38(3): 389-416.

Boudreau, B.P., 1997. Diagenetic Models and their Implementation, Springer, New York.

Boynton, W.R. and Bailey, E.M., 2008. Sediment Oxygen and Nutrient Exchange Measurements from Chesapeake Bay, Tributary Rivers and Maryland Coastal Bays: Development of a Comprehensive Database and Analysis of Factors Controlling Patterns and Magnitude of Sediment-Water Exchanges, Technical Report Series No. TS-542-08, University of Maryland Center for Environmental Science - Chesapeake Biological Laboratory, Solomons, Maryland, June, 2008.

Brady, D.C., Testa, J.M., DiToro, D.M., Boynton, W.R., and Kemp, M.W., 2013. Sediment flux modeling: Calibration and application for coastal systems, *Estuarine, Coastal and Shelf Science*, 117: 107-124, doi: http://dx.doi.org/10.1016/j.ecss.2012.11.003

Burdige, D.J., 1991. The kinetics of organic matter mineralization in anoxic marine-sediments, *Journal of Marine Research*, 49(4): 727-761, doi: 10.1357/002225091784995710.

Caffrey, J.M. and Miller, L.G., 1995. A comparison of two nitrification inhibitors used to measure nitrification rates in estuarine sediments, *FEMS Microbiology Ecology*, 17: 213-220.

Caffrey, J.M., Hammond, D.E., Kuwabara, J.S., Miller, L.G., and Twilley, R.R., 1996. Benthic Processes in South San Francisco Bay: The Role of Organic Inputs and Bioturbation, in San Francisco Bay: The Ecosystem, Hollibaugh, J.T. ed., Proceedings of the 75th Annual Meeting of the Pacific Division/American Association for the Advancement of Science, held at San Francisco, CA, June 19-24, 1994.

Caffrey, J.M., Cloern, J.E., and Grenz, C., 1998. Changes in production and respiration during a spring phytoplankton bloom in San Francisco Bay, California, USA: implications for net ecosystem metabolism, *Marine Ecology Progress Series*, 172:1-12.

Cerco, C.F., Kim, S-C., and Noel, M.R., 2010. The 2010 Chesapeake Bay Eutrophication Model, A Report to the U.S. Environmental Protection Agency Chesapeake Bay Program and the U.S. Army Corps of Engineers Baltimore District, by U.S. Army Engineer Research and Development Center, Vicksburg, MS, December, 2010. Available at: http://www.chesapeakebay.net/publications/title/the_2010_chesapeake_bay_eutrophication_model1

Cerco, C.F. and Noel, M.R., 2017. The 2017 Chesapeake Bay Water Quality and Sediment Transport Model, A Report to the U.S. Environmental Protection Agency Chesapeake Bay Program, by

U.S. Army Engineer Research and Development Center, Vicksburg, MS, May, 2017 Draft Report.

Chapra, S.C., Gawde, R.K., Auer, M.T., Gelda, R.K., and Urban, N.R., 2015. Sed2K: Modeling Lake Sediment Diagenesis in a Management Context, *Journal of Environmental Engineering*, 141(3). doi: https://doi.org/10.1061/(ASCE)EE.1943-7870.0000897

Cornwell, J.C., P.M. Gilbert and M.S. Owens, 2014. Nutrient fluxes from the sediments in the San Francisco Bay Delta, *Estuaries and Coasts*, 37:1120 – 1133, doi: 10.1007/s12237-013-9755-4

Crauder, J., Downing-Kunz, M.A., Hobbs, J.A., Manning, A.J., Novick, E., Parchaseo, F., Wu, J., Schoellhamer, D.H., Senn, D.B., Shellenbarger, G.G., Thompson, J. and Yee, D., 2016. Lower South Bay Nutrient Synthesis. San Francisco Estuary Institute & Aquatic Science Center, Richmond. CA. Contribution #732.

DiToro, D.M., 2001. Sediment Flux Modeling, Wiley-Interscience, New York.

Fueller, C.C., van Green, A., Baskaran, M., and Anima, R., 1999. Sediment chronology in San Francisco Bay, California, defined by ^{210}Pb, ^{234}Th, ^{137}Cs, ^{239,240}Pu, Marine Chemistry, 64(1-2):7-27, doi: https://doi.org/10.1016/S0304-4203(98)00081-4

Grenz, C., Cloern, J.E., Hager, S.W., and Cole, B.E., 2000. Dynamics of nutrient cycling and related benthic nutrient and oxygen fluxes during a spring phytoplankton bloom in South San Francisco Bay (USA), *Marine Ecological Progress Series*, 197:67-80.

Hagy III, J.D., W.R. Boynton, and D.A. Jasinski, 2005. Modelling phytoplankton deposition to Chesapeake Bay sediments during winter-spring: interannual variability in relation to river flow, *Estuarine, Coastal and Shelf Science*, 62: 25-40, doi:10.1016/j.ecss.2004.08.004.

Hammond, D.E., Fuller, C., Harman, D., Hartman, B., Korosec, M., Miller, L.G., Rea, R., Warren, S., Berelson, W., and Hager, S.W., 1985. Benthic fluxes in San Francisco Bay, *Hydrobiologia*, 129: 69-90.

Holleman, R., Nuss, E., and Senn, D., 2017. San Francisco Bay Interim Model Validation Report, San Francisco Estuary Institute, Contribution No. 850, December 2017.

Kuwabara, J.S., Topping, B.R., Parchaso, F., Engelstad, A.C. and Greene, V.E., 2009, Benthic flux of nutrients and trace metals in the northern component of San Francisco Bay, California: U.S. Geological Survey Open-File Report 2009-1286, 26 p.

Lesen, A.E., 2006. Sediment organic matter composition and dynamics in San Francisco Bay, California, USA: seasonal variation and interactions between water column chlorophyll and the benthos, *Estuarine, Coastal and Shelf Science*, 66: 501-512, doi: 10.1016/j.ecss.2005.10.003.

Novak, E., Holleman, R., Jabusch, T., Sun, J., Trowbridge, P., Senn, D., Guerin, M., Kendall, C., Young, M., and Peek, S., 2015. Characterizing and quantifying nutrient sources, sinks and

transformations in the Delta: synthesis, modeling, and recommendations for monitoring, prepared for California Department of Water Resources, December 2015.

Paraska, D.W., Hipsey, M.R., and Salmon, S.U., 2014. Sediment diagenesis models: Review of approaches, challenges and opportunities, *Environmental Modelling and Software*, 61: 297-325, doi: http://dx.doi.org/10.1016/j.envsoft.2014.05.011

Testa, J., Brady, D., DiToro, D., Boynton, W., Cornwell, J., and Kemp, W., 2013. Sediment flux modeling: Simulating nitrogen, phosphorus, and silica cycles, *Estuarine, Coastal and Shelf Science*, 131: 245-263, doi: http://dx.doi.org/10.1016/j.ecss.2013.06.014

Wang, Y., and Van Cappellen, P., 1996. A multicomponent reactive transport model of early diagenesis: Application to redox cycling in coastal marine sediments, *Geochimica et Cosmochimica Acta*, 60(16): 2993-3014.

Zhang, Z., R. Holleman, E. Nuss and D. Senn, 2018. *Nutrient limits phytoplankton growth during a historical bloom event in San Francisco Bay*, Presented at the 10th Biennial Bay-Delta Science Conference, Sacramento, CA, September 10-12, 2018.